Observations of Sun-Induced Chlorophyll fluorescence (SIF), Photochemical Reflectance Index (PRI) and Chlorophyll:Carotenoid Index (CCI) during spring recovery in two evergreen conifers from the Boreal Forest.

by

Rebeca Campos Valverde

A thesis submitted in partial fulfillment of the requirements for the degree of

Master of Science

Department of Earth and Atmospheric Sciences

University of Alberta

Abstract

Northern hemisphere evergreen forests assimilate a significant fraction of global atmospheric CO_2. Conifers undergo winter-downregulated photosynthetic activity and spring-onset photosynthetic activation. Currently, increased temperatures are leading to shifts in photosynthetic phenology (early spring-onset, longer growing season), which has important implications in terrestrial GPP. How these species are adapting to these changes is highly uncertain. Evergreen conifer's foliage remains green year-round, making the photosynthetic transition between spring and winter "invisible" to classical remote sensing (RS) techniques such as the Normalized Difference Vegetation Index (NDVI). However, conifers adjust their carotenoid pigment content between seasons, to modulate photosynthesis and relieve excess energy. These changes can be detected using a series of RS techniques such as the Photochemical Reflectance Index (PRI), the Chlorophyll/Carotenoid Index (CCI) and the Sun induced chlorophyll fluorescence signal (SIF). To better understand the mechanisms and timing of this invisible transition, we conducted a series of leaf-scale experiments to explore the biophysical link between SIF, PRI, CCI and air temperature in two dominant conifer species: lodgepole pine (*Pinus contorta*) and black spruce (*Picea mariana)*, in Alberta, Canada. Our results provide strong evidence that during the spring recovery, SIF parameters, and carotenoid reflectance-based vegetation indices are closely tied to temperature changes and positively correlated with each other. We were able to track the relative-timing of the photosynthetic reactivation of both species during the spring recovery and we gained knowledge about how these two conifer species' metrics differ slightly in kinetics. In particular, the activation of SIF emission was earlier in lodgepole pine (*P. contorta*) than in black spruce *(P. mariana*). We conclude that together these metrics are reliable optical methods for detecting spring transition across evergreen conifer tree species and can help lay the foundation for improved remote sensing methods of monitoring the changing photosynthetic activity of boreal forests. These findings are important because the boreal ecosystem is a major contributor to the global climate system. Thus, reducing uncertainties in the timing and drivers of the spring transition could generate a better understanding of how this biome is responding to a changing climate, and how it may in turn affect climate.

Acknowledgements

The completion of my thesis work would not have been possible without many sources of support:

Thank you to my supervisor Dr. John A. Gamon for being an excellent mentor and for his guidance, support, and patience during my path through grad school.

Thank you also to my committee members, Dr. Martin Sharp, Dr. Karl F Huemmrich and Dr. John Waldron for their helpful feedback.

Thank you to current and former graduate students who have provided their help and advice: Alexandra Hennig, Kyle Springer, and Chris Wong.

Thank you to our collaborators from University of Valencia, Luis Alonso and Shari Van Wittenberghe who advised me in the use of the FluoWat leaf-clip.

Thank you to my family, my parents Mari and Carlos and to my siblings Carlomagno and Karolina for their unconditional support and love.

And thanks to all my friends from grad school in Canada and my friends from Costa Rica for always being there for me and for constantly believe in me: Branko, Natalie, Birgitta, Hellen, Peter Carlson, Sofi, Pam, Dani, Joe, Eric Timmer, Calla, Avni, Nikita, Makoto, Jason, Brandon, Nancy, José Luis, Laura, Meli, Andrea, and Pedro.

Table of contents

List of Tables

List of Figures

Abbreviations

A: Antheraxanthin, V: Violaxanthin , Z: Zeaxanthin

BS: black spruce (*Picea mariana*)

CCI: Chlorophyll/Carotenoid ratio index

Chl:Car : Chlorophyll/Carotenoid ratio

DS : dark current signal

F*yield*: Sun induced chlorophyll fluorescence yield.

I: Irradiance

LP: lodgepole pine (*Pinus contorta*)

L_λ= (spectral) radiance in units of $Wm^{-2}s^{-1}$ nm^{-1}

NIR: near-infrared

nm: nanometer

nm: nanometers

PAR: Photosynthetically Active Radiation (radiation between 400 and 700 nm). Also used to indicate the flux of solar radiation between 400 and 700 nm, either in micromoles quanta m^{-2} s^{-1} or in energy units, (e.g., watts m^{-2} sr^{-1})

PRI : Photochemical reflectance Index

R_λ= uncalibrated (spectral) radiance (machine units)

SIF 685: Sun induced chlorophyll fluorescence at 685 nm

SIF 745: Sun induced chlorophyll fluorescence at 745 nm

SIF ratio: Ratio of sun induced chlorophyll fluorescence at 685 and 745 nm

SIF: Sun Induced chlorophyll Fluorescence

sr: steradian

T_λ = transmittance

W: Watts

WR: White reference calibration panel

WR650: White reference calibration panel with a 650nm short pass filter in place

λ = wavelength

ρ: (spectral) needle reflectance (ρ_λ)

Chapter 1 – General Introduction

The boreal forest is found in the high latitudes of Europe, Asia, and North America, and covers an area of 12 million km^2. This ecosystem represents a quarter of the world's total forest biomass (Kneeshaw et al. 2011), contains some of the most extensive unmanaged forest areas in the world and stores a substantial part of the global carbon mass (MacDonald, 2010). Canada possesses 28% of the world's boreal forest, which is dominated by mixed stands of evergreen conifers and broadleaf deciduous tree species (Natural Resources Canada, 2019). Since evergreen conifers exchange massive quantities of carbon with the atmosphere, these forests are important to the global carbon budget. However, this boreal ecosystem is currently facing a challenge: the mean annual air temperatures in these regions haven risen at a rate of 0.6°C per decade over the last 30 years (Song et al. 2018), which is twice the global average rate (IPCC, 2014). This warming is altering ecological processes and natural disturbance regimes (Caccianiga, 2006; Payette, 2006; Hogg, Brandt & Michaelian, 2008; van Mantgem et al. 2009).

Some of the reasons why the northern hemisphere terrain is warming so fast include increases in atmospheric greenhouse gas forcing caused by anthropogenic emissions (Rangwala et al. 2013), a decrease in the production and release of sulfate aerosols (Friedman et al. 2013), the North American hemispheric asymmetry in land area distribution in comparison with other continents (Stouffer et al. 1989; Manabe et al. 1991), and changes in the polar jet stream circulation (Francis & Skific, 2015) among other reasons. In addition to this, the rise in boreal forest temperatures is accelerated by a phenomenon known as "*Arctic amplification*". This is a consequence of the loss of sea ice, land ice, and snow from the Arctic region and a consequent decrease in the Earth's albedo. When bright and reflective ice melts, a darker Earth surface is

revealed. This amplifies the warming trend because the darker ocean or land surfaces absorb more heat from the sun than do the snow and ice covered surfaces (NASA's Earth Observatory, 2018). This amplification has also been reported over land (Chapin et al. 2005). It has been projected that, by the end of the century, the climate of a biome such as the northern boreal forest could become drastically drier and/or warmer, opening doors to the expansion of native or invasive forest pests, (or to similar situations such as the "outbreaks" of the mountain pine beetle) experienced in Canada (Gauthier et al. 2015). Fire frequency, area, and severity are also expected to increase considerably (Shvidenko & Schepaschenko, 2013), along with drought-induced tree mortality (Lian et al. 2020). The noticeable warming of the boreal forest in recent decades has been linked to an earlier onset of the growing season and to phenological variation in evergreen vegetation, which lead to modifications in forest productivity, and changes in the boreal carbon budget (Ulsig et al. 2017). Changes in air temperature can alter the timing of the spring and fall transition periods, altering the timing and length of the growing season, and directly impacting vegetation phenology and the productivity of evergreen tree species (Richardson et al. 2013; Friedl et al. 2014). Recent remote sensing studies indicate that the growing season length is increasing in the northern hemisphere (Gonsamo, Chen, & Ooi, 2018).

As a result of these changes, boreal tree species could be responding to longer growing seasons via increased photosynthesis or higher productivity, which would likely increase gross CO_2 uptake (Estiarte & Peñuelas, 2015; Bowling, et al. n.d., Luus et al. 2017), a process that is often referred to as "greening". However, there is also abundant evidence of the opposite situation, "browning," which is associated with increases in tree mortality. Piao et al. (2020) stated that the rise in photosynthetic activity in most of Siberia is associated with spring warming, but they also suggested that the slope of the regression relationship between leaf area index (LAI) and air

temperature increases with soil moisture but decreases with increasing air temperatures. This implies that the contribution of rising air temperatures to the current "greening" trend will weaken or even disappear under continued global warming. According to Allen et al. (2014) forest mortality has increased in tandem with rising CO_2 and air temperatures (over the 20^{th} century), and is highly connected to terrestrial warming and the increase in extreme drought events. Moreover, hotter, drier summers lead to increases in the frequency of forest fires. Both of these effects can increase outbreaks of insect pests, increasing tree mortality (Angert et al. 2005; Michaelian et al. 2011). The warming over the northern hemisphere can lead to enhanced vegetation carbon uptake, due to a longer growing season (Barichivich et al. 2013; Goetz, Bunn, Fiske, & Houghton, 2005). On the other hand, it can also lead to a higher rate of carbon release from forest dieback (Hogg et al. 2008)

The phenological response of the vast evergreen conifer forests in Boreal regions to warmer temperatures remains highly uncertain. As changes in meteorological and climatic conditions start to have substantial impacts on forest ecology and plant physiology, the photosynthetic and respiratory activities of boreal conifer tree species are expected to change, along with their impact on global values of Gross Primary Productivity (GPP) and Net Primary Productivity (NPP). GPP is the equivalent of the CO_2 assimilation or photosynthetic rate but is expressed over a large area over a long period, while NPP accounts for the combined effect of plant photosynthesis and respiration on the environment over time (Randerson et al. 2002). Calculating accurate values of GPP and NPP for the boreal forest is a priority, due to its immense impact on the terrestrial carbon budget production (up to 30% of the terrestrial CO_2 uptake (Hari & Kulmala, 2009).

The light-use efficiency model (LUE) is a common method to quantify plant productivity within an ecosystem. It relies on remote sensing approaches to model seasonal variations in photosynthetic plant efficiency and GPP. As outlined by Gamon (2015), this model is derived from crop studies by Monteith (1977), who stated that dry matter yield can be expressed as a function of the amount of intercepted solar radiation (IPAR, which is typically expressed as the incoming photosynthetically active radiation or photosynthetic photon flux density (PPFD), and the efficiency (Ɛ) which expresses how much of that radiation is converted to biomass per unit time, as shown in Figure 1-1.

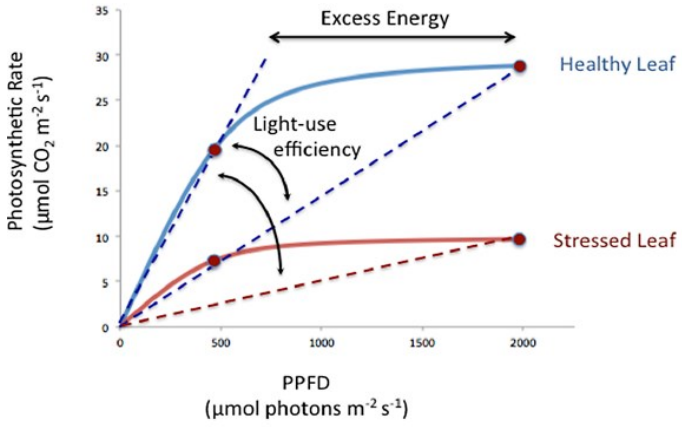

Figure 1-1. Modeled photosynthetic light-response curves (rectangular hyperbola) for healthy and stressed leaves, illustrating a decline in light-use efficiency (LUE) as a response to changes in PPFD, also typically termed the photon (or quantum) yield, from (Gamon, 2015).

In the remote sensing context, a common formulation of the light use efficiency (LUE) model has evolved from the fundamental concept of Monteith (1977). Here, efficiency is expressed in terms of how GPP varies as a function of absorbed radiation, and of the efficiency (Ɛ) with which that absorbed radiation is converted to fixed carbon. The fraction of the absorbed

photosynthetically active radiation taken up by vegetation is called fAPAR (Peñuelas et al. 1995; Peñuelas, Filella, Gamon, & Field, 1997; Gitelson & Gamon, 2015).

Equation 1. $GPP = PPFD \times fAPAR \times (\text{Ɛ})$

Where:
GPP: Gross primary production
PPFD: photosynthetic photon flux density
*f*APAR: fraction of absorbed photosynthetic active radiation.
Ɛ: Efficiency

This quantification is a complex task in the boreal forest. Access to evergreen coniferous ecosystems can be very complicated because these ecosystems are located in remote geographical locations and experience harsh weather conditions over long periods of the year. These conditions, have made the installation and maintenance of environmental-monitoring equipment very challenging (Bowling; Frankenberg & Logan, 2018). The remote and inaccessible nature of these forests has restricted the ability to collect quality data (in time and space) within them. This is why, over recent decades; researchers have dedicated considerable effort to apply remote sensing technologies to the observation of the photosynthetic activity of evergreen conifers.

However, the evergreen conifer ecosystem is physiologically complex, and researchers have encountered challenges using remote sensing techniques. Data-driven estimates of photosynthesis (LUE) across Boreal regions have had often relied on satellite-derived proxies such as the normalized difference vegetation index (NDVI) or the enhanced vegetation index (EVI). These greenness-based indices have a lot of limitations when applied to evergreen systems, and do not provide a direct proxy for the LUE models, especially in high latitude ecosystems (Wang et al. 2015). This because, the vegetation of northern ecosystems undergoes marked seasonal shifts

in light-use efficiency (LUE), which result in strong changes in photosynthetic dynamics over the course of a year, while canopy structure and green leaf/needle area remain relatively constant. In such cases, greenness-based vegetation indices (e.g., NDVI) that are responsive to changes in green leaf/needle area, typically fail to detect the seasonal photosynthetic dynamics (Gamon et al. 2016). Due to difficulties in assessing evergreen complex physiology using NDVI, researchers have explored new methods for detecting seasonal changes in the boreal forest that are more sensitive to physiological changes affecting the efficiency term of the LUE model. These new methods are based on the idea studying the links between photosynthetic efficiency, seasonal pigment composition, and their response to environmental variables such as temperature and radiation. To understand this, we need to explore the physiology of evergreen conifers and their multiple adaptative mechanisms.

Evergreen conifers have evolved specific physiological features to survive in the harsh high latitude climates (Gillies & Vidaver, 1990). These physiological features function as strategies that allow conifers to survive intense periods of winter cold. One of them is, that evergreen conifer trees keep their pigmented and constant foliage over the year, but undergo a photosynthetic downregulation process during winter, when light use efficiency (LUE) is drastically reduced. This process is analogous to hibernation/winter dormancy, starts slowly in the fall and continues through the winter until photosynthetic activation is triggered in spring. This photosynthetic acclimation is accompanied by gradual changes in chlorophyll and carotenoid pigments(Adams III & Demmig-Adams, 1994), which also leads to an optical response.

The detection of spring activation in evergreen conifers is tied to the activation of photosynthetic mechanisms directly connected to the start of the growing season, and must be

taken into account when quantifying terrestrial carbon uptake or GPP. (Luus et al. 2017; Bowling, Frankenberg & Logan, 2018; Magney et al. 2019). Spring activation involves changes in carotenoid pigment concentrations (or photoprotective pigments) and chlorophyll pigments in leaves and needles (Huner, Öquist & Sarhan, 1998), and these seasonal pigments changes in evergreen photosynthetic pigments have been reported for years (Adams III & Demmig-Adams, 1994; Huner, Öquist, & Sarhan, 1998; Wong and Gamon, 2015; and Gamon et al. 2016). In addition, more recent work by Magney et al. (2019) confirmed that the strong seasonality of GPP in a subalpine evergreen is modulated by changes in photosynthetic efficiency and the acclimatization of photoprotective pigments in needles (experiments were performed on *P. contorta and P. engelmannii*), and Wong et al. (2020) demonstrated the potential of photoprotective carotenoids to remotely detect leaf development in the spring and leaf senescence during the fall in evergreen and mixed deciduous forests, at both the leaf and canopy scales, in a Canadian forest. These findings indicate that seasonal changes in photoprotective pigments can be detected with new remote sensing methods, including fluorescence and reflectance indices. Because these methods can be applied remotely, they could potentially help us to overcome the difficulties and challenges of detecting and monitoring the activation of evergreen photosynthesis during the spring and, its decline during the fall.

Evergreen conifers dissipate excess light energy through reactions mediated by a particular group of carotenoids, the xanthophyll pigments violaxanthin, antheraxanthin and zeaxanthin (Öquist & Huner, 2003). The xanthophyll cycle is an energy dissipation process that is induced by the accumulation of protons in the thylakoid lumen, which is triggered by excess light (saturation or excess energy, as shown in Figure 1-2). It happens when acidification of the lumen induces an enzymatic conversion of the carotenoid violaxanthin into antheraxanthin and zeaxanthin (Gilmore

& Yamamoto, 1993). Then, zeaxanthin triggers a kind of ‘‘lightning rod’’ mechanism. This mechanism is involved in catching the light (like an antenna) and facilitating the dissipation of excess energy (Barbara Demmig-Adams & Adams, 1996a), thus avoiding photo-damage to chlorophyll by reactive oxygen species (ROS). The xanthophyll cycle acts at a daily scale, from minutes to hours, reducing and increasing photosynthetic pigments in the face of possible environmental stressors such as high irradiance, drought, heat or cold. This process is linked to non-photochemical quenching (NPQ), a decline in chlorophyll fluorescence under stress. The xanthophyll cycle and the carotenoid pigments provide photoprotection and provide fundamental information about the daily LUE of evergreen-conifers (Wong & Gamon, 2015).

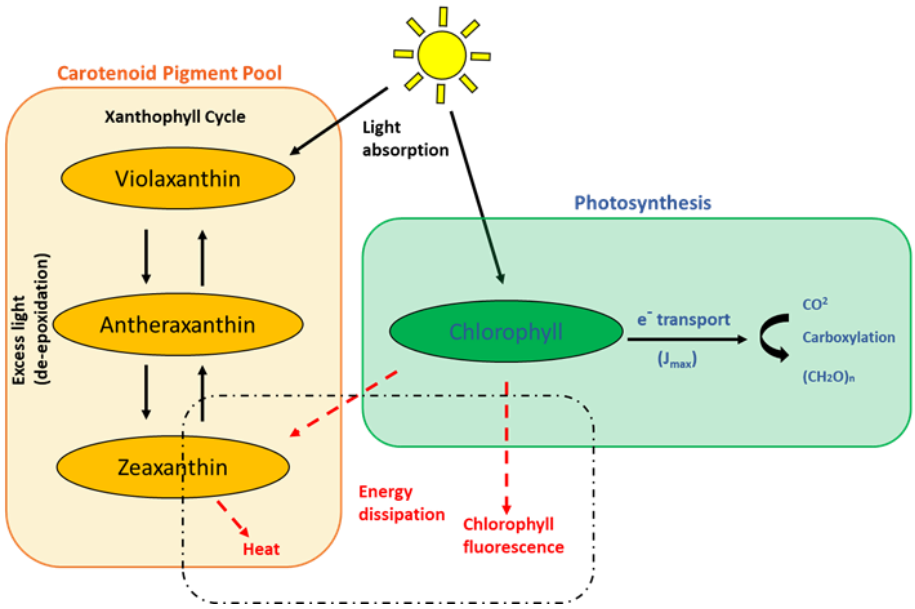

Figure 1-2. Distribution of absorbed radiation within a leaf, showing processes of productive photosynthesis (dark blue text and arrows), energy dissipation (red text and arrows) also called NPQ, regulatory processes associated with the xanthophyll cycle (black text and arrows within

box on left), and the carotenoid and chlorophyll pigment concentrations, modified from Gamon (2015).

Photoprotective responses involving pigments or NPQ can be classified based on two different time scales as the short-term xanthophyll cycle and long-term pigment pool size adjustments (Gamon & Berry, 2012). Over winter, evergreen plants do not use the xanthophyll cycle at a daily time scale as they do in summer, because it is too cold to operate biochemical processes (Gillies & Vidaver, 1990). In contrast, they shift to using a seasonal-scale or a 'sustained' version of the xanthophyll cycle and later, after winter, they gradually disconect this process and start a transition to reactivate photochemistry as spring approaches (Öquist & Huner, 2003).This can be observed in figure 1-3, and is also known as sustained NPQ (Porcar-Castell et al. 2012).

The sustained NPQ, while related to the xanthophyll cycle, is often associated with seasonal changes in the ratio between carotenoid and chlorophyll pigments concentration (Car: Chl) rather than by the diurnal xanthophyll cycle (a daily interconversion is not present) (Busch, Huner, & Ensminger, 2009; Fréchette, Wong, Junker-Frohn, Chang, & Ensminger, 2015; Wong & Gamon, 2015). This means that during winter, the xanthophyll cycle gets "stuck" in an energy dissipation state (sustained NPQ), displaying high concentrations of zeaxanthin. Similarly, the overall carotenoid levels gradually increase relative to chlorophyll from the fall through the winter and start to decrease with the onset of spring (Figure 1-3). In some (Gamon et al. 2016), but not all (Bowling et al. 2018; Walter-McNeill et al. 2021) cases, the levels of chlorophyll decline along with the winter increase in carotenoid levels. The sustained NPQ provides photoprotection at a seasonal scale, and provides information about the seasonal dynamics of evergreen-conifers during seasonal transitions.

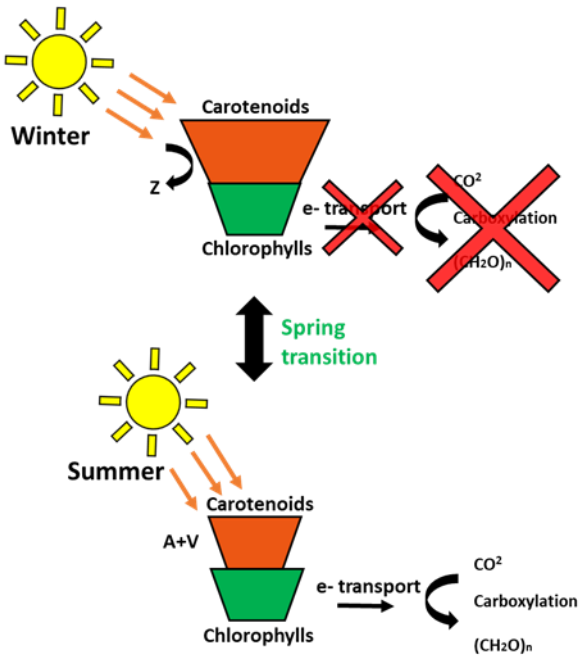

Figure 1-3. Hypothesized shifts in concentrations of chlorophyll and carotenoid pigments during the transition from winter to spring and the reactivation of photosynthesis, during winter when electron transport stops, discontinuing the carboxylation process converting CO_2 to carbohydrates (denoted with a red X). Modified from Gamon (2020).

The remote sensing approach to assessing the daily interconversion of the xanthophyll cycle uses a reflectance index known as the photochemical reflectance index (PRI) (Gamon, Serrano & Surfus, 1997). Over diurnal periods, PRI captures the photoprotective conversion of the xanthophyll cycle pigment violaxanthin into antheraxanthin and zeaxanthin in response to light to facilitate the distribution of absorbed light energy (Gamon, Peñuelas & Field, 1992; Gamon et al. 1995). Specifically, PRI tracks the conversion of the xanthophyll cycle pigments based on changes in spectral reflectance at 531 nm in comparison to a reference waveband at 570 nm. On a longer time-scale, PRI tracks the seasonal transitions in pigment pools associated with sustained changes in pigment pools and NPQ (Wong and Gamon 2015 a&b). However, this index suffers from a

small “signal-to-noise” ratio and cannot be measured by most current satellites (Gamon et al. 2016).

To track seasonal pigment variation on the chlorophyll and carotenoid shifting ratios, a new vegetation index was proposed by Gamon et al. (2016). This is called the chlorophyll: carotenoid index (CCI, sometimes called “MODIS PRI”). Recent studies by Springer et al.(2017); and Wong et al. (2019, 2020) have used this index to explore the sustained energy dissipation process of boreal species. Springer et al. (2017) confirmed that CCI was able to track photosynthetic phenology in both deciduous and evergreen species, reflecting seasonal changes in both pigment pool size and canopy structural changes. Wong et al. (2020) were able to accurately capture seasonal variation of photosynthetic pigment (Chl:Car) composition by using carotenoid-sensitive vegetation indices such as PRI and CCI, confirming that both indices can act as proxies for LUE and photosynthesis, at both leaf and canopy scales. In summary, both optical indices share a high potential for tracking the ‘invisible’ phenology in evergreen conifer trees.

A second method of observing or monitoring the photosynthetic phenology associated with seasonal pigment and NPQ adjustments is known as Sun-induced chlorophyll fluorescence (SIF). This method allows us to detect dissipation of excess absorbed energy (Fig 1-4). During normal photosynthetic activity, a small fraction of the absorbed light can be dissipated through re-emission as chlorophyll fluorescence, producing a weak signal at wavelengths longer than those at which absorption occurs (Rajewicz, Atherton, Alonso, & Porcar-Castell, 2019). Nowadays, the sun induced chlorophyll fluorescence signal can be detected from space using high-resolution spectra that can resolve absorption bands, which are known as “Fraunhofer bands” and “telluric lines”. These bands are “windows” or “gaps” in the solar spectrum that are due to absorption in the Sun’s

and Earth's atmospheres. Thanks to those gaps we can use passive remote sensing techniques to explore the link between this signal and photochemical acclimation in evergreen conifers. At the same time, new methods involving filters have been developed for leaf-level assessment, such as the FluoWat leaf-clip that has the ability to measure SIF by cutting off the light spectrum with a short pass filter (650 nm), allowing us to observe and track the SIF fluorescence signal from needle and leaf scale (Figure 1-4). These observations can help to validate airborne and satellite data.

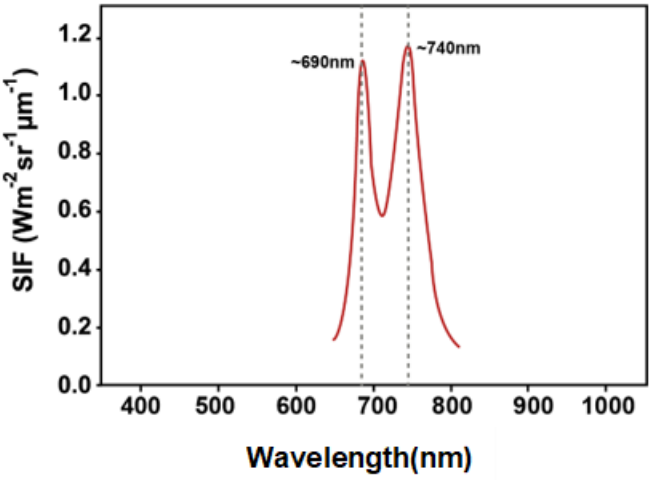

Figure 1-4. Sun induced chlorophyll fluorescence spectrum in the region between 650 and 800 nm.

SIF has attracted a lot of interest, because it is thought to provide a more effective proxy for photosynthesis than most reflectance-based metrics like NDVI (Springer et al. 2017; Bowling et al. 2018., n.d.), especially in evergreen conifer forest stands where reflectance-based indices (such as NDVI and EVI) can be problematic. Because chlorophyll fluorescence energy dissipation occurs as a direct result of light absorption by the chlorophyll complex during photosynthesis, it can more closely track the actual photosynthetic process, more closely than indices based on canopy structure (e.g., NDVI and EVI) (Rossini et al. 2015). Based on this, the SIF signal carries additional information on the photoregulatory status associated with photoprotective pigment

changes and affecting PRI and CCI. For these reasons, SIF may provide a complementary optical measure of seasonal photosynthetic activity in evergreens (Figure 1-5).

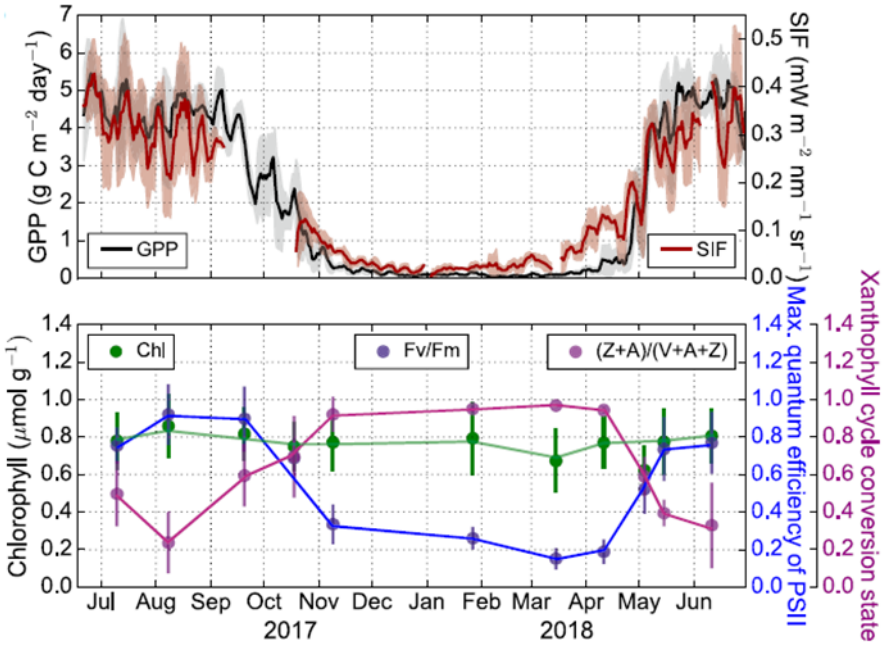

Figure 1-5. Annual cycle of photosynthesis, SIF, and pigment composition from a winter-dormant Colorado conifer forest, illustrating a) strong linkages between GPP, solar-induced fluorescence (SIF) and b) sustained version of xanthophyll cycle (NPQ) in comparison with Chlorophyll content and Photochemistry (Max quantum efficiency of PSII). Modified from: Magney et al. 2019.

The SIF signal can be tracked over the seasons as shown in Figure 1-5 (Magney et al. 2019). Another advantage of SIF is that can be useful as an indicator of photosynthetic activation of evergreen conifers. Recent studies have demonstrated the strong link between GPP and space-borne retrievals of SIF at broad scales and in evergreen conifers ecosystems (Luus et al. (2017); Magney et al. (2019); Walther et al. (2016), and the SIF fluorescence signal can be potentially time-linked to other photosynthetic acclimation processes, such as the sustained NPQ, as

mentioned by Springer (2017) and may also, potentially, be related to photosynthetic pigment (chlorophyll a+b and carotenoid pigment pool) ratios.

The SIF fluorescence signal brings a great opportunity to understand the physiological dynamics of evergreen conifers that can also, potentially, be linked to other remote sensing-derived indices such as the PRI and CCI. In this study, we asked how closely SIF followed the seasonal patterns of PRI and CCI that are related to photosynthetic phenology and pigment changes in evergreen conifers. If these metrics are well correlated, then, together, they could provide complementary remote sensing methods for tracking changes in seasonal phenology and the global carbon cycle.

For this project, we aimed to improve our ability to assess both the timing of activation of photosynthesis during spring-onset and the associated changes in pigments through a new proximal (leaf-level) sampling method that might improve our understanding of remote sensing approaches. Here we compared three vegetation indices (NDVI, PRI, CCI) with SIF at the leaf-scale for two temperate evergreen species from Alberta, Canada. Our goals were to explore the relationship and kinetics between photosynthetic pigments, reflectance-based indices (NDVI, PRI, CCI) and the SIF spectral signal during the transition between the winter downregulation and the spring activation of photosynthesis, under natural outdoor conditions and in a temperature-controlled environment. Our key goal was to compare leaf-scale SIF to reflectance-based metrics (CCI, PRI and NDVI) with the hope of adding to our understanding of the phenology and physiology of Boreal evergreen conifers, which play a critical role in global photosynthesis.

Literature Cited

Adams III, W. W., & Demmig-Adams, B. (1994). Carotenoid composition and down regulation of photosystem II in three conifer species during the winter. *Physiologia Plantarum*, *92*(3),

451–458. https://doi.org/https://doi.org/10.1111/j.1399-3054.1994.tb08835.x

Allen, M., Barros, V., Broome, J., Cramer, W., Christ, R., Church, J., … Yohe, G. (2014). *{IPCC fifth assessment synthesis report - Climate Change 2014 synthesis report}* (P. Aldunce, T. Downing, S. Joussaume, Z. Kundzewicz, J. Palutikof, J. Skea, … Z. Xiao-Ye, Eds.). Retrieved from citeulike-article-id:13416115

Angert, A., Biraud, S., Bonfils, C., Henning, C., Buermann, W., Pinzon, J., … Fung, I. (2005). Drier summers cancel out the CO_2 uptake enhancement induced by warmer springs. *Proceedings of the National Academy of Sciences of the United States of America*, *102*, 10823–10827. https://doi.org/10.1073/pnas.0501647102

Barichivich, J., Briffa, K. R., Myneni, R. B., Osborn, T. J., Melvin, T. M., Ciais, P., … Tucker, C. (2013). Large-scale variations in the vegetation growing season and annual cycle of atmospheric CO_2 at high northern latitudes from 1950 to 2011. *Global Change Biology*, *19*(10), 3167–3183. https://doi.org/10.1111/gcb.12283

Bowling, D., Frankenberg, C., Logan, B., & G. J. G. 2019. (n.d.). *Collaborative Proposal: MRA: Seasonality of photosynthesis of temperate and boreal conifer forests across North America.*

Bowling, D., Logan, B., Hufkens, K., Aubrecht, D., Richardson, A., Burns, S., … Eiriksson, D. (2018). Limitations to winter and spring photosynthesis of a Rocky Mountain subalpine forest. *Agricultural and Forest Meteorology*, *252*, 241–255. https://doi.org/10.1016/j.agrformet.2018.01.025

Busch, F., Huner, N., & Ensminger, I. (2009). Biochemical constrains limit the potential of the photochemical reflectance index as a predictor of effective quantum efficiency of photosynthesis during the winter spring transition in Jack pine seedlings. *Functional Plant Biology*, *36*. https://doi.org/10.1071/FP08043

Chapin, F. S., Sturm, M., Serreze, M. C., McFadden, J. P., Key, J. R., Lloyd, A. H., … Welker, J. M. (2005). Role of Land-Surface Changes in Arctic Summer Warming. *Science*, *310*(5748), 657 LP – 660. https://doi.org/10.1126/science.1117368

Demmig-Adams, B., & Adams, W. W. (1996). The role of xanthophyll cycle carotenoids in the protection of photosynthesis. *Trends in Plant Science*, *1*(1), 21–26. https://doi.org/10.1016/S1360-1385(96)80019-7

Estiarte, M., & Peñuelas, J. (2015). Alteration of the phenology of leaf senescence and fall in winter deciduous species by climate change: effects on nutrient proficiency. *Global Change Biology*, *21*(3), 1005–1017. https://doi.org/10.1111/gcb.12804

Francis, J., & Skific, N. (2015). Evidence linking rapid Arctic warming to mid-latitude weather patterns. *Philosophical Transactions. Series A, Mathematical, Physical, and Engineering Sciences*, *373*. https://doi.org/10.1098/rsta.2014.0170

Fréchette, E., Wong, C., Junker-Frohn, L., Chang, C., & Ensminger, I. (2015). Zeaxanthin-independent energy quenching and alternative electron sinks cause a decoupling of the relationship between the photochemical reflectance index (PRI) and photosynthesis in an evergreen conifer during spring. *Journal of Experimental Botany*, *66*. https://doi.org/10.1093/jxb/erv427

Friedl, M. A., Gray, J. M., Melaas, E. K., Richardson, A. D., Hufkens, K., Keenan, T. F., … O'Keefe, J. (2014). A tale of two springs: using recent climate anomalies to characterize the sensitivity of temperate forest phenology to climate change. *Environmental Research Letters*, *9*(5), 54006. https://doi.org/10.1088/1748-9326/9/5/054006

Friedman, A. R., Hwang, Y.-T., Chiang, J. C. H., & Frierson, D. M. W. (2013). Interhemispheric Temperature Asymmetry over the Twentieth Century and in Future Projections. *Journal of Climate*, *26*(15), 5419–5433. https://doi.org/10.1175/JCLI-D-12-00525.1

Gamon, J., Fred Huemmrich, K., Wong, C., Ensminger, I., Garrity, S., Y. Hollinger, D., … Penuelas, J. (2016). A remotely sensed pigment index reveals photosynthetic phenology in evergreen conifers. In *Proceedings of the National Academy of Sciences* (Vol. 113). https://doi.org/10.1073/pnas.1606162113

Gamon, J A, Peñuelas, J., & Field, C. B. (1992). A narrow-waveband spectral index that tracks diurnal changes in photosynthetic efficiency. *Remote Sensing of Environment*, *41*(1), 35–44. https://doi.org/https://doi.org/10.1016/0034-4257(92)90059-S

Gamon, J A, Serrano, L., & Surfus, J. S. (1997). The Photochemical Reflectance Index: An Optical Indicator of Photosynthetic Radiation Use Efficiency across Species, Functional Types, and Nutrient Levels. *Oecologia*, *112*(4), 492–501. Retrieved from http://www.jstor.org/stable/4221805

Gamon, John A, & Berry, J. A. (2012). Facultative and constitutive pigment effects on the Photochemical Reflectance Index (PRI) in sun and shade conifer needles. *Israel Journal of Plant Sciences*, *60*(1–2), 85–95. https://doi.org/10.1560/IJPS.60.1-2.85

Gamon, John A, Field, C. B., Goulden, M. L., Griffin, K. L., Hartley, A. E., Joel, G., … Valentini, R. (1995). Relationships Between NDVI, Canopy Structure, and Photosynthesis in Three Californian Vegetation Types. *Ecological Applications*, *5*(1), 28–41. https://doi.org/10.2307/1942049

Gauthier, S., Bernier, P., Kuuluvainen, T., Shvidenko, A. Z., & Schepaschenko, D. G. (2015). Boreal forest health and global change. *Science*, *349*(6250), 819 LP – 822. https://doi.org/10.1126/science.aaa9092

Gillies, S. L., & Vidaver, W. (1990). Resistance to photodamage in evergreen conifers. *Physiologia Plantarum*, *80*(1), 148–153. https://doi.org/10.1111/j.1399-3054.1990.tb04389.x

Gilmore, A. M., & Yamamoto, H. Y. (1993). Linear models relating xanthophylls and lumen acidity to non-photochemical fluorescence quenching. Evidence that antheraxanthin explains zeaxanthin-independent quenching. *Photosynthesis Research*, *35*(1), 67–78. https://doi.org/10.1007/BF02185412

Gitelson, A. A., & Gamon, J. A. (2015). The need for a common basis for defining light-use efficiency: Implications for productivity estimation. *Remote Sensing of Environment*, *156*, 196–201. https://doi.org/https://doi.org/10.1016/j.rse.2014.09.017

Goetz, S., Bunn, A., Fiske, G., & Houghton, R. (2005). Satellite-observed photosynthetic trends across boreal North America associated with climate and fire disturbance. In *Proceedings of*

the National Academy of Sciences of the United States of America (Vol. 102). https://doi.org/10.1073/pnas.0506179102

Gonsamo, A., Chen, J. M., & Ooi, Y. W. (2018). Peak season plant activity shift towards spring is reflected by increasing carbon uptake by extratropical ecosystems. *Global Change Biology*, *24*(5), 2117–2128. https://doi.org/10.1111/gcb.14001

Hari, P., & Kulmala, L. (2009). Boreal Forest and Climate Change. In *Advances in Global Change Research*. https://doi.org/10.1007/978-1-4020-8718-9_9

Hogg, E. H. (Ted), Brandt, J. P., & Michaelian, M. (2008). Impacts of a regional drought on the productivity, dieback, and biomass of western Canadian aspen forests. *Canadian Journal of Forest Research*, *38*(6), 1373–1384. https://doi.org/10.1139/X08-001

Huner, N. P. A., Öquist, G., & Sarhan, F. (1998). Energy balance and acclimation to light and cold. *Trends in Plant Science*, *3*(6), 224–230. https://doi.org/https://doi.org/10.1016/S1360-1385(98)01248-5

Lian, X., Piao, S., Li, L. Z. X., Li, Y., Huntingford, C., Ciais, P., … McVicar, T. R. (2020). Summer soil drying exacerbated by earlier spring greening of northern vegetation. *Science Advances*, *6*(1), eaax0255. https://doi.org/10.1126/sciadv.aax0255

Luus, K. A., Commane, R., Parazoo, N. C., Benmergui, J., Euskirchen, E. S., Frankenberg, C., … Lin, J. C. (2017). Tundra photosynthesis captured by satellite-observed solar-induced chlorophyll fluorescence. *Geophysical Research Letters*, *44*(3), 1564–1573. https://doi.org/10.1002/2016GL070842

Magney, T., R. Bowling, D., A. Logan, B., Großmann, K., Stutz, J., D. Blanken, P., … Frankenberg, C. (2019). Mechanistic evidence for tracking the seasonality of photosynthesis with solar-induced fluorescence. *Proceedings of the National Academy of Sciences of the United States of America*. https://doi.org/10.1073/pnas.1900278116

Manabe, S., Stouffer, R. J., Spelman, M. J., & Bryan, K. (1991). Transient Responses of a Coupled Ocean–Atmosphere Model to Gradual Changes of Atmospheric CO_2. Part I. Annual Mean Response. *Journal of Climate*, *4*(8), 785–818. https://doi.org/10.1175/1520-0442(1991)004<0785:TROACO>2.0.CO;2

MICHAELIAN, M., HOGG, E. H., HALL, R. J., & ARSENAULT, E. (2011). Massive mortality of aspen following severe drought along the southern edge of the Canadian boreal forest. *Global Change Biology*, *17*(6), 2084–2094. https://doi.org/10.1111/j.1365-2486.2010.02357.x

Monteith JL. (1977). Climate and the efficiency of crop production in Britain. *Philosophical Transactions of the Royal Society of London. B, Biological Sciences*, *281*(980), 277–294. https://doi.org/10.1098/rstb.1977.0140

NASA's Earth Observatory. (2013). Arctic amplification. Retrieved May 10, 2019, from https://climate.nasa.gov/news/927/arctic-amplification/

Öquist, G., & Huner, N. P. A. (2003). Photosynthesis of Overwintering Evergreen Plants. *Annual Review of Plant Biology*, *54*(1), 329–355. https://doi.org/10.1146/annurev.arplant.54.072402.115741

Peñuelas, J., Filella, I., Gamon, J. A., & Field, C. (1997). Assessing photosynthetic radiation-use efficiency of emergent aquatic vegetation from spectral reflectance. *Aquatic Botany*, *58*(3), 307–315. https://doi.org/https://doi.org/10.1016/S0304-3770(97)00042-9

Porcar-Castell, A., Garcia Plazaola, J. I., J Nichol, C., Kolari, P., Olascoaga, B., Kuusinen, N., … Nikinmaa, E. (2012). Physiology of the seasonal relationship between Photochemical Reflectance Index and photosynthetic Light Use Efficiency. In *Oecologia* (Vol. 170). https://doi.org/10.1007/s00442-012-2317-9

R. Springer, K., Wang, R., & Gamon, J. (2017). Parallel Seasonal Patterns of Photosynthesis, Fluorescence, and Reflectance Indices in Boreal Trees. In *Remote Sensing* (Vol. 9). https://doi.org/10.3390/rs9070691

Rajewicz, A. P., Atherton, J., Alonso, L., & Porcar-Castell, A. (2019). Leaf-Level Spectral Fluorescence Measurements: Comparing Methodologies for Broadleaves and Needles. *Remote Sensing* , Vol. 11. https://doi.org/10.3390/rs11050532

Rangwala, I., Sinsky, E., & Miller, J. (2013). Amplified warming projections for high altitude regions of the Northern Hemisphere mid-latitudes from CMIP5 models. *Environmental Research Letters*, *8*, 24040. https://doi.org/10.1088/1748-9326/8/2/024040

Richardson, A. D., Keenan, T. F., Migliavacca, M., Ryu, Y., Sonnentag, O., & Toomey, M. (2013). Climate change, phenology, and phenological control of vegetation feedbacks to the climate system. *Agricultural and Forest Meteorology*, *169*, 156–173. https://doi.org/https://doi.org/10.1016/j.agrformet.2012.09.012

Ronald, S., Manabe, S., & Bryan, K. (1989). Interhemispheric asymmetry in climate response to a gradual increase of atmospheric CO2. *Nature*, *342*. https://doi.org/10.1038/342660a0

Rossini, M., Nedbal, L., Guanter, L., Ač, A., Alonso, L., Burkart, A., … Rascher, U. (2015). Red and far red Sun-induced chlorophyll fluorescence as a measure of plant photosynthesis. *Geophysical Research Letters*, *42*(6), 1632–1639. https://doi.org/https://doi.org/10.1002/2014GL062943

Shvidenko, A., & Schepaschenko, D. (2013). Climate Change and Wildfires in Russia. *Contemporary Problems of Ecology*, *6*, 683–692. https://doi.org/10.1134/S199542551307010X

Ulsig, L., Nichol, J. C., Huemmrich, F. K., Landis, R. D., Middleton, M. E., Lyapustin, I. A., … Porcar-Castell, A. (2017). Detecting Inter-Annual Variations in the Phenology of Evergreen Conifers Using Long-Term MODIS Vegetation Index Time Series. *Remote Sensing* , Vol. 9. https://doi.org/10.3390/rs9010049

Walter-McNeill, A., Garcia, M. A., Logan, B. A., Bombard, D. M., Reblin, J. S., Lopez, S., … Bowling, D. R. (2021). Wide variation of winter-induced sustained thermal energy dissipation in conifers: a common-garden study. *Oecologia*. https://doi.org/10.1007/s00442-021-05038-y

Walther, S., Voigt, M., Thum, T., Gonsamo, A., Zhang, Y., Köhler, P., … Guanter, L. (2016). Satellite chlorophyll fluorescence measurements reveal large-scale decoupling of photosynthesis and greenness dynamics in boreal evergreen forests. *Global Change*

Biology, *22*(9), 2979–2996. https://doi.org/10.1111/gcb.13200

Wang, X., Piao, S., Xu, X., Ciais, P., MacBean, N., Myneni, R. B., & Li, L. (2015). Has the advancing onset of spring vegetation green-up slowed down or changed abruptly over the last three decades? *Global Ecology and Biogeography*, *24*(6), 621–631. https://doi.org/10.1111/geb.12289

Wong, C. Y. S., D'Odorico, P., Arain, M. A., & Ensminger, I. (2020). Tracking the phenology of photosynthesis using carotenoid-sensitive and near-infrared reflectance vegetation indices in a temperate evergreen and mixed deciduous forest. *New Phytologist*, *226*(6), 1682–1695. https://doi.org/10.1111/nph.16479

Wong, C. Y. S., D'Odorico, P., Bhathena, Y., Arain, M. A., & Ensminger, I. (2019). Carotenoid based vegetation indices for accurate monitoring of the phenology of photosynthesis at the leaf-scale in deciduous and evergreen trees. *Remote Sensing of Environment*, *233*, 111407. https://doi.org/https://doi.org/10.1016/j.rse.2019.111407

Wong, C. Y. S., & Gamon, J. A. (2015). The photochemical reflectance index provides an optical indicator of spring photosynthetic activation in evergreen conifers. *New Phytologist*, *206*(1), 196–208. https://doi.org/10.1111/nph.13251

Chapter 2 – Observations of Sun-Induced Chlorophyll fluorescence (SIF), Photochemical Reflectance Index (PRI) and Chlorophyll:Carotenoid Index (CCI) during spring recovery in two evergreen conifers.

Introduction

The boreal forest biome, is one of the most important global reservoirs of stored carbon and is also the home of a unique biological community that provides a variety of ecosystem services. The floristic composition of the Boreal Forest is dominated by cold-hardy evergreen conifers of the genera *Picea, Abies and Pinus* (La Roi, 1967). After tropical forests, the boreal forest biome stores the second-largest quantity of carbon in the planet, with estimates of total storage of 367.3–1,715.8 Pg C (Astrupet al. 2018) with an annual sink of 0.5 ± 0.1 Pg C y^{-1} (Pan et al. 2011). The boreal forest's major role in the global carbon budget, has generated a need to understand the impact of climate change on photosynthetic activity and the growing season length, especially for evergreen conifers species that represent 10% of the global forested area (Keenan et al. 2015). Therefore, our capability to monitor boreal tree's vital role in the terrestrial carbon balance is crucial to gaining an understanding of the changing global carbon cycle.

Boreal regions are characterized by strong seasonality, with a long winter season consisting of a short photoperiod with temperatures well below 0ºC, and a short summer season with a longer photoperiod and temperatures exceeding 20ºC. These extreme variations in environmental temperature and light between the summer and winter seasons, have shaped the physiology and phenology of evergreen conifers. As a part of these adaptations, evergreen trees have evolved wintertime and summertime photosynthetic acclimation strategies (Savitch et al. 2002). The

transitions (spring and fall) between winter and summer, are of particular interest, as these appear to be changing with climate change (Williams, Henry & Sinclair, 2015; IPCC report, 2021).

A fundamental feature of evergreen conifers is the maintenance of green needles over the winter months. This characteristic allows evergreen conifers to be more energetically efficient during the spring (Hänninen, 2016), because they do not need to reinvest energy, carbon, and nitrogen in the production of new leaves (Savitch et al. 2002). On the other hand, the maintenance of evergreen foliage during winter brings its own challenges. Under freezing temperatures, needles are exposed to high light intensities, frost, and desiccation (Sutinen et al. 2001). These combined threats during winter lead inhibition of photosynthetic CO_2 assimilation (also known as photoinhibition or photosynthetic downregulation), because it is too cold for biochemical processes of photosynthesis to operate (Öquist & Martin, 1980), yet light is still being absorbed. The exposure of photosynthetic tissues to continued illumination can cause an overexcitation of the photosynthetic apparatus and increases the probabilities of damage by photooxidation (Powles, 2003). To defend themselves, conifers protect their needles' internal structure against damage by using photoprotective mechanisms to maintain *photostasis*, defined as the tendency of a photosynthetic organism to keep a balance between the absorbed light energy absorbed through photochemistry and subsequent energy utilization by means of metabolism and growth (Huner, Öquist & Melis, 2003).

During the growing season, to maintain daily photostasis and avoid photodamage during exposure to daily environmental stressors (heat, cold, excess light…), evergreen conifers dissipate the absorbed energy not used by photochemistry as heat. This photoprotective mechanism, is related to non-photochemical quenching (NPQ) of chlorophyll fluorescence, governed by the xanthophyll cycle, and involves the de-epoxidation of violaxanthin to antheraxanthin and

zeaxanthin (V-A-Z carotenoid pigments) (Adams III & Demmig-Adams, 1994). In winter, to maintain photostasis, evergreen conifers engage in a sustained version of the xanthophyll deepoxidation to constantly dissipate energy; this mechanism is sometimes called sustained non-photochemical quenching (NPQ), as it results in long-term suppression of chlorophyll fluorescence (Barbara Demmig-Adams & Adams, 1996b). Sustained NPQ is often indicated by an increased concentration of xanthophyll cycle and other photoprotective carotenoid pigments in winter (Huner et al.1998)

Because seasonal and diurnal energy dissipation involve the acclimation of pigments, they also affects leaf optical properties (Wong, 2014). The Photochemical Reflectance Index (PRI), was developed by (Gamon et al. 1992; Peñuelas, Filella, & Gamon, 1995; Gamon et al, 1997) to track the short-term xanthophyll cycle response. This response has been exhaustively studied at diurnal scales, in different species and ecosystems, and its dynamics are well understood (Adams III & Demmig-Adams, 1994; Demmig-Adams & Adams, 1996; Öquist & Huner, 2003; Verhoeven, 2014). Similarly, the corresponding diurnal PRI response has been well-documented (Gamon, Serrano, & Surfus, 1997; Gamon & Bond, 2013; Peñuelas, Filella, Gamon & Field, 1997). The PRI can also be used to track seasonal pigment responses, which has been recently studied by Wong & Gamon (2015). To track the seasonal xanthophyll cycle and associated seasonal pigment responses, the Chlorophyll : Carotenoid index (CCI) has also been used recently (Gamon et al. 2016; Springer, 2017; Magney et al. 2019; Wong et al. 2019, 2020; Pierrat et al. 2021). Over seasonal time scales, this index is functionally similar to the PRI, but has the added benefit that it can be assessed from broadband (e.g. MODIS) satellite bands (Gamon et al. 2016). Both PRI and CCI can be used to explore photosynthetic activation and deactivation mechanisms in evergreen conifer species, especially to study the spring transition. While the diurnal and seasonal PRI

responses both involve pigments, the two PRI responses differ in their kinetics and mechanisms, and have been termed the facultative and constitutive responses, respectively (Gamon & Berry, 2012).

When energy is absorbed by the plant leaf, it can be directed into three different possible paths (Butler & Strasser, 1977), photochemistry (or productive photosynthesis), fluorescence, and dissipation as heat (also known as non-photochemical quenching of fluorescence, NPQ). Chlorophyll fluorescence emission represents a balance between these three processes. In the absence of environmental stress conditions, plants take the majority of absorbed energy (APAR) and direct it towards photochemistry. Along with this absorption, an emission of SIF occurs, that largely reflects the amount of absorbed radiation (APAR) (Mohammed et al., 2019). Under these favorable conditions the SIF signal is thought to be an indicator of the amount of radiation absorbed, and hence a direct indicator of photosynthetic rate. Under non-favorable conditions for photosynthesis, the quantum yield of photosynthesis and the quantum yield of fluorescence (i.e. the fraction of APAR photons that are re-emitted from photosynthesis as fluorescence) drop and dissipation as heat (NPQ) increases (Du, Liu, Liu, & Hu, 2017). In summer, this dissipation is temporary, while, in winter, it is sustained due to the extended cold. Because the SIF signal can also detect this downregulation, it detects these declines in photosynthesis with stress (Porcar-Castell et al. 2014).

The recent discovery of a satellite solar-induced fluorescence (SIF) signal and the development of techniques to isolate the signal from the background radiance (Frankenberg et al. 2011; Joiner et al. 2011) has spurred further interest in SIF emission, and has encouraged the development of leaf-level methods (e.g., the FluoWat leaf-clip; Van Wittenberghe et al. (2013). The SIF signal is characterized by two peaks: 685-690nm (red) and 740-745nm (far-red) (Sun et

al. 2018) and these peaks can now be detected using a spectrometer in combination with filters that can isolate the SIF signal from background radiation (Meroni et al. 2009b). Wider possibilities of SIF data collection and its potentially close relationship to photosynthetic activity has attracted the attention of the scientific community. The Fluorescence Explorer (FLEX) mission that will be launched in the near future by the European Space Agency is the first satellite mission that is specifically intended for fluorescence retrieval from space along with pigment data via PRI, CCI, and other pigment-based indices (Drusch et al. 2016).

Because SIF emission is dynamic and connected to stress events and to the regulation of photosynthetic activity as a means of photoprotection, the interpretation of the SIF satellite retrieval can be complex. NPQ responses and their connection with the SIF emission and pigment responses in the context of seasonally changing environmental conditions need further exploration. Historically, most fluorescence work has focused on leaf-level studies, and this information has not yet been fully connected with the observations made by satellites at coarse spatial, and multiple temporal-scales, potentially generating errors in GPP models derived from satellite signals. Similarly, most fluorescence studies have not paid close attention to pigment dynamics, which can be assessed in situ via PRI and CCI. This highlights the importance of gaining knowledge and understanding of how well the SIF signal relates to both APAR and NPQ (CCI and PRI) mechanisms from leaf scale to landscape scale (Porcar-Castell et al. 2014; Magney et al. 2019; Pinto et al. 2020) and how much a combination of these remote sensing techniques could help us to detect the seasonal reactivation and deactivation of photosynthetic activity.

To understand the seasonal controls of boreal photosynthetic activity, including the mechanisms of activation of photosynthesis during the spring-summer transition in evergreen conifers from the Boreal Forest, we need to explore the complex kinetics and environmental

conditions surrounding photosynthetic acclimation mechanisms. In this study, we evaluated the Photochemical Reflectance Index (PRI) and the Chlorophyll:Carotenoid Index (CCI) in two dominant evergreen conifers: *Picea mariana* (black spruce) and *Pinus contorta (*lodgepole pine), with the purpose of comparing the kinetics between these carotenoid reflectance indices and Sun induced chlorophyll fluorescence (SIF) emission. Additionally, we assessed how well the SIF signal, CCI, and PRI can track changes in air temperature during the spring transition, and how this can help us to identify changes in the start and duration of the summer growing season, because such changes directly influence forest ecosystem productivity (Richardson et al. 2010; Buermann et al. 2018). We expected to find that these three optical metrics would have similar seasonal patterns, and that, in combination, they could track the changes in temperature during spring activation as an indicator of seasonal pigment shifts tied to the timing of the photosynthetic activation. Our expectation was that the seasonal dynamics of the SIF signal and carotenoid-based reflectance indices using leaf-scale and Boreal Forest species, would offer complementary information that could be helpful for future satellite missions (e.g., FLEX mission) and provide a foundation for monitoring the seasonal carbon dynamics of the important Boreal Forest biome.

Materials and Methods

For this experiment, we used two evergreen conifer species, lodgepole pine (*Pinus contorta D.*) and black spruce (*Picea mariana (Mill.)*). The six-year-old lodgepole pine individuals and three-year-old black spruce individuals were bought during 2020, from a local nursery (TreeTime Services Inc, Alberta). At the beginning of the study, we preselected healthy individuals and established them on the south-facing rooftop of the Biological Science building at the University of Alberta, Canada. There, all plants were planted or repotted in a 1:2 soil mixture of sandy topsoil and potting soil (Sunshine Mix 4, Sun Gro Horticulture, Agawam, MA, USA) with added slow-

release fertilizer (Nutricote 14-14-14, Sun Gro Horticulture, Agawam, MA, USA). Plants were potted in 2.83 L pots (CP412CH, Stuewe & Sons, Tangent, OR, USA) and arranged by species into synthetic stands (1.5 m x 1.5 m plots) for their long-term acclimation. Plants were located on the rooftop exposed to seasonal weather similar to boreal forest conditions and watered throughout the non-freezing periods to avoid water stress. Data collection took place from February 2020 to October 2020, covering the winter-spring transition and the summer season.

To collect meteorological data, we set up a weather station adjacent to the plants to provide photosynthetic photon flux density (PPFD) and irradiance (S-LIB-M003, Onset, Bourne, MA, USA), air temperature and relative humidity (S-THB-M002, Onset, Bourne, MA, USA), collected every minute on a datalogger (U30-NRC, Onset, Bourne, MA, USA). Irradiance obtained from the pyranometer was converted to PPFD (µmoles quanta m^{-2} s^{-1}). The weather data were aggregated into 15-minute averages that were later filtered to 3-hours, "noon" average values (from 11:30 AM to 2:30 PM). The sensors were set up at the same height as the canopy and located within 3-5 m of the plants to provide representative conditions of incoming PPFD and ambient temperatures experienced by the leaves.

Measurements of reflectance and fluorescence emission for this experiment were conducted by using the FluoWat leaf-clip (Fig 1). Sun-induced chlorophyll fluorescence (SIF) was measured under natural light conditions using a high spectral resolution spectrometer (UniSpec-SC, PP Systems, Amesbury, MA, USA) attached to an optical fibre (UNI684, PP Systems, Amesbury, MA, USA). Both instruments were coupled with the FluoWat leaf clip (Van Wittenberghe et al. 2013). The SIF emission signal (650–850 nm) was measured by setting a short-pass filter cutting off light above 650 nm. This way only SIF was measured, as light in this spectral region cannot originate from reflection of light above 650 nm. Measurements were executed under

sunny and clear sky conditions with an incident sun illumination on the previously sun-exposed leaf position under a 45° illumination angle. Needles were collected from exposed branches and selected from the side of the tree that was exposed to the direct sunlight at midday. After this, needles were set on black electrical tape (one next to another taking care not to leave space in-between). Five to eight healthy needles per sample were measured. For this study, we explored the following SIF parameters: SIF *total* : $\int_{690}^{740} f(\lambda)\, d\lambda$, APAR, SIF *yield* (SIF *total* / APAR), far-red SIF (SIF 740nm), red SIF (SIF 640nm), far-red SIF/ red SIF ratio, summarized in Table 2-1. For further details of how we collected, calibrated, and analysed SIF data, see the Appendix I.

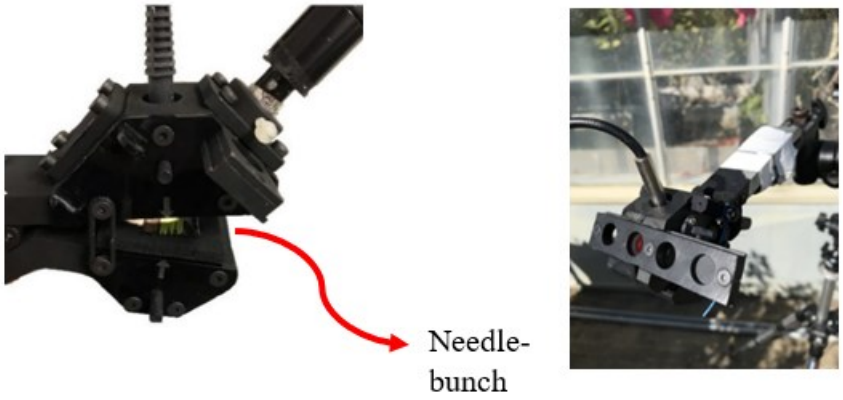

Figure 2-1. FluoWat leaf-clip (Van Wittenberghe, S; Verrelst, J; Alonso L; Hermans, I; Delegido, J; Valcke, R; Moreno, J; Samson, 2013).

The seasonal acclimation of PRI and CCI was monitored for both evergreen species twice per week from February 2020 to October 2020 in the case of *Picea mariana* and from March 2020 to October 2020 in the case of *Pinus contorta*. Spectral data collection was performed from about 11:00 to 14:00 (within 1-2 hours of solar noon), exclusively on sunny days to ensure consistent high light during the midday sample collection. In addition to SIF, reflectance indices were calculated using leaf reflectance (ρ_λ) from each measurement using the equations below.

Table 2-1. Vegetation reflectance indices and Sun Induced Chl florescence(SIF) parameters studied in this methodology.	
Normalized Difference Vegetation Index (NDVI)	$\frac{\rho 800\text{nm} - \rho 630\text{nm}}{\rho 800\text{nm} + \rho 630\text{nm}}$
Photochemical Reflectance index (PRI)	$\frac{\rho 531\text{nm} - \rho 570\text{nm}}{\rho 531\text{nm} + \rho 570\text{nm}}$
Chlorophyll/Carotenoid index (CCI)	$\frac{\rho 531\text{nm} - \rho 630\text{nm}}{\rho 531\text{nm} + \rho 630\text{nm}}$
SIF*total*	SIF *total*= $\int_{690}^{740} f(\lambda)\, d\lambda$
red SIF (SIF $_{680\text{nm}}$)	690nm
far-red SIF (SIF $_{740\text{nm}}$)	740nm
far-red SIF/ red SIF ratio	740nm/690nm
F*yield*	SIF *total* / APAR
F*yield* 690	690nm/APAR
F*yield* 740	740nm/APAR

To examine the kinetics of both the spring recovery and the subsequent summer period, data were collected from February 2020 to October, incorporating winter, spring- and summer-adapted- needles. For comparative purposes, the values of all the parameters were normalized from zero to one. A sigmoidal fit of photosynthetic parameters incorporating stable winter and summer days and transitional spring recovery was estimated using the R studio 4.1.1, package 'sigmoid'. To compare the timing of the photosynthetic spring recovery, the half-max value was also calculated from the sigmoidal fit using Igor Pro (WaveMetrics, Portland, OR, USA). We also applied a sigmoidal fit to all parameters but as a function of temperature using a non-linear regression analysis, that was executed in R version 4.1.1, using the same package ('sigmoid'). This

made it possible to compare and estimate the kinetics between photosynthetic parameters and temperature.

Results

- Meteorological measurements

Average midday temperature and PPFD values for the outdoors experiment showed strong seasonal patterns typical of boreal regions (Fig. 2-2). In winter, minimum midday temperatures ranged from -20°C in the colder days of January to 1°C at the end of February. Average midday PPFD ranged from 100 μmol m^{-2} s^{-1} to 450 μmol m^{-2} s^{-1} during the last week of February. During the transition between spring and summer, from March to May, the lowest midday temperature reported was -17.5 °C and the maximum was 23°C; PPFD ranged from 800 μmol m^{-2} s^{-1} to 1200 μmol m^{-2} s^{-1} at the end of May. Midday temperatures typically exceeded 15°C in summer months accompanied by PPFD values between 1000 and 1400 μmol m^{-2} s^{-1}, from May to August. Midday summer temperatures (>15°C) persisted throughout September, with temperatures rarely below 10°C until mid-October. Maximum temperatures were observed at the end of July and during August (>25°C). Exceptionally low winter PPFD values are reported in these results because the sun was shaded by an adjacent building (CCIS) near the winter solstice.

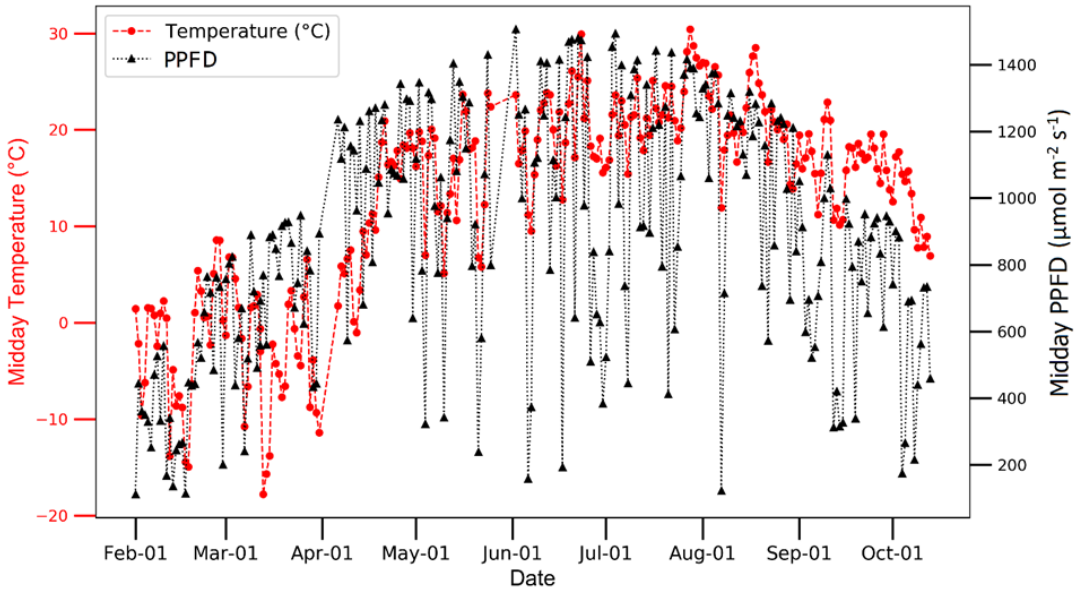

Figure 2-2. Seasonal dynamics of Temperature (°C) and incoming Photosynthetic Photon Flux Density PPFD (µmol m-2 s-1) during the experiment, data collected from January 2020 to October 2020, Edmonton, AB, CA. Temperature and PAR are expressed as midday average values from 11:00 AM to 3:00 PM. Red circles denote temperature and grey triangles denote incoming PPFD.

- Seasonal dynamics of needle– spectral reflectance and Sun induced chlorophyll fluorescence (SIF).

Over the course of the experiment, needle reflectance spectra and SIF spectra showed seasonal variation in both species (Fig 2-3). For black spruce (*P. mariana)*, spectral reflectance shape changed gradually with temperature increments during the winter-summer transition, as shown in Fig 2-3A. These changes were particularly clear over most of the spectrum and included changes in the shape of the "green hump", indicating a fundamental shift in the xanthophyll cycle pigments (531 nm) from winter to summer. The SIF spectral shape presented a similar behaviour (Fig 2-3C) over the different seasons. Winter presented SIF values near zero while during the spring to summer transition SIF presented a clear shape of the signal, peaking in both SIF bands

[690nm and 740 nm], and the summer spectral shape presented the maximum SIF values obtained for both SIF bands during the experiment.

In the case of lodgepole pine (*Pinus contorta*) in Fig 2-3B, major reflectance spectral differences were observed between the winter and spring spectra. Spring reflectance presented the highest values in the 531nm band and a shift in the red edge, indicating a shift in the xanthophyll cycle pigments (531nm) and chlorophyll (red edge) during this season. The seasonal response in SIF spectral shape for these species was similar to that of black spruce. During winter, red, and far-red SIF bands presented very low (near zero) values, while in spring, there was a marked rise in both SIF bands, and summer produced the highest SIF values in both spectral bands (Figure 2-3D).

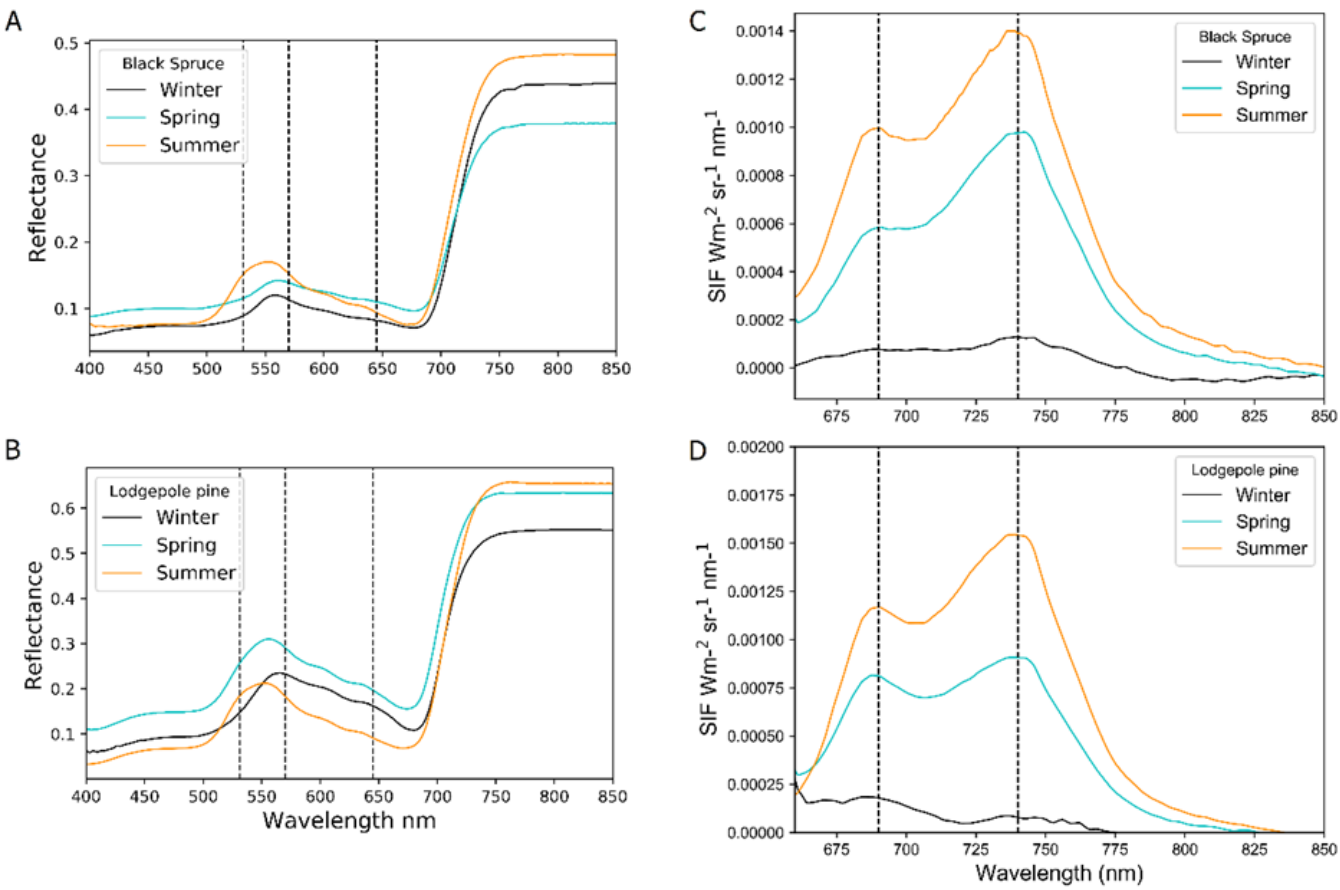

Figure 2-3. Column A, Seasonal dynamics of average needle-spectral reflectance for (A) black spruce (*P. mariana*) and (B) lodgepole pine (*P. contorta*) from winter (black), spring (cyan)and summer (orange), in Edmonton, AB. Vertical dotted lines represent the wavebands used for deriving PRI (531 and 570 nm) and CCI (531 and 645 nm). Each line represents a seasonal reflectance average value obtained every season : Winter = January and February (n=36), Spring = march and April (n=36), Summer = May, June, and July n=54). Column B, Seasonal dynamics of Spectral SIF emission (Wm^{-2} $sr^{-1}nm^{-1}$) at the needle-scale for (C) black spruce *(P. mariana*) and (D) lodgepole pine (*P. contorta*), transition from winter (black), spring (cyan), and summer (orange), Edmonton, AB. Data were collected twice per week from February 2020 to October 2020. The SIF spectrum was collected using a FluoWat leaf-clip and short-pass 650 nm filter attached to a spectrometer, and data were collected using sunlight at around midday under only sunny and clear sky conditions. Each line represents a seasonal SIF average value obtained during: Winter = January and February (n=36), Spring = march and April (n=36), Summer= May, June, and July n=54).

- Seasonal dynamics of needle spectral carotenoid-reflectance indices and SIF.

For both species, PRI patterns closely followed temperature and increased gradually, over several months, from winter minimum values to summer-growing season maxima, following the spring transition (Fig 2.4 B). Spruce PRI and pine PRI increased slightly (ca. 0.01) towards the end of the summer. PRI values decreased gradually in the fall (Sept-Oct). Spruce PRI and pine PRI were able to track seasonal temperature and SIF dynamics during winter and the spring-summer transition, however, we also noticed a decoupling of PRI and SIF in both species after reaching PRI summer values in both species (Fig 2-4).

The CCI (Fig 2-4C) values obtained for black spruce individuals, went from the lowest values in winter to intermediate values during April and May, to maximum summer values (from June to August). These transitions coincided with seasonal temperature changes (Fig 2-4 A), and CCI values followed the SIF dynamics during the spring transition (April to June). Over the summer (July-Aug), spikes in the CCI (0.27) corresponded with periods of high temperatures (>30°C), and these were particularly noticeable in lodgepole pine. CCI values started to decay into transitional fall values at the end of September. For lodgepole pine-CCI (Fig 2-4 F), the values showed a similar pattern to black spruce during winter and the spring transition into summer. However, we observed that, during the summer months, there was a decoupling of CCI from temperature (Fig 2-4 D) and SIF dynamics. The pine-CCI values started to decline in September, in contrast to the SIF values that continued to increase during September and October. However, SIF values in October also exhibited high variability between individuals as observed in Figure 2-4 below.

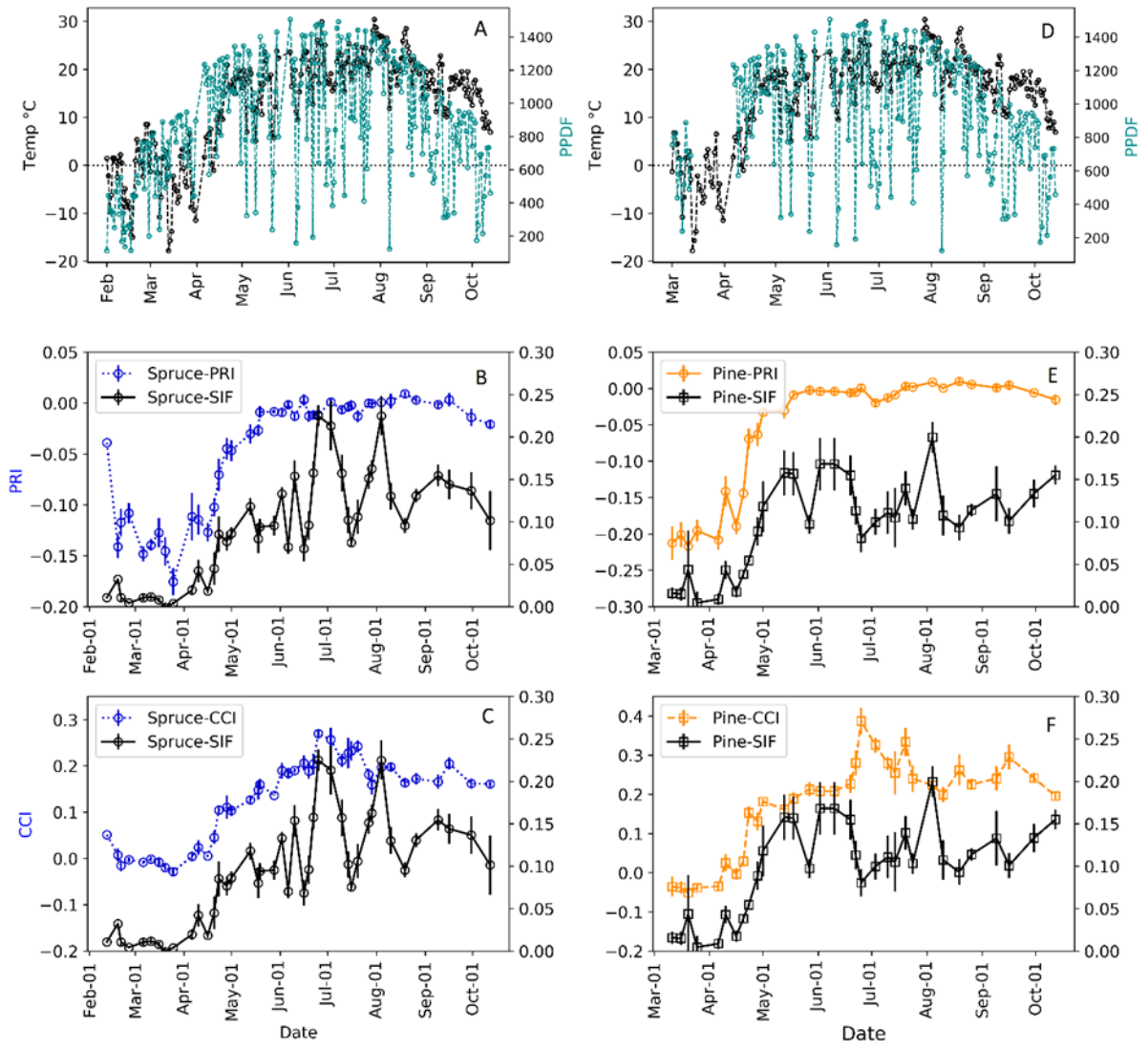

Figure 2-3. Seasonal dynamics of needle spectral carotenoid-reflectance indices and SIF*total* for two evergreen species, along with corresponding transitions in temperature and PPFD, in Edmonton, AB. Black spruce results (A,B,C): (A) Temperature (black circles) and Photosynthetic Photon Flux Density (PPFD, in micromoles m^{-2} s^{-1}) (cyan); (B) PRI (blue circles) and SIF*total* (black circles); C) CCI (blue circles) and SIF*total* (black circles). Lodgepole pine results (D,E,F): (D) Temperature (black) and PPFD (cyan); E) PRI (orange squares) and SIF (black squares), (F) CCI (orange squares) and SIF (black squares). Data points were collected twice per week from February 2020 to October 2020 in the case of black spruce, for lodgepole pine data were collected from March 2020 to October 2020. Dots represent daily averages, and both sets of data were

collected only during sunny and clear sky days. Error bars denote the standard error of the daily average (n = 18), samples collected every collection date = 3 from 6 individuals.

- Sun induced chlorophyll fluorescence seasonal responses of key parameters.

To fully explore the SIF signal, we studied different SIF-parameters for both species that are presented (as monthly averages) in Fig. 2-5. For black spruce, *P. mariana,* fig 2-5A shows how the total SIF emission signal evolved during the different seasons. Winter presented values near zero, spring-summer transition presented a clear shape, peaking in both bands [690nm and 740 nm], and summer presented the maximum SIF values obtained for both SIF bands [690nm and 740 nm]. The 740 nm band always had higher values than the 690 nm band. SIF total (Fig. 2-5A) showed that SIF values started to increase in April, with a slight decline in June. SIF peaked in July-September and started to decline again in October-November. SIF *yield* (Fig. 2-5B) behaved in a very similar way; however, it did not show the decline during June that was exhibited by SIF *total*. This decline in the SIF signal was also detected by SIF *yield* $_{[740]}$ (Fig. 2-5 D). SIF [690,740 nm] in (fig 2-5C) started to climb during April and declined towards the end of September. Only the 740nm band showed the decline in SIF values during June.

Lodgepole pine (*P. contorta*) SIF parameters are summarized in the right column of Fig. 2-5. SIF *total* (fig. 2-5F) displayed an abrupt increase from April to May, with a slight decrease during July, followed by a slight increase towards October. $SIF_{[740nm]}$ and $SIF_{[690nm]}$ in Fig 2-5H showed similar patterns to SIF total. By contrast, the SIF yield values (Fig. 2-5 I) showed an abrupt increase in May, followed by a more gradual increase from May to October.

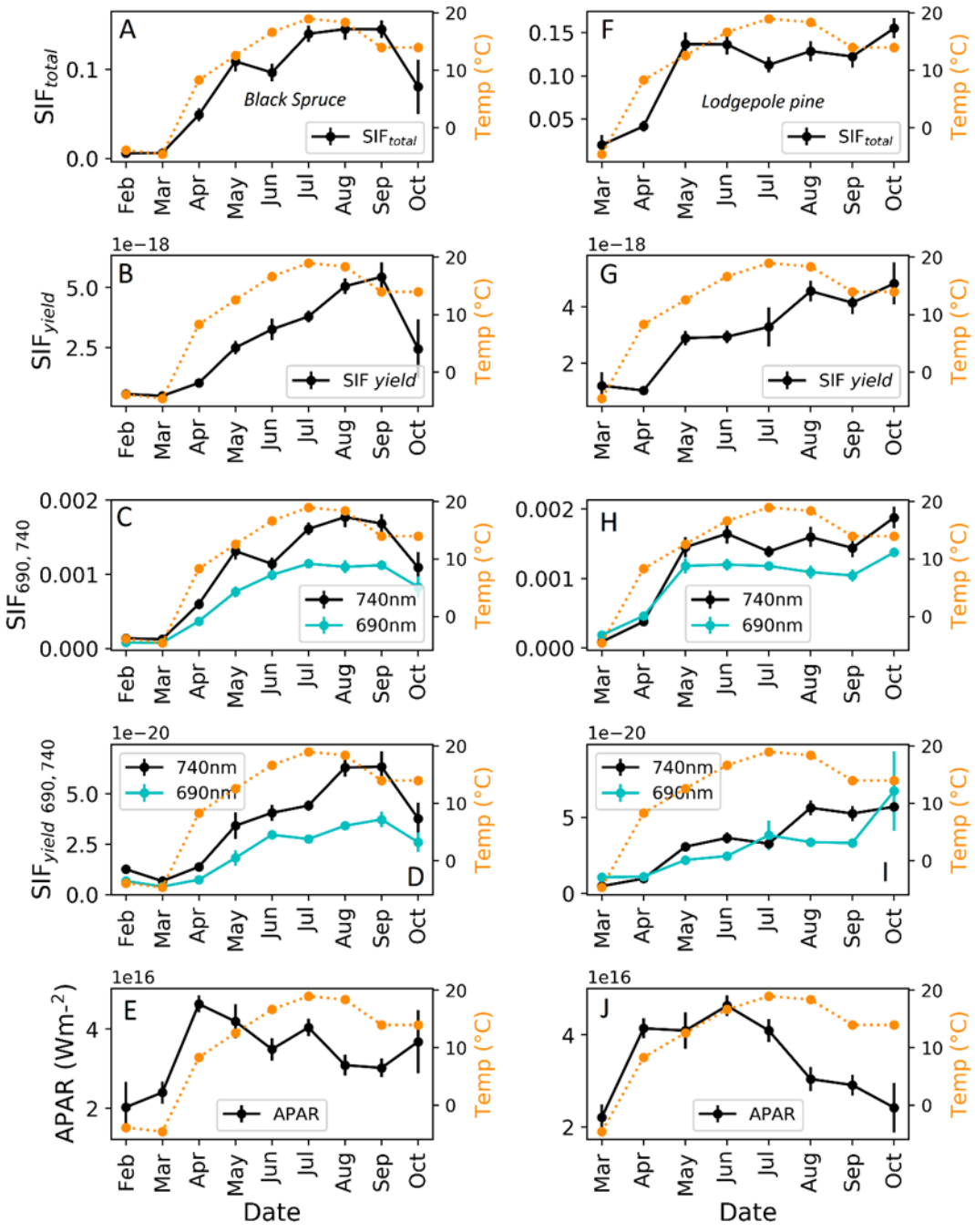

Figure 2-4. Seasonal dynamics of Sun-induced chlorophyll fluorescence (SIF) parameters (SIF total Wm^{-2} $sr^{-1}nm^{-1}$ (black circles), SIF *yield*, SIF_{740} (black circles) and SIF_{690} (cyan circles), $SIF_{yield\ 740nm}$ (black circles) and $SIF_{yield\ 690nm}$ (cyan circles), APAR (Wm^{-2}), in Edmonton, AB. Black spruce results (A-E) and lodgepole pine results (F-J). Right axis shows the monthly average temperature °C (orange circles) in all the plots. Data were collected twice per week from February

2020 to October 2020 in the case of black spruce, for lodgepole pine data were collected starting in March 2020. Data points were only collected during sunny and clear sky days. Error bars denote the standard error of the monthly average (n = 108). Temperature data are presented as average midday values between 11:00 AM and 2:00 PM, the timeframe when we collected the SIF signal.

- Seasonal sigmoidal fits for all parameters for black spruce (*P. mariana*) and lodgepole pine (*P. contorta*).

A sigmoidal fit was applied to all key parameters to evaluate the kinetics of spring recovery (Fig. 2-6). This smoothed fit enabled the analysis of the dates when photosynthetic parameters start to recover and help us to identify when the half-maximum value was reached for comparison between metrics. Also, to better observe the kinetics (dynamics) of these parameters, we combined all the sigmoidal results in Fig. 2-7. All parameters for both species showed a noticeable transition from winter values to summer values around April 22nd and May 29th.

For *P. mariana* SIF fluorescence recovered the most gradually and last, reaching the half-maxima value at the beginning of May. The PRI presented the earliest recovery – during April 26th. The CCI closely followed the PRI, with a half-max value at early-May. The order and rate of spring recovery for each parameter can be more clearly seen in Figure 2-7, which overlays the sigmoidal fits for a better visual comparison of the responses shown in Figure 2-6.

For *P. contorta,* CCI recovered most gradually, with a half value at the end of April. PRI and SIF, with similar half-maximum dates, made a more abrupt recovery (Figure 2-7B). Both species displayed a PRI and CCI that closely followed the seasonal temperature variations during the experiment. However, after the spring transition, SIF showed a high degree of noise and an apparent decoupling from temperature. Comparing these species in general, *P. contorta* exhibited an earlier recovery than *P. mariana* (Table 2-2).

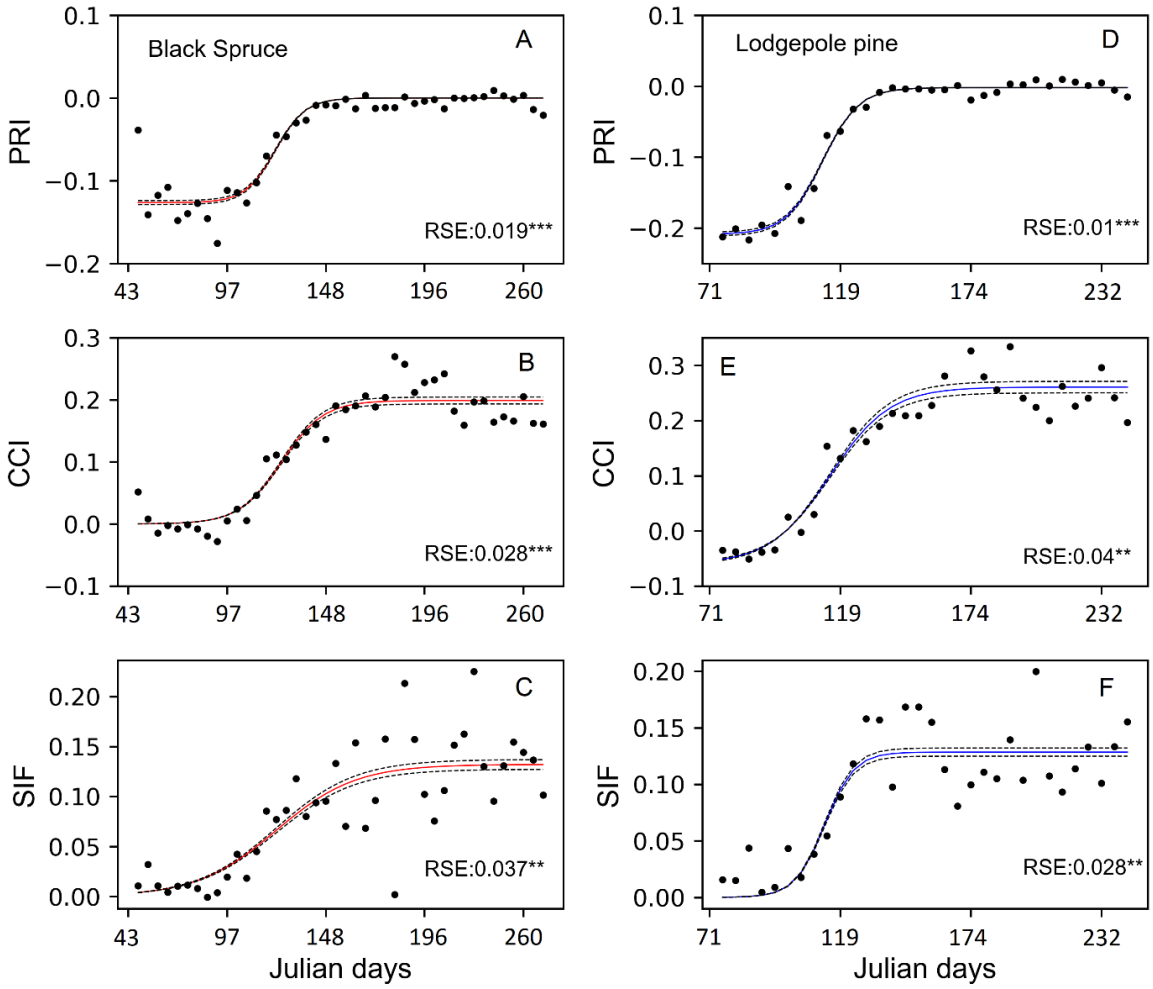

Figure 2-5. Seasonal sigmoidal fits for key parameters (PRI, CCI and SIF in Wm^{-2} sr^{-1} nm^{-1}), results for black spruce (*Picea mariana*) are showed in the first column from A-C in red color. And lodgepole pine (*Pinus contorta*) results are showed in second column from E-F in blue color. Dashed lines represent the residual standard error of the non-regression model. Data was collected from February to October 2020 in the case of black spruce, and from March to October for lodgepole pine.

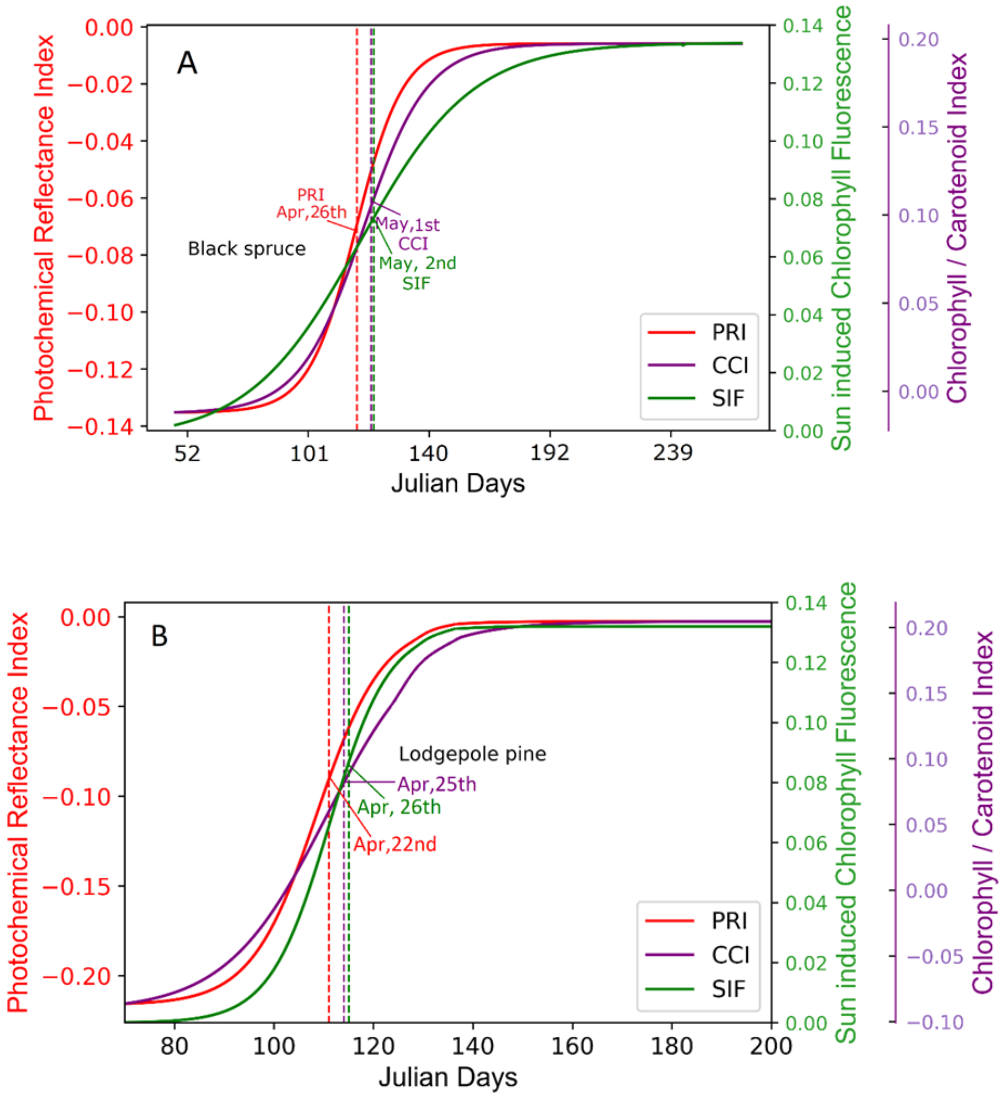

Figure 2-6. Seasonal sigmoidal fits for key parameters (PRI, CCI and SIF Wm-2 sr-1 nm-1), results for black spruce (*Picea mariana*) are shown in panel A. Lodgepole pine (*Pinus contorta*) results are shown in panel B. Vertical lines indicate dates of half-maximum values (see also Table 2-2), Data were collected from February to October 2020 in the case of black spruce, and from March to October for lodgepole pine.

Table 2-2. The half-maximum values for the sigmoidal fits of photosynthetic parameters during the 2020 spring recovery for *Picea mariana* and *Pinus contorta*.

	Black spruce, *P. mariana*		Lodgepole pine, *P. contorta*	
Parameter	Date	Julian days	Date	Julian days
PRI	April 26th	117	April 22nd	113
CCI	May 1st	122	April 25th	116
SIF	May 2nd	123	April 26th	117

- Seasonal sigmoidal fits for all parameters for black spruce *(P. mariana*) and lodgepole pine (*P. contorta)* as a function of temperature.

To interpret the temperature responses of key parameters (PRI, CCI, and SIF emission) during spring, a sigmoidal fit was applied, and plotted as a function of temperature in Fig 2-8. For *P. mariana* (black spruce), Fig 2-8 (A-C), lower values of PRI, CCI and SIF were found under cold and freezing temperatures (< -10℃ - 0℃). Half-maximum values (see Table 2-3) were found in temperatures that were from 9℃ to 15℃; summer values were observed after 12-15℃. In the case of *P. contorta* (lodgepole pine), PRI and CCI (Fig. 2-8(D-E)) winter values occurred under freezing temperature and parameters started to reach the half-maximum values after 6℃. The half-maximum value was observed between 5℃ to 12℃ and fully summer values were reported after reaching temperatures above 12℃. For the SIF emission, half-maximum values were reached at 6℃, transitional values were seen between 5℃ and 12℃, and summer values after 12℃.

From the sigmoidal fit, showed in Fig 2-9, wee can observe that, relative to CCI and PRI parameters, the SIF emission transitions (half-maximum temperature) occurred at about the same temperature (10-11℃) for *P. mariana* , but at lower temperature (around 6℃) for *P. contorta*.

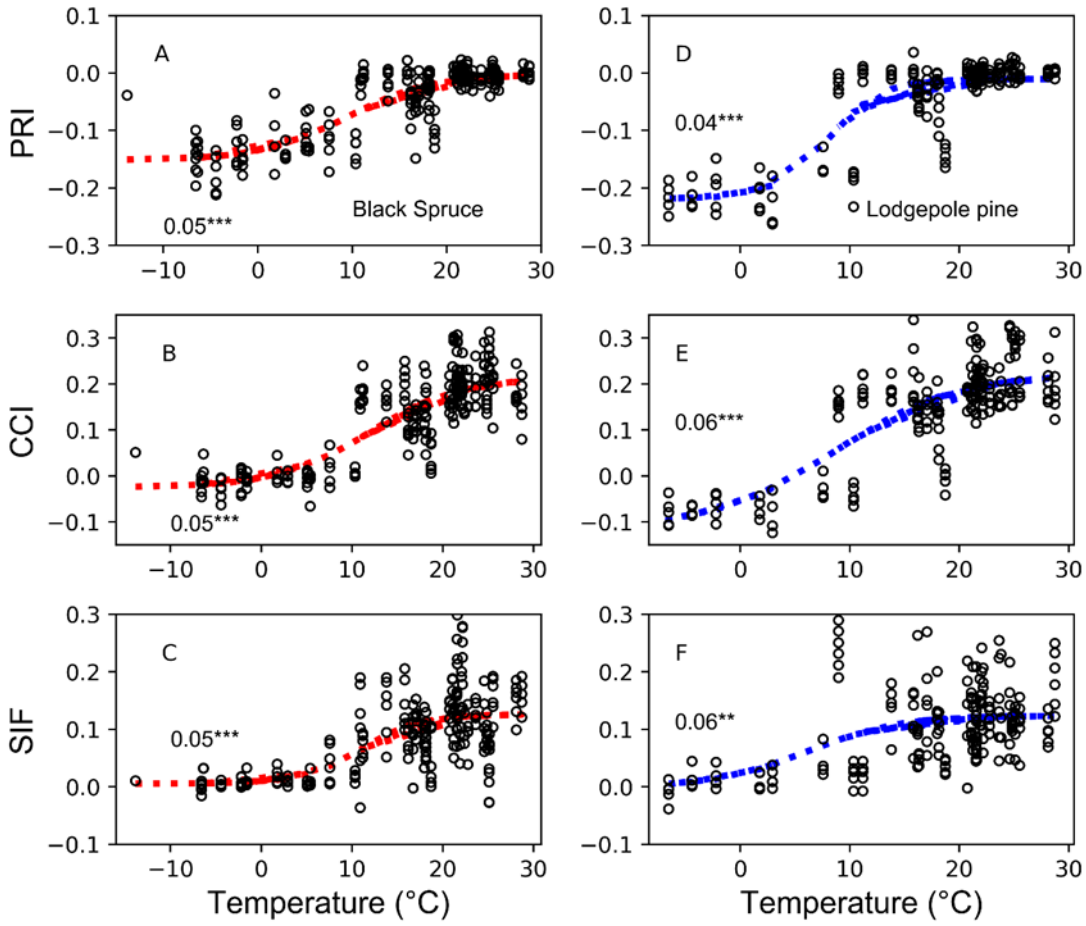

Figure 2-7. Sigmoidal fits for a non-linear regression model between temperature (℃) and the Sun induced chlorophyll fluorescence signal (SIF), the Photochemical Reflectance Index (PRI) and the Chlorophyll:Carotenoid Index (CCI). Figures A-C in the first row represent the results for black spruce (*Picea mariana*) and D-F represent the results from lodgepole pine (*Pinus contorta*). RSE indicates the residual standard error of the model.

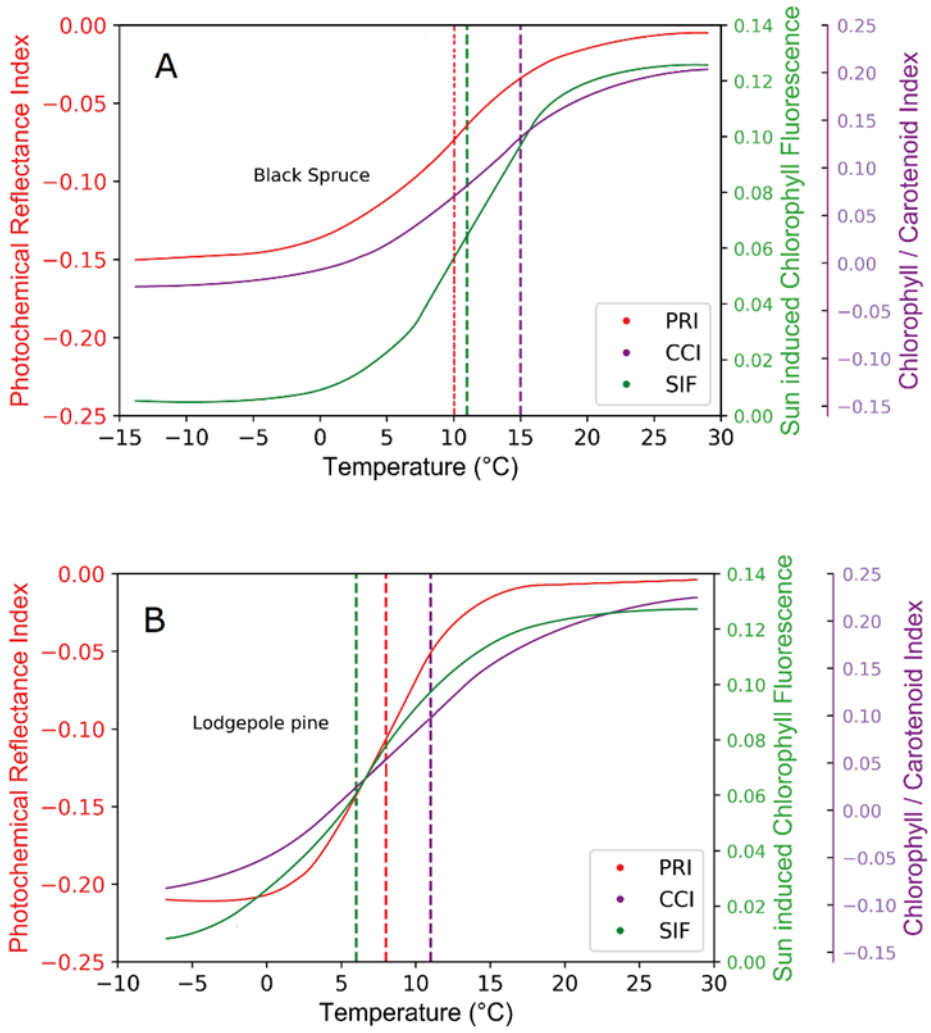

Figure 2-8. Overlaid sigmoidal fits, showing the temperature kinetics of PRI (red line), CCI (purple line) and SIF (green line) parameters during the 2020 spring recovery for (A) black spruce, *P. mariana* and (B) lodgepole pine, *P. contorta.* The dates for the observations range from winter in February to the end of June for P. mariana and from March to June for P. contorta. Red (PRI), green (SIF) and purple (CCI) dotted lines represent the temperature when the half-maximum values were reached.

Table 2-3. The half-recovery temperatures for the temperature-sigmoid fit of photosynthetic parameters during the 2020 spring recovery for *P.mariana* and *P. contorta.*		
Metric	*Picea mariana* (black spruce)	*Pinus contorta* (lodgepole pine)
PRI	9 ℃	8℃
CCI	10℃	11℃
SIF	15℃	6℃

Discussion

During the spring onset, environmental conditions start to gradually reverse from freezing to warmer temperatures. These temperature changes trigger the spring recovery of photosynthetic mechanisms in evergreen conifers (Huner et al. 1998; Öquist & Huner, 2003). These mechanisms differ very slightly in kinetics (Wong & Gamon, 2015), and appear to be directly related to carbon uptake dynamics (Wong and Gamon 2015; Gamon et al. 2016; Pierrat et al. 2021). A key question for this project, is how the SIF signal compares to carotenoid-based reflectance indices (PRI and CCI) – do they have the same kinetics and temperature response or not? To answer these questions about spring recovery, we explored two dominant evergreen conifer species from the Canadian Boreal Forest, black spruce (*Picea mariana*) and lodgepole pine (*Pinus contorta*).

Evergreen cold-hardening involves an increase in carotenoid content in order to enhance photoprotection during winter stress when photosynthesis is downregulated, a process that is entirely reversible during spring recovery (Öquist & Huner, 2003). These pigment changes influence needle-reflectance properties and can be monitored by using the correct reflectance wavelengths and indices (J. Gamon et al., 2016). Based on that, we found but similar responses in

the seasonal dynamics of optical indices at the needle-scale among our two conifer species. Spectral reflectance illustrated a gradual change between winter, spring, and summer in both species, showing the seasonal changes of the constitutive effects of carotenoid pigment pool size, and the facultative effects of the xanthophyll cycle activity. Similar results also have been reported in previous reflectance work (Wong, 2014; Wong et al. 2019).

Using CCI and PRI to track seasonal variations in this study we were able to observe the spring-summer transition, and results reported here are similar to what had been observed previously by (Wong, 2014; Springer et al. 2017; Wong et al. 2020), for the Canadian boreal forest. Specifically, during the spring recovery, both species displayed PRI and CCI values that closely followed the temperature transitions. These indices were closely related to SIF *total* and SIF *yield*, as has been observed by Magney et al. (2019), who stated that both GPP and SIF are regulated by seasonal changes in photoprotective pigments, and that SIF is directly related to needle physiology. However, in this needle-scale experiment, for both conifer species, we found that after the spring transition, SIF showed a high degree of noise and apparent decoupling from temperature and the Chl:Car reflectance indices (PRI and CCI). The SIF decoupling from temperature, CCI and PRI, could imply that after the transition into summer, the SIF emission is controlled by different environmental drivers such as PAR, soil volumetric water content (VWC) increased by precipitation, snow melt or both, soil temperature, and vapor pressure deficit (VPD), as reported by Pierrat et al. (2021).

We found similar temperature responses of SIF, PRI, and CCI, but slightly different kinetics and timing between *P.mariana and P. contorta* over the course of the spring recovery and growing season length, similar to results presented by (Wong, 2014; Springer, 2018). Both species showed a noticeable transition from winter values to summer values from April 23rd – May 29th.

During this period, PRI and SIF recovered earlier, suggesting the reactivation of the xanthophyll cycle (mostly associated with daily photoprotection) and indicating changes in the efficiency of photosynthetic processes. CCI, was the last parameter to recover, suggesting that Carotenoid: Chlorophyll ratios likely need more time and energy to adjust to chlorophyll and carotenoid concentrations. These last results have been observed before by Wong (2014) and also by Pierrat et al. (2021), who reported that in a first stage of spring recovery, the increase in SIF *total* marked the reactivation of photosynthesis and transpiration by evergreen trees, and that a second stage, was marked by a reduction in 'bulk' photoprotective pigments content, that was also confirmed by an increase in – the Chlorophyll : Carotenoid Index (CCI).

We also found that the responses of SIF to temperature were slightly different between the two conifer species. The activation of SIF*total* during spring, determined as the temperature of the half-maximum value, occurred at a higher temperature range for black spruce (around 10-11°C), than for lodgepole pine (around ~6°C). A similar observation was made by Yang et al. (2020), who showed that two dominant conifer species utilized fundamentally different mechanisms to manage spring recovery of photosynthetic activity, but that this difference may in part reflect the divergent positions these two species occupy in the ecosystem. Similarly, in this study, we detected that SIF parameters were still active in lodgepole pine during October but were in decline in black spruce around mid-September, suggesting a slightly longer growing season for lodgepole Pine individuals. These results agree with a recent study presented by Walter-McNeill et al. (2021) who pointed out that plants obtained from different locations but living under common environmental conditions can present variations in the engagement and disengagement of energy dissipation mechanisms.

Using proximal remote sensing tools like the FluoWat leaf clip in this study, we were able to track the emission of the Sun induced chlorophyll fluorescence (SIF) signal in two evergreen conifers (*P. mariana* and *P. contorta*), and to track the relative-timing of the photosynthetic reactivation of both species during the spring recovery. Here, we gained knowledge about how these two conifer species differ slightly in kinetics, in particular the activation of SIF emission, which was earlier in lodgepole pine (under lower temperatures) than in black spruce. PRI and CCI were able to track seasonal temperature changes, however, their kinetics differed slightly between the two species. From this we suggest that, for different conifer species, the reactivation of the photosynthetic processes and the disconnection of photoprotective mechanisms may not be perfectly simultaneous but and can vary across species and ecosystems. However, during spring recovery, all parameters under study – SIF, PRI and CCI – were clearly correlated across species, and with air temperature.

We learned that optical metrics responded in a similar way to temperature during the spring transition. However, these metrics, exhibited slightly different kinetics, and these kinetics differed slightly between species, with one species lodgepole pine having a slightly earlier response at a colder temperature than the other (black spruce). The optical metrics PRI, CCI and SIF are known indicators of the underlying mechanisms that govern the photosynthetic phenology of spring transition, suggesting that the photosynthetic responses may differ slightly between species and ecosystems, and with the role these species play within the forest. Other papers such as (Linkosalo et al. 2014; Wong et al. 2020; Yang et al. 2020; Walter-McNeill et al. 2021; Pierrat et al. 2021), have also emphasized slight variation in physiological and phenological species differences between conifers.

We suggest that carotenoid-based vegetation indices such as the photochemical reflectance index (PRI) and chlorophyll/carotenoid index (CCI) are promising tools to remotely track the invisible phenology of photosynthesis by assessing carotenoid pigment dynamics. These metrics can be used together as complementary data to interpret the SIF emission signal during the spring recovery in evergreen conifers and combined they might provide useful indicators to explore and study these species differences. Therefore, future SIF observations (e.g., leaf/needle, canopy, and satellite such as FLEX mission (Kraft et al. 2017) should consider including these metrics together.

We highlight these results, because, by understanding how different evergreen species respond to the spring recovery using a combination of remote sensing techniques, we can better understand the information contained in spatially integrated remote sensing time series data and perhaps more accurately determine the start and the end, and therefore the length of the growing season. Future studies should include sampling of photosynthesis and pigment levels during this transition. These measurements were not possible during this study due to practical and logistical reasons. The time involved in repeated sampling both fluorescence and reflectance under midday sun exposure did not allow for simultaneous pigment sampling and gas exchange, hence our study focused on comparing SIF (considered a photosynthetic metric) to the established pigment indices PRI and CCI. Lodgepole pine and black spruce are two dominant species that form part of the boreal forest, an ecosystem that stores the second-largest quantity of carbon on the planet. Their spring-recovery photosynthetic dynamics need to be accounted for when estimating CO_2 sequestration by the boreal forest, and this study offers highly valuable ground-based information to better track and interpret spring recovery of photosynthetic dynamics in the boreal forest.

Literature Cited

Adams III, W. W., & Demmig-Adams, B. (1994). Carotenoid composition and down regulation of photosystem II in three conifer species during the winter. *Physiologia Plantarum*, *92*(3), 451–458. https://doi.org/https://doi.org/10.1111/j.1399-3054.1994.tb08835.x

Astrup, R., Bernier, P. Y., Genet, H., Lutz, D. A., & Bright, R. M. (2018). A sensible climate solution for the boreal forest. *Nature Climate Change*, *8*(1), 11–12. https://doi.org/10.1038/s41558-017-0043-3

Buermann, W., Forkel, M., O'Sullivan, M., Sitch, S., Friedlingstein, P., Haverd, V., … Richardson, A. D. (2018). Widespread seasonal compensation effects of spring warming on northern plant productivity. *Nature*, *562*(7725), 110–114. https://doi.org/10.1038/s41586-018-0555-7

Butler, W., & Strasser, R. (1977). Tripartite model for the photochemical apparatus of green plant photosynthesis. *Proceedings of the National Academy of Sciences of the United States of America*, *74*, 3382–3385. https://doi.org/10.1073/pnas.74.8.3382

Demmig-Adams, B., & Adams, W. W. (1996). The role of xanthophyll cycle carotenoids in the protection of photosynthesis. *Trends in Plant Science*, *1*(1), 21–26. https://doi.org/https://doi.org/10.1016/S1360-1385(96)80019-7

Drusch, M., Moreno, J., Del Bello, U., Franco, R., Goulas, Y., Huth, A., … Verhoef, W. (2016). The FLuorescence EXplorer Mission Concept-ESA's Earth Explorer 8. *IEEE Transactions on Geoscience and Remote Sensing*, *PP*, 1–12. https://doi.org/10.1109/TGRS.2016.2621820

Du, S., Liu, L., Liu, X., & Hu, J. (2017). Response of Canopy Solar-Induced Chlorophyll Fluorescence to the Absorbed Photosynthetically Active Radiation Absorbed by Chlorophyll. *Remote Sensing* , Vol. 9. https://doi.org/10.3390/rs9090911

Frankenberg, C., B. Fisher, J., Worden, J., Badgley, G., Saatchi, S., Lee, J.-E., … Yokota, T. (2011). New global observations of the terrestrial carbon cycle from GOSAT: Patterns of plant fluorescence with gross primary productivity. In *GEOPHYSICAL RESEARCH LETTERS* (Vol. 38). https://doi.org/10.1029/2011GL048738

Gamon, J., Fred Huemmrich, K., Wong, C., Ensminger, I., Garrity, S., Y. Hollinger, D., … Penuelas, J. (2016). A remotely sensed pigment index reveals photosynthetic phenology in evergreen conifers. In *Proceedings of the National Academy of Sciences* (Vol. 113). https://doi.org/10.1073/pnas.1606162113

Gamon, J A, Peñuelas, J., & Field, C. B. (1992). A narrow-waveband spectral index that tracks diurnal changes in photosynthetic efficiency. *Remote Sensing of Environment*, *41*(1), 35–44. https://doi.org/https://doi.org/10.1016/0034-4257(92)90059-S

Gamon, J A, Serrano, L., & Surfus, J. S. (1997). The Photochemical Reflectance Index: An Optical Indicator of Photosynthetic Radiation Use Efficiency across Species, Functional Types, and Nutrient Levels. *Oecologia*, *112*(4), 492–501. Retrieved from http://www.jstor.org/stable/4221805

Gamon, John A, & Bond, B. (2013). Effects of irradiance and photosynthetic downregulation on the photochemical reflectance index in Douglas-fir and ponderosa pine. *Remote Sensing of Environment*, *135*, 141–149. https://doi.org/https://doi.org/10.1016/j.rse.2013.03.032

Hänninen, H. (2016). *Boreal and Temperate Trees in a Changing Climate*. https://doi.org/10.1007/978-94-017-7549-6

Huner, N., Öquist, G., & Melis, A. (2003). Photostasis in Plants, Green Algae and Cyanobacteria: The Role of Light Harvesting Antenna Complexes. In *Light-Harvesting Antennas in Photosynthesis* (Vol. 13, pp. 401–421). https://doi.org/10.1007/978-94-017-2087-8_14

Huner, N. P. A., Öquist, G., & Sarhan, F. (1998). Energy balance and acclimation to light and cold. *Trends in Plant Science*, *3*(6), 224–230. https://doi.org/https://doi.org/10.1016/S1360-1385(98)01248-5

Joiner, J., Yoshida, Y., Vasilkov, A. P., Yoshida, Y., Corp, L. A., & Middleton, E. M. (2011). First observations of global and seasonal terrestrial chlorophyll fluorescence from space. *Biogeosciences*, *8*(3), 637–651. https://doi.org/10.5194/bg-8-637-2011

Keenan, R. J., Reams, G. A., Achard, F., de Freitas, J. V, Grainger, A., & Lindquist, E. (2015). Dynamics of global forest area: Results from the FAO Global Forest Resources Assessment 2015. *Forest Ecology and Management*, *352*, 9–20. https://doi.org/https://doi.org/10.1016/j.foreco.2015.06.014

Kraft, S., Bello, U. Del, Harnisch, B., Bouvet, M., Drusch, M., & Bézy, J.-L. (2017). Fluorescence imaging spectrometer concepts for the Earth explorer mission candidate flex. *Proc.SPIE*, *10564*. https://doi.org/10.1117/12.2309086

La Roi, G. H. (1967). Ecological Studies in the Boreal Spruce-Fir Forests of the North American Taiga. I. Analysis of the Vascular Flora. *Ecological Monographs*, *37*(3), 229–253. https://doi.org/10.2307/1948439

Linkosalo, T., Heikkinen, J., Pulkkinen, P., & Mäkipää, R. (2014). Fluorescence measurements show stronger cold inhibition of photosynthetic light reactions in Scots pine compared to Norway spruce as well as during spring compared to autumn . *Frontiers in Plant Science* , Vol. 5. Retrieved from https://www.frontiersin.org/article/10.3389/fpls.2014.00264

Magney, T., R. Bowling, D., A. Logan, B., Großmann, K., Stutz, J., D. Blanken, P., … Frankenberg, C. (2019). Mechanistic evidence for tracking the seasonality of photosynthesis with solar-induced fluorescence. *Proceedings of the National Academy of Sciences of the United States of America*. https://doi.org/10.1073/pnas.1900278116

Meroni, M., Rossini, M., Guanter, L., Alonso, L., Rascher, U., Colombo, R., & Moreno, J. (2009). Remote sensing of solar-induced chlorophyll fluorescence: Review of methods and applications. *Remote Sensing of Environment*, *113*(10), 2037–2051. https://doi.org/https://doi.org/10.1016/j.rse.2009.05.003

Mohammed, G. H., Colombo, R., Middleton, E. M., Rascher, U., van der Tol, C., Nedbal, L., … Zarco-Tejada, P. J. (2019). Remote sensing of solar-induced chlorophyll fluorescence (SIF) in vegetation: 50 years of progress. *Remote Sensing of Environment*, *231*, 111177.

https://doi.org/https://doi.org/10.1016/j.rse.2019.04.030

Nichol, J. C., Drolet, G., Porcar-Castell, A., Wade, T., Sabater, N., Middleton, M. E., … Atherton, J. (2019). Diurnal and Seasonal Solar Induced Chlorophyll Fluorescence and Photosynthesis in a Boreal Scots Pine Canopy. *Remote Sensing* , Vol. 11. https://doi.org/10.3390/rs11030273

Öquist, G., & Huner, N. P. A. (2003). Photosynthesis of Overwintering Evergreen Plants. *Annual Review of Plant Biology*, *54*(1), 329–355. https://doi.org/10.1146/annurev.arplant.54.072402.115741

ÖQUIST, G., & MARTIN, B. (1980). Inhibition of photosynthetic electron transport and formation of inactive chlorophyll in winter stressed Pinus silvestris. *Physiologia Plantarum*, *48*(1), 33–38. https://doi.org/https://doi.org/10.1111/j.1399-3054.1980.tb03215.x

Pan, Y., Birdsey, R. A., Fang, J., Houghton, R., Kauppi, P. E., Kurz, W. A., … Hayes, D. (2011). A Large and Persistent Carbon Sink in the World's Forests. *Science*, *333*(6045), 988 LP – 993. https://doi.org/10.1126/science.1201609

PEÑUELAS, J., FILELLA, I., & GAMON, J. A. (1995). Assessment of photosynthetic radiation-use efficiency with spectral reflectance. *New Phytologist*, *131*(3), 291–296. https://doi.org/https://doi.org/10.1111/j.1469-8137.1995.tb03064.x

Peñuelas, J., Filella, I., Gamon, J. A., & Field, C. (1997). Assessing photosynthetic radiation-use efficiency of emergent aquatic vegetation from spectral reflectance. *Aquatic Botany*, *58*(3), 307–315. https://doi.org/https://doi.org/10.1016/S0304-3770(97)00042-9

Pierrat, Z., Nehemy, M., Roy, A., Magney, T., Parazoo, N., Laroque, C., … Stutz, J. (2021). Tower-Based Remote Sensing Reveals Mechanisms Behind a Two-phased Spring Transition in a Mixed-Species Boreal Forest. *Journal of Geophysical Research: Biogeosciences*, *126*. https://doi.org/10.1029/2020JG006191

Pinto, F., Celesti, M., Acebron, K., Alberti, G., Cogliati, S., Colombo, R., … Rascher, U. (2020). Dynamics of sun-induced chlorophyll fluorescence and reflectance to detect stress-induced variations in canopy photosynthesis. *Plant, Cell & Environment*, *43*(7), 1637–1654. https://doi.org/https://doi.org/10.1111/pce.13754

Porcar-Castell, A., Garcia Plazaola, J. I., J Nichol, C., Kolari, P., Olascoaga, B., Kuusinen, N., … Nikinmaa, E. (2012). Physiology of the seasonal relationship between Photochemical Reflectance Index and photosynthetic Light Use Efficiency. In *Oecologia* (Vol. 170). https://doi.org/10.1007/s00442-012-2317-9

Porcar-Castell, A., Tyystjärvi, E., Atherton, J., Tol, C., Flexas, J., E Pfündel, E., … Berry, J. (2014). Linking chlorophyll a fluorescence to photosynthesis for remote sensing applications: Mechanisms and challenges. In *Journal of experimental botany* (Vol. 65). https://doi.org/10.1093/jxb/eru191

Powles, S. (2003). Photoinhibition of Photosynthesis Induced by Visible Light. *Annu Rev Plant Physiol*, *35*, 15–44. https://doi.org/10.1146/annurev.pp.35.060184.000311

R. Springer, K., Wang, R., & Gamon, J. (2017). Parallel Seasonal Patterns of Photosynthesis, Fluorescence, and Reflectance Indices in Boreal Trees. In *Remote Sensing* (Vol. 9).

https://doi.org/10.3390/rs9070691

Richardson, A., Black, T., Ciais, P., Delbart, N., Friedl, M., Gobron, N., … Varlagin, A. (2010). Influence of spring and autumn phenological transitions on forest ecosystem productivity. *Philosophical Transactions of the Royal Society B-Biological Sciences, v.365, 3227-3246 (2010)*, *365*. https://doi.org/10.1098/rstb.2010.0102

Savitch, L. V, Leonardos, E. D., Krol, M., Jansson, S., Grodzinski, B., Huner, N. P. A., & Öquist, G. (2002). Two different strategies for light utilization in photosynthesis in relation to growth and cold acclimation. *Plant, Cell & Environment*, *25*(6), 761–771. https://doi.org/https://doi.org/10.1046/j.1365-3040.2002.00861.x

Springer, K. (2018). *Monitoring Phenology of Boreal Trees Using Remote Sensing*. University of Alberta.

Sun, Y., Frankenberg, C., Jung, M., Joiner, J., Guanter, L., Köhler, P., & Magney, T. (2018). Overview of Solar-Induced chlorophyll Fluorescence (SIF) from the Orbiting Carbon Observatory-2: Retrieval, cross-mission comparison, and global monitoring for GPP. *Remote Sensing of Environment*, *209*, 808–823. https://doi.org/https://doi.org/10.1016/j.rse.2018.02.016

Sutinen, M.-L., Arora, R., Wisniewski, M., Ashworth, E., Strimbeck, R., & Palta, J. (2001). *Mechanisms of Frost Survival and Freeze-Damage in Nature*. https://doi.org/10.1007/978-94-015-9650-3_4

Van Wittenberghe, S; Verrelst, J; Alonso L; Hermans, I; Delegido, J; Valcke, R; Moreno, J; Samson, R. (2013). Methodology, Fluowat leaf clip develped by Luis Alonso. In *Enviromental Pollution* (pp. 29–37). Valencia.

Van Wittenberghe, S., Alonso, L., Verrelst, J., Hermans, I., Delegido, J., Veroustraete, F., … Samson, R. (2013). Upward and downward solar-induced chlorophyll fluorescence yield indices of four tree species as indicators of traffic pollution in Valencia. *Environmental Pollution*, *173*, 29–37. https://doi.org/https://doi.org/10.1016/j.envpol.2012.10.003

Verhoeven, A. (2014). Sustained energy dissipation in winter evergreens. *New Phytologist*, *201*(1), 57–65. https://doi.org/10.1111/nph.12466

Walter-McNeill, A., Garcia, M. A., Logan, B. A., Bombard, D. M., Reblin, J. S., Lopez, S., … Bowling, D. R. (2021). Wide variation of winter-induced sustained thermal energy dissipation in conifers: a common-garden study. *Oecologia*. https://doi.org/10.1007/s00442-021-05038-y

Williams, C. M., Henry, H. A. L., & Sinclair, B. J. (2015). Cold truths: how winter drives responses of terrestrial organisms to climate change. *Biological Reviews*, *90*(1), 214–235. https://doi.org/https://doi.org/10.1111/brv.12105

Wong, C. (2014). *Seasonal photosynthetic activity in evergreen conifer leaves monitored with spectral reflectance*. Univesity of Alberta.

Wong, C. Y. S., D'Odorico, P., Arain, M. A., & Ensminger, I. (2020). Tracking the phenology of photosynthesis using carotenoid-sensitive and near-infrared reflectance vegetation indices in a temperate evergreen and mixed deciduous forest. *New Phytologist*, *226*(6), 1682–1695.

https://doi.org/10.1111/nph.16479

Wong, C. Y. S., D'Odorico, P., Bhathena, Y., Arain, M. A., & Ensminger, I. (2019). Carotenoid based vegetation indices for accurate monitoring of the phenology of photosynthesis at the leaf-scale in deciduous and evergreen trees. *Remote Sensing of Environment*, *233*, 111407. https://doi.org/https://doi.org/10.1016/j.rse.2019.111407

Wong, C. Y. S., & Gamon, J. A. (2015). The photochemical reflectance index provides an optical indicator of spring photosynthetic activation in evergreen conifers. *New Phytologist*, *206*(1), 196–208. https://doi.org/10.1111/nph.13251

Yang, Q., Blanco, N., Hermida Carrera, C., Lehotai, N., Hurry, V., & Strand, Å. (2020). Two dominant boreal conifers use contrasting mechanisms to reactivate photosynthesis in the spring. *Nature Communications*, *11*, 128. https://doi.org/10.1038/s41467-019-13954-0

Chapter 3 - Needle-scale reflectance and SIF responses during a simulated spring transition in *Picea mariana* (black spruce), an evergreen conifer species.

Introduction

Past and current studies have shown that conifers in cold climates experience large seasonal variability in their photosynthetic status (Gillies & Vidaver, 1990). These plants exhibit a gradual decline of photosynthetic activity during late summer and autumn, a strong inhibition during winter, and a complete recovery during spring and summer (Öquist & Huner, 2003). The photosynthetic decay and spring recovery that these plants experience during the year provide us with an opportunity to observe and understand their phenology at a whole ecosystem level, by using both leaf-scale and satellite-scale data. However, the unique ecophysiology of cold-climate conifers has represented a major challenge to global remote sensing-based approaches over decades, because the quantification of photosynthetic activity by using vegetation indices based on "greenness" detection has not been sufficiently sensitive to track variations in the photosynthetic activity of evergreen conifers (Gamon et al. 2016; Magney et al. 2019; Wong et. al 2019). This is a result of their evergreen needles, which make it difficult to assess seasonal photosynthetic activity based on "greenness" indices such as the Normalized Difference Vegetation Index (NDVI). Therefore, two of the challenges encountered during recent decades have been how to accurately track the photosynthetic status of evergreen conifers at a large scale, and how to validate interpretations of these data.

Specifically, conifer species have evolved a remarkable series of photosynthetic strategies to couple with winter. These include the capacity for thermal dissipation of excess energy, which is the conversion of light energy absorbed by chlorophyll into heat (Demmig-Adams & Adams

1992; Adams III & Demmig-Adams 1994), also known as the xanthophyll cycle (non-photochemical quenching NPQ). This mechanism is capable of downregulating the photosynthetic status during winter, a process that is facilitated by the de-epoxidation of the carotenoid violaxanthin to antheraxanthin(A) and zeaxanthin (Z). (Demmig-Adams & Adams, 1996b; Verhoeven 2014).

During the decade of the 1990s, Gamon et al. (1992) & Gamon et al. (1993), started to study and explore the variations of the 531 nm band reflectance signal produced by carotenoids in leaves, and developed the Photochemical Reflectance Index (PRI), an index capable of tracking the xanthophyll cycle using measurements of spectral reflectance. They related this to photosynthetic activity at an hourly/daily scale. More recently, the Chlorophyll/Carotenoid Index (CCI) was developed (Gamon et al. 2016; Springer, Wang, & Gamon, 2017; Wong et al., 2019). This index is similar to PRI and is an alternative carotenoid-sensitive vegetation index for tracking photosynthethic phenology in deciduous and evergreen trees at the canopy and stand scales (Gamon et al. 2016; Wong et al. 2022). However, the link between the CCI and photosynthethic activity at the needle-scale has yet to be fully explored. Understanding the fundamental behaviour of the CCI at the needle scale is is important for better assessing photosynthesis at the global scale.

In addition to this, other opportunities, based-on global remote-sensing, have recently become available to better track changes in evergreen conifers using measurements of sun-induced chlorophyll fluorescence (SIF) (Jeong et al. 2017). Several studies have shown an almost linear relationship between SIF and photosynthesis (Louis et al., 2005; Nichol et al., 2019; van der Tol et al., 2016), demonstrating its high potential for quantifying plant physiological variability and in quantifying the productivity of evergreen conifers when compared to most existing remote-

sensing approaches based on NDVI (Raczka et al. 2019). SIF studies from various ecosystems and scales have emerged, at leaf, (Rajewicz et al. 2019), tower-based (Magney et al. 2019; Pierrat et al. 2021), airborne, and satellite scales (Wieneke et al. 2016; Bandopadhyay, Rastogi, & Juszczak, 2020; Siegmann et al. 2021; Walther et al, 2016; Jeong et al. 2017 & Raczka et al. 2019). With the same goal, using multispectral and hyperspectral reflectance measurements, other researchers (Springer, Wang, & Gamon, 2017; Wong et al. 2019, Pierrat et al. 2022) have reported that PRI and CCI are able to improve the remote assessment of the photosynthetic phenology of evergreen tree species in different boreal forest settings. These recent experiments have explored changes in phenology in response to temperature and/or precipitation variability in high-latitude forests by combining the biological response of SIF with optical vegetation indices such as PRI and CCI. However, how these metrics are linked at the needle scale remains to be understood.

Currently, global/satellite remote sensing faces an additional challenge, particularly in northern latitudes, where climate change is affecting temperature conditions, impacting growing season length through earlier spring onset and/or delayed fall senescence (Berra & Gaulton, 2021). Because of this, changes in the physiology and phenology of evergreen conifers in response to variability on temperature and/or precipitation are expected (Montgomery et al, 2020). Therefore, one of the current challenges for satellite-based remote sensing remains how to accurately track the onset, duration, and end of the growing season of evergreen conifers. An evaluation of PRI, CCI and SIF at the needle-scale in relation to seasonal temperature transitions could lead us to better approaches to monitoring and understanding the impacts of climate change on seasonal photosynthetic regulation in evergreen conifers.

In chapter 2, we studied *Picea mariana* and *Pinus contorta* under natural weather conditions typical of the boreal forest. We found evidence that the PRI, CCI and SIF metrics were highly related during the spring onset, and that temperature played a direct role in the activation of SIF, the deactivation of the sustained xanthophyll cycle (sustained NPQ), and the reactivation of the xanthophyll cycle (NPQ). However, that study followed plants exposed to naturally varying conditions, making it hard to be sure whether temperature, as opposed to other environmental factors (e.g., daylength) was the driving variable. Based on these results, we decided to conduct a second needle-scale experiment designed to capture the response of SIF, PRI, CCI and NDVI to a gradual increment in temperature within a controlled environment, simulating the spring-onset of growth in boreal evergreen conifers using *Picea mariana* (black spruce) seedlings. The main goals of this experiment were (1) to study the response of SIF to an increase in temperature under controlled conditions, (2) to further explore the relationship between SIF and reflectance-based vegetation indices such as PRI, CCI and NDVI under these controlled conditions; and (3) to compare our results to chlorophyll and carotenoid pigment data, which required destructive sampling, and had not been obtained in the previous experiment.

Materials and methods

- Plant materials and controlled environment

Previous to this experiment, we preselected healthy three-year-old black spruce individuals, that were obtained for the previous experiment (from TreeTime Nursery Inc, , Alberta, Canada). We first established them on (?) the south-facing rooftop of the Biological Science building at the University of Alberta, Canada. There, all plants were potted in a 1:2 soil mixture of sandy topsoil and sunshine mix (Sunshine Mix 4, Sun Gro Horticulture, Agawam, MA, USA) with added slow-

release fertilizer (Nutricote 14-14-14, Sun Gro Horticulture, Agawam, MA, USA). After this, plants were potted in 2.83 L pots (CP412CH, Stuewe & Sons, Tangent, OR, USA). and arranged by species into synthetic stands (1.5 m x 1.5 m plots) for their long-term acclimation. Plants were located in the rooftop, exposed to seasonal weather conditions similar to those encountered in the boreal forest and watered throughout the non-freezing periods to avoid water stress, Fig 3-1.

During late winter, when daytime temperatures approached 5°C, six individuals were moved into a growth chamber (Converso CMP 3244: Controlled Environments Ltd, Winnipeg, MB, Canada) in which the trees were exposed to a steady temperature under constant light conditions. Data collection took place from March to May 2020, from 13:00 to 15:00 PM every time. Temperature was maintained at 5 °C for the first ten days of the experiment and was set to increase by 5°C every ten-days (see figure 3-1) until it reached 30°C. Relative humidity was set at 20% (simulating low humidity conditions in Edmonton, Alberta). Light conditions were established at a photosynthetic photon flux density (PPFD) of approximately 700-800 μmol m^{-2} s^{-1} with a photoperiod of 14 h, throughout the experiment. Measurements were made every three days, and the plants were watered every 3 days and every 2 days when temperatures where higher than 15°C in order to prevent desiccation and heat stress.

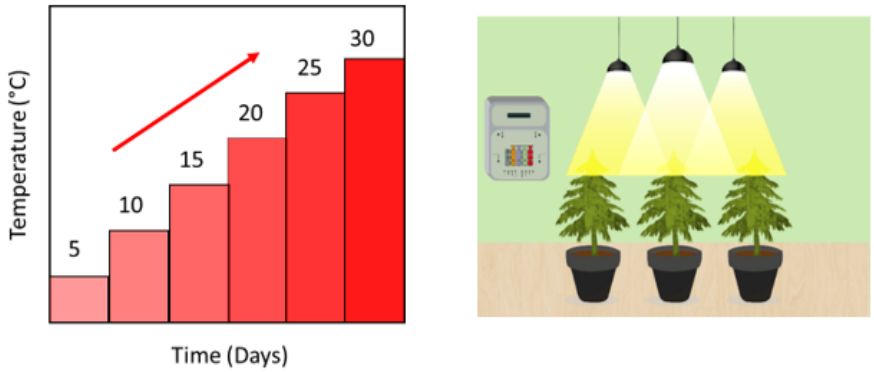

Figure 3-1.Design of the chamber experiment, where temperature was increased every ten days and an example of tree location inside the growing chamber.

- Needle reflectance and Sun Induced chlorophyll fluorescence measurements

Measurements of the reflectance and fluorescence emission signals for this experiment were made using the FluoWat leaf-clip (Fig 3-2) attached to a field spectrometer (UniSpec-SC, PP Systems, Amesbury MA, USA). In this case, chlorophyll fluorescence ("SIF") was measured under artificial light conditions. While using a high spectral resolution spectrometer (UniSpec-SC, PP Systems, Amesbury, MA, USA) we attached an optical fibre (UNI684, PP Systems, Amesbury, MA, USA), and a halogen light source with a custom fiber optic, both instruments coupled with the FluoWat leaf clip (Alonso L. et al., 2013; Van Wittenberghe et al., 2013).

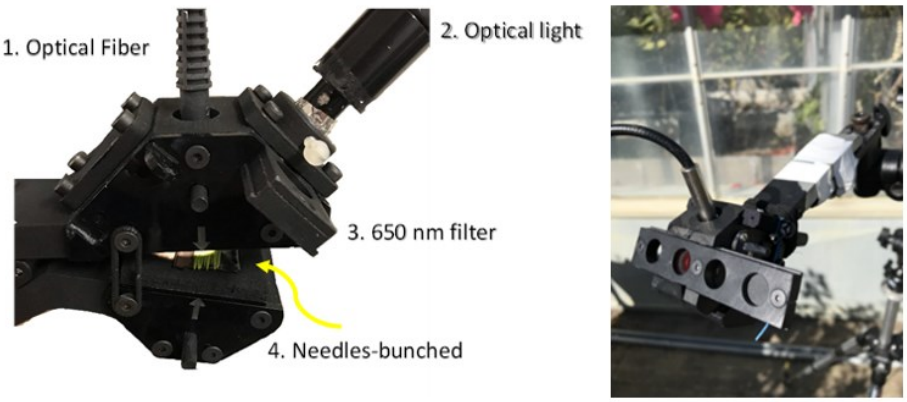

Figure 3-2. (1) FluoWat leaf-clip (Alonso, L. et al. 2007) coupled with a spectrometer (UniSpec, PP Systems, Amesbury MA) which enables measurement of the SIF spectrum by selectively filtering the incoming light. (2) External halogen light source. (3) Short pass 650nm filter (Edmund optics, 12.5 Diameter, OD 4.0) (3) Needle-bunches were arranged vertically, one next to another, using black masking tape.

The SIF emission signal (650–850 nm) was measured by setting a short-pass filter cutting off light above 650 nm (12.5mm Diameter, OD 4.0, Edmund Optics). This way primarily SIF was measured, as (except for light leaks) light in this spectral region cannot originate from reflection of light above 650 nm with the filter in place. Measurements were executed under a 45° illumination angle. Five-eight healthy needles from each tree were measured per sample. We explored the following SIF parameters: APAR, SIF total, SIF *yield* (SIF *total* / APAR), far-red SIF (SIF 740nm), red SIF (SIF 680nm), far-red SIF/ red SIF ratio, as described in Chapter 2. To see further details in how we collected, calibrated, corrected light leaks, and analysed SIF data, review the Appendix I. In addition to SIF, reflectance indices were calculated using leaf reflectance (ρ_λ) from each measurement and the appropriate equations were applied (Table 3-1).

Table 3-1. Vegetation reflectance indices and Sun Induced Chl florescence(SIF) parameters studied in this methodology.	
Normalized Difference Vegetation Index (NDVI)	
Photochemical Reflectance index (PRI)	$\frac{\rho 800\text{nm} - \rho 630\text{nm}}{\rho 800\text{nm} + \rho 630\text{nm}}$
Chlorophyll/Carotenoid index (CCI)	$\frac{\rho 531\text{nm} - \rho 570\text{nm}}{\rho 531\text{nm} + \rho 570\text{nm}}$
SIF*total*	$\frac{\rho 531\text{nm} - \rho 630\text{nm}}{\rho 531\text{nm} + \rho 630\text{nm}}$
red SIF (SIF_{680nm})	SIF *total*= $\int_{690}^{740} f(\lambda)\, d\lambda$
far-red SIF (SIF_{740nm})	$F690\text{nm}$
far-red SIF/ red SIF ratio	$F740\text{nm}$
F_{yield}	$F740\text{nm}/F690\text{nm}$
$F_{yield\ 690}$	SIF *total* / APAR
$F_{yield\ 740}$	$F690\text{nm}/\text{APAR}$
	$F740\text{nm}/\text{APAR}$

- Photosynthetic pigments

Needle samples for pigment analysis were collected immediately after spectral measurements (flash-frozen in liquid nitrogen) and stored at −80 °C upon arrival in the laboratory (There was a time gap of an hour and half between collecting the samples, measurements and storing the samples in the -80C freezer, however needle material was always submerged in liquid nitrogen). Once in the lab, the leaves were cut into three 1 cm long segments, measured with a fine caliper for leaf area, and immediately stored in liquid nitrogen again. Following Wong (2014), needle samples were later transferred to a -80 °C freezer for long-term storage. For pigment analyses, batches of 6 leaf samples from a given date and time were pooled together and analyzed using high-performance liquid chromatography (HPLC) (1260 Infinity, Agilent Technologies,

Santa Clara, CA, USA). HPLC sampling following the Thayer and Björkman (1990) method was used to find the concentrations of various carotenoid and chlorophyll pigments. The HPLC system had previously been calibrated using pigment standards from DHI (DHI LAB Products, Hørsholm, Denmark).

The carotenoid: chlorophyll ratio was calculated as the sum of all carotenoids, including neoxanthin, violaxanthin, antheraxanthin, lutein, zeaxanthin, and β-carotene, expressed on a total chlorophyll (a and b) basis (mmol mol^{-1} Chl a+b) The epoxidation state (EPS) of the xanthophyll cycle was calculated as:

$$\text{EPS} = \frac{V+0.5A}{V+A+Z}$$

The EPS is an expression of the non-photoprotective (dark state) pigment composition of the xanthophyll cycle. The letters indicate absolute concentration (μmol m^{-2}) of each xanthophyll pigment violaxanthin (V), antheraxanthin (A) and zeaxanthin (Z).

Results

- Exploring SIF spectral signal, Red-SIF, and Far-red SIF as a function of temperature.

In this experiment we explored the SIF spectral signal as a function of temperature. All temperatures presented a clear SIF needle-spectrum, shown in Fig 3-3. The lowest values were observed at 5°C and the highest values were observed at 15°C. At higher temperatures, SIF tended to diminish slightly.

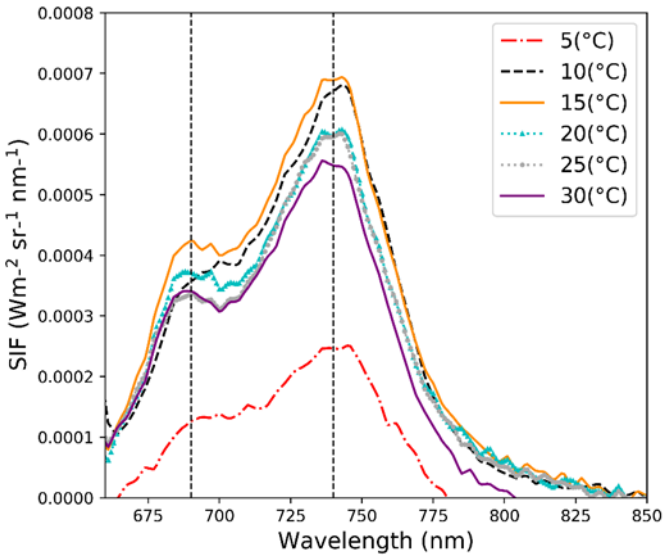

Figure 3-3. Needle-scale SIF dynamic response of six three-year-old black spruce (P. mariana) individuals to a gradual increase of temperature in a controlled environment, during a simulation of the spring to summer transition, when temperatures ranged from 5°C to 30°C. Lines represent the average of all the spectral data points for each temperature (sample size = 18) represents the data from average reflectance, collected from three individuals, three different dates.

- Contribution of needle spectral reflectance changes through the experiment.

The spectral reflectance of black spruce needles showed significant variation over the course of the experiment in response to a gradual increment in temperature, as shown in Fig. 3-4. In this figure, the variation of spectral reflectance as a function of temperature was often visibly larger in the near infrared region, from 700 to 1000 nm than in the visible region. In the visible region, from 450 nm to 700 nm, the differences in spectral reflectance appeared to be smaller relative to temperature increases. However, the relative changes in the visible bands (400-700 nm) were clearer when expressing this reflectance as ratio spectra (Fig 3-5), as these bands spectrally changed shape with temperature. This allowed us to observe the relative changes, especially from 5°C to 10°C (Fig 3-5 A,B,C), 5°C to 15°C (Figure 3-5 D,E,F) and 5°C-30°C (Figure 3-5 G,H,I).

In addition to distinct spectral changes at 531 nm (indicative of shifts in the xanthophyll cycle pigments, Gamon et al. 1990, 1992, 1993), the reflectance in the visible spectrum also tended to increase with temperature and time, suggesting changes in pigment pool sizes.

Even if in the visible region (from 400 to 700nm) differences in needle-spectra were less marked, these differences were clearly detected at 531 nm (relative to 570 or 645 nm), the wavelengths used to quantify PRI and CCI (carotenoid-based vegetation indices). According to this reflectance analysis, the gradual variations in needle-spectral reflectance in response to temperature were reflected in the NDVI, PRI and CCI bands (see Fig 3-4). However, these variations were not equally well represented by all three vegetation indices as NDVI remained almost unchanged over the course of the experiment (showed in Fig 3-7) . PRI and CCI were both able to follow the gradual increase in temperature (Fig. 3-7). Both indices showed a sharp increase between the transition from 5°C to 10 °C, and above 10°C, both indices continued moderately growing.

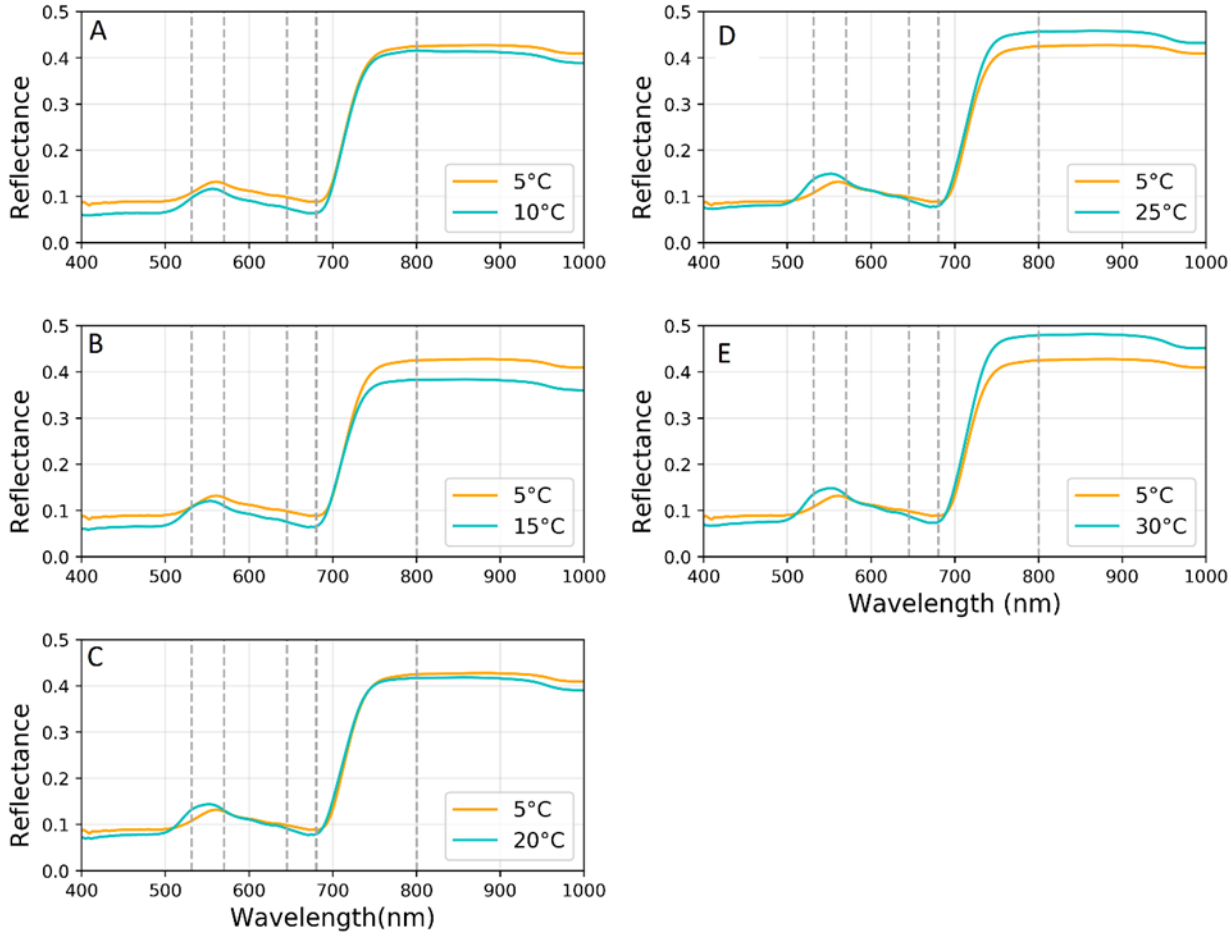

Figure 3-4. Transitional dynamics of average needle-spectral reflectance for black spruce (P. mariana) while exposed to a gradual increase in temperature. Vertical dotted lines represent the wavebands used for deriving NDVI (680 and 800 nm), PRI (531 and 570 nm) and CCI (531 and 645 nm). Each line represents the temperature average value obtained from a total of n=18.

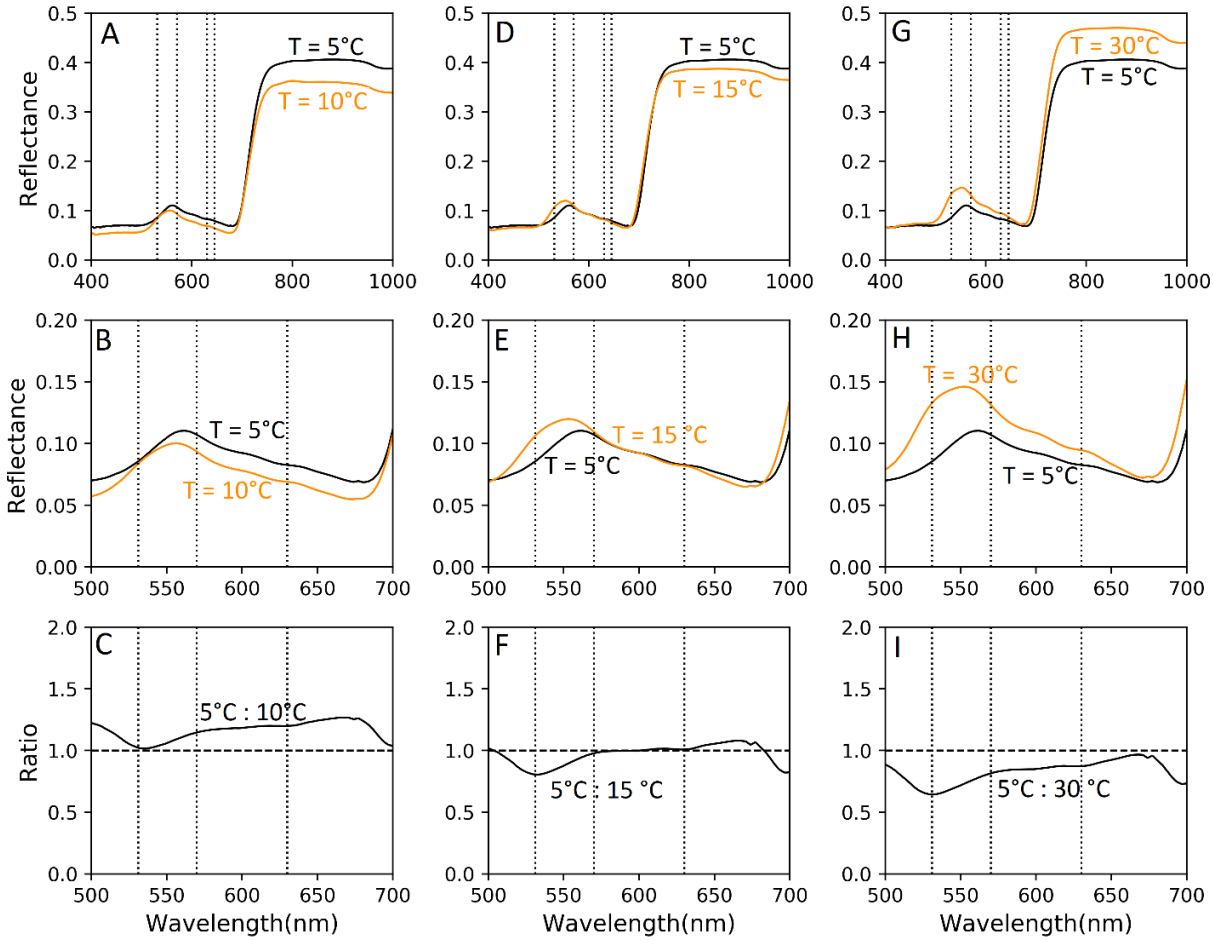

Figure 3-5. Needle spectra of P. mariana at three temporal scales and temperature transitions of the spring simulation experiment, left columns (A,B,C) represent the transition between 5°C (black lines) and 10°C (orange lines). Middle vertical column: (D,E,F) show the transition between 5°C (black lines) and 15°C (orange lines) and right column (G,H,I) show the transition between 5°C (black lines) and 30°C (orange lines). Top panels (A,D,G) are leaf reflectance spectra of the visible and near-infrared regions. Middle horizontal panels (B,E,H) are leaf reflectance spectra expanded from 500 to 600 nm. Bottom panels (C,F,I) are the ratio of the temporal change in reflectance at contrasting temperatures (referenced to 5 degrees). Vertical dashed lines denote location of the PRI (531 and 570 nm) and CCI (531 and 645 nm) bands. n = 18.

- Carotenoid and chlorophyll concentrations changed during the 5°C - 15°C experiment, simulating spring transition temperatures.

Parallel to the spectral shifts described above, Z+A/(A+Z+V), Zeaxanthin pigment concentrations decreased, and EPS increased, with temperature increases (Fig. 3-6). Of all pigment metrics for *P. marina,* EPS, and (Z+A)/(A+Z+V) and Zeaxanthin, matched the best with PRI and CCI, as shown by the Pearson [R] correlations analysis, presented in Table 3-2. Chlorophyll: Carotenoid ratios did not present significant changes over the course of the study (Fig 3-6 A). However, zeaxanthin (Fig 3-6 C) pigment concentrations decreased with a rise in temperature. Similarly, gradual decline in the xanthophyll cycle conversion state (Z+A/ A+Z+V) was evident with an increase in temperature (Fig 3-6 E); and EPS increased with temperature (Fig 3-6 F) correlating best with CCI results (0.74***) and PRI (0.71***)(Table 3-2).

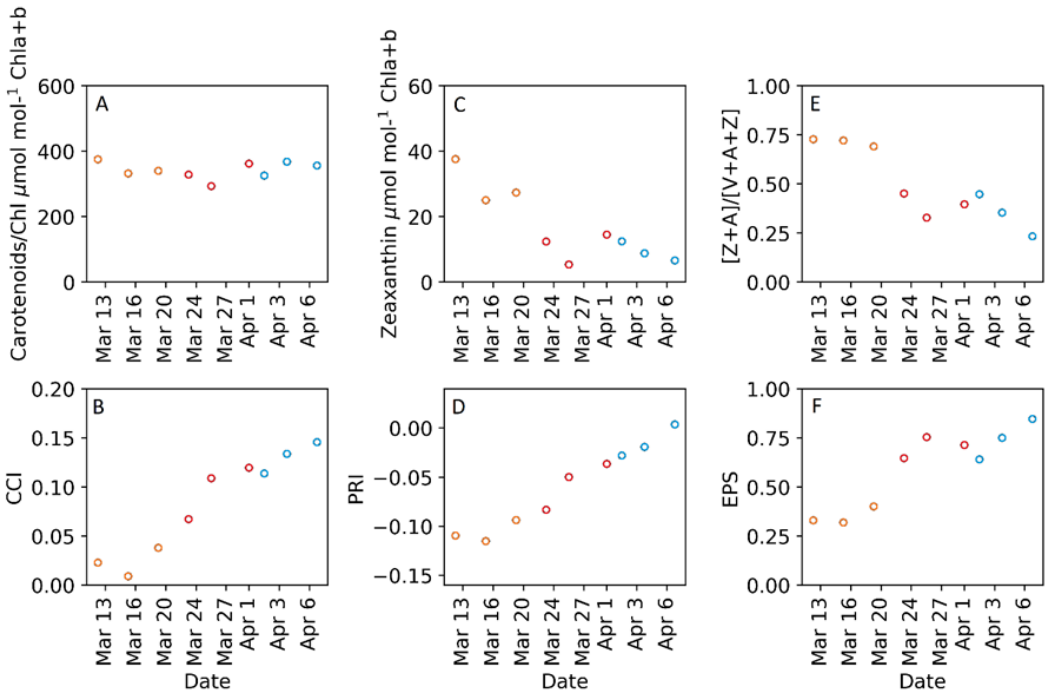

Figure 3-6. Transitional dynamics of (a) total Car/Chl (µmol Car mol^{-1} Chl a+b) , (b) Chlorophyll / Carotenoid index (CCI), (c) Zeaxanthin (µmol mol^{-1} Chl a+b), (d) Photochemical reflectance index (PRI); (e) Xanthophyll cycle conversion state (Z+A/V+A+Z) or sustained photoprotection, (f) EPS((V+0.5A)/(V+A+Z)) in response to a gradual increment in temperature (orange circles = 5°C, red circles = 10°C and light blue circles = 15°C). Samples were pooled, SE not presented.

- Response of SIF parameters and vegetation indices to a gradual increase of temperature while simulating the spring transition.

SIF parameters and Carotenoid-based vegetation indices (CCI and PRI) from black spruce (*P. mariana*) showed a marked variation over the course of the experiment in response to the gradual incrementation in temperature. Both, PRI and CCI (Fig 3-7; A and B), tracked the temperature increment of the experiment very well. These results contrasted with the NDVI index results (Fig 3-7 C), that did not show noticeable variation over the course of the study. On the other hand, the SIF parameters, such as SIF_{total}, $SIF_{yield,}$ $SIF_{yield\ 690nm}$ and $SIF_{yield\ 740\ nm,}$ shown in Fig 3-7 (D,E,F), displayed a parallel increase in values during the initial transition from 5℃ to 15℃ (these temperatures are signaled in the figure by using orange, red and blue markers in all the plots), However, after an initial increase at lower temperatures, we observed a noticeable decrease in SIF metrics with higher temperatures (above 15℃) (Fig. 3-7).

To complement our results and understand better the link between our parameters during the initial temperature transition from 5℃ to 15℃ that simulates the spring recovery, we compared the metrics we had by using Pearson's correlation coefficient [R] and calculated corresponding probability (p) values. These results are shown below in the Table 3.2. We found that all the SIF parameters exhibited significant and positive correlations with temperature (R > 0.70***), CCI and PRI metrics were also strongly correlated with temperature (R >0.80***), and from the Chl and Car pigment, EPS was the best correlated to temperature R. > 0.68***).

CCI and PRI exhibited positive and strong significant relationships with SIF *total*. The carotenoid-reflectance indices (PRI and CCI), also exhibited significant and positive correlations with other SIF parameters. For example, $F_{yield\ 690}$ exhibited slightly stronger correlations than F_{yield} and $F_{yield\ 740.}$ The pigment metrics, EPS, Zeaxanthin, and the xanthophyll cycle conversion state

(Z+A/V+A+Z) were well correlated with the $F_{yield\ 690\ \&\ 740nm}$ bands. NDVI was not significantly correlated with the metrics studied, and results are not shown in Table 3.2.

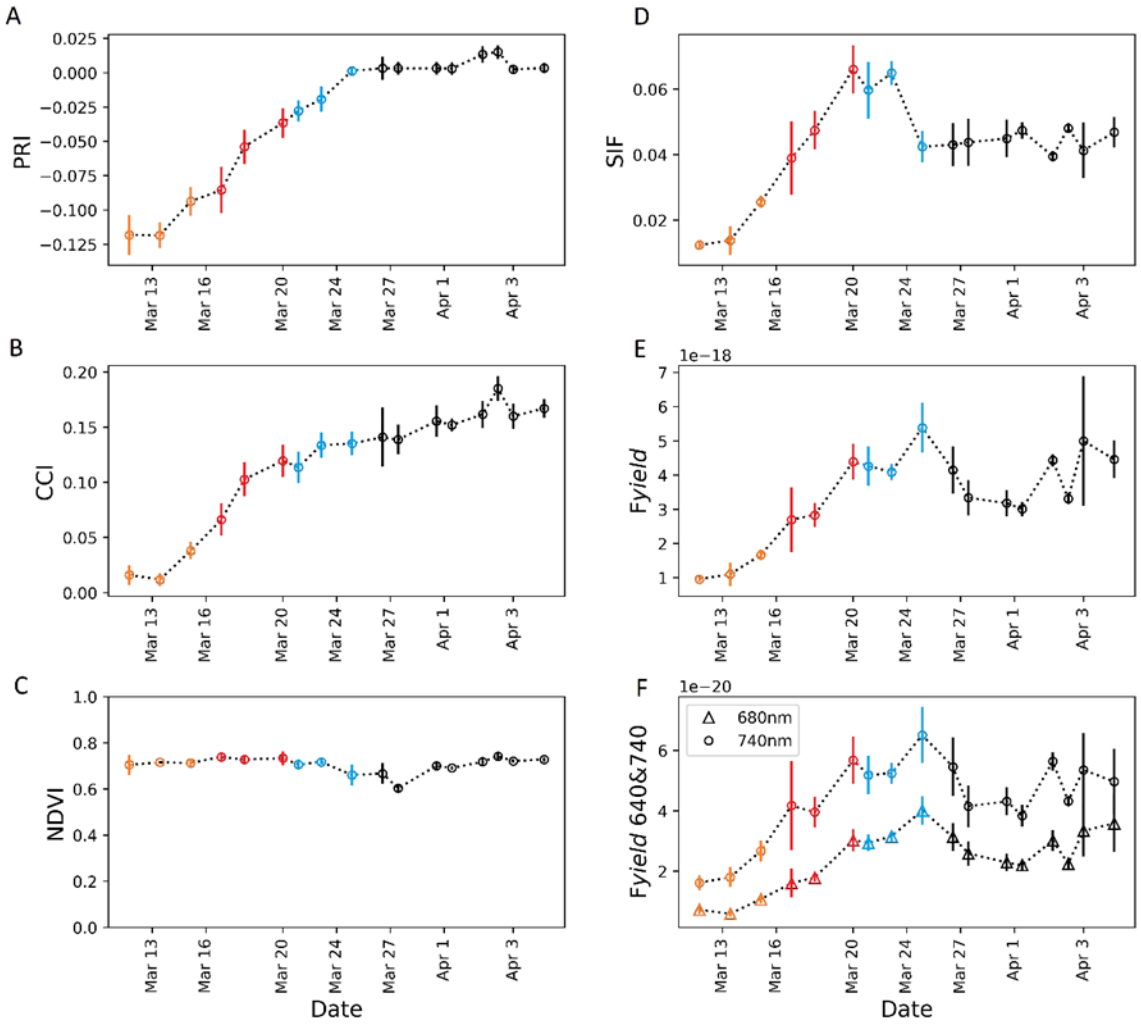

Figure 3-7. Needle-scale dynamic response of three-year old black spruce (P. mariana) individuals to a gradual increase of temperature in a controlled environment, during a simulation of spring transition; a) PRI, (b) CCI Fyield , (c) NDVI, (d) SIFtotal (Wm-2 sr-1nm-1), (e) Fyield and (f) Fyield 690nm (triangles) and Fyield 740nm (circles). Marker colors represent the temperature transition: 5°C – orange, 10°C – red, blue – 15°C, and black : 20-30°C. Vertical lines represent the standard error of the mean (n=6).

Table 3-2. Pearson's [R] correlations between SIF parameters, carotenoid-reflectance indices, and chlorophyll and carotenoid pigments, SIF *total* (Wm^{-2} $sr^{-1}nm^{-1}$); F_{yield} (SIF total/APAR) $F_{yield690}$ (SIF_{690}/APAR), $F_{yield740}$ (SIF_{740}/APAR); VAZ/Chl, ratio of total xanthophylls per total chlorophylls; EPS, Epoxidation State; Z, Zeaxanthin; [Z+A]/[V+A+Z], Xanthophyll cycle conversion state; Photochemical Reflectance Index (PRI) and Chlorophyll/Carotenoid Index (CCI). p value > 0.05: no symbol; p value <0.05: *; p value <0.01: **; p value <0.001: ***.

Temperature interval = 5°C – 15°C.

	T °C	SIF	FY	FY690	FY740	PRI	CCI	VAZ/Chl	EPS	Z	[Z+A]/[V+A+Z]
Temp °C	1										
SIF	0.67***	1									
F_{yield}	0.74***	0.86***	1								
$F_{yield690}$	0.81***	0.78***	0.94***	1							
$F_{yield740}$	0.68***	0.84***	0.96***	0.89***	1						
PRI	0.82***	0.68***	0.78***	0.80***	0.75***	1					
CCI	0.80***	0.67***	0.68***	0.74***	0.68***	0.85***	1				
VAZ/Chl	0.24***	0.30***	0.20***	0.32***	0.13***	0.31***	0.30***	1			
EPS	0.72***	0.53***	0.62***	0.64***	0.61***	0.71***	0.74***	-0.81***	1		
Z	-0.68***	-0.54***	-0.60***	-0.57***	-060***	-0.58***	-0.66***	0.08***	-0.80***	1	
[Z+A]/[V+A+Z]	-0.71***	-0.50***	-0.62***	-0.62***	-0.64***	-0.70***	-0.71***	-0.23***	-0.97**	-0.97***	1

Discussion

In this temperature experiment, we studied the response of evergreen conifer individuals of black spruce (*Picea mariana*) to a gradual increase in temperature similar to what it is experienced in nature during spring recovery, but under more controlled conditions provided by a growth chamber. Our goal was to compare and validate the performance and relationship of optical metrics and pigment content while simulating the spring recovery phenology stage. Overall, our results indicate that PRI (reversible xanthophyll cycle or NPQ) and CCI (non-reversible xanthophyll cycle/sustained NPQ) are outstanding indicators of the spring transition for black spruce (*P. mariana*). These indices were strongly related to temperature (over the full temperature range from 5 to 30 degrees C) and to fluorescence metrics (only between 5 to 15 degrees C). We were able to corroborate that these indices are also sensitive to variations in xanthophyll cycle pigments in response to increasing temperatures. These indices are clearly driven by reflectance changes in the dynamic 531 nm reflectance band (figure 3-5), a key wavelength that has been shown to correlate both with both photosynthetic light-use efficiency and with the epoxidation state of the xanthophyll cycle pigments (Gamon et al. 1992; Gamon et al. 1993)

We detected a clear division in temperature responses, between two thermal periods, 5°C to 15°C, and 15°C to 30°C. In the first period, PRI, CCI and SIF metrics all increased sharply with the increment in temperature. These observations indicated the reactivation of the rapidly-reversible xanthophyll cycle, as indicated by the decline in leaf levels of zeaxanthin, and by the increased epoxidation state of the xanthophyll cycle pigments (figure 3-7). These results are consistent with a relaxation of the (wintertime) xanthophyll cycle (sustained NPQ) from a de-epoxidized winter state to an active summer state that has been observed under natural conditions during spring activation in evergreen conifers (Öquist & Huner, 2003; Demmig-Adams & Adams,

2006). Parallel to these results obtained for pigments and pigment indices during the same temperature period (5-15°C), we observed clear changes in SIF parameters. The SIF*total,* Red-SIF and Far-Red-SIF bands increased progressively, suggesting the reactivation of the photosystem II activity. These increases in SIF metrics during spring recovery are consistent with recent work presented by (Magney et al. 2016; Springer et al. 2017 and Pierrat et al. 2021). These optical metrics based on fluorescence and reflectance function as indicators of the onset of photosynthesis (similar to the spring recovery period under natural conditions), as has been previously observed by Walther et al. (2016) and Luus et al.(2017) using SIF satellite scale data or leaf-level studies. Interestingly, above 15 degrees C, the SIF metrics failed to track either the temperature changes or the pigment changes as is discussed further below.

In contrast with the remarkable performance of SIF parameters and carotenoid-sensitive vegetation indices (PRI and CCI) in tracking the gradual increase in temperature (5-15°C), NDVI results were relatively invariant, suggesting little to no change in Chl pigment levels or leaf structure during the experiment. This finding is consistent with the chlorophyll/carotenoid pigment ratios, which were relatively stable during this experiment (figure 3-7A). This failure of NDVI to track seasonal change in physiology for evergreen conifers is consistent with a large body of literature reporting the inability of NDVI to track photosynthesis in evergreens (Gamon et al. 1995; Gamon et al. 2016; Magney et al. 2019)

In the case of pigment concentration (during periods when air temperatures ranged from 5°C to 15°C), we observed a strong seasonal variation in the xanthophyll cycle pigment conversion state (Z+A/VAZ). These values went from winter values (higher values) to spring values (lower values), showing a clear relaxation of the sustained wintertime xanthophyll cycle pigment state

(between 5°C and 15°C). The Zeaxanthin pigment concentration followed the same pattern as (Z+A/VAZ), with the highest levels when air temperature was ~ 5°C and lowest levels when it was ~ 15°C. These results were expected because, during spring recovery, the process of winter downregulation starts to reverse, and this process includes a reduction of photoprotective xanthophyll cycle pigments, especially the zeaxanthin pigment (Ottander et al. 1995; Hüner et al. 1998; Öquist and Hüner, 2003; Adams et al. 2004; Ensminger et al. 2004; Demmig-Adams and Adams, 2006). Unlike other studies (Wong and Gamon 2015; Gamon et al. 2016), we observed that the overall Chl:Car ratio did not show changes during this first period. It is possible that this phenomenon of changing Chl:Car ratio does not always occur and may be temperature or species dependent. Walter-McNeill et al. (2021) obtained similar results, in a common-garden experiment. They reported that seasonal differences in needle Chlorophyll content in most of the (30) evergreen conifer individuals sampled (49) did not exhibit a significant change. It is also possible that the relatively compressed time period or constraints of potted culture with no nutrient addition limited the ability for pigment synthesis which might have affected this result. This finding has important implications in the interpretation of remotely sensed SIF. Many studies suggest that SIF is driven primarily by seasonal changes in photosynthetic activity associated with absorbed radiation and chlorophyll content (Rascher et al. 2015; Magney et al. 2019). However, our results indicate that, at least for evergreens during spring transition, this change in fluorescence activity is driven primarily by changes in regulatory processes associated with xanthophyll cycle activity. Clearly, in our study, SIF dynamics cannot be explained by trends in NDVI or seasonal chlorophyll content.

In our needle-scale SIF results related to temperature, we observed a clear increase in SIF bands during the 5-10°C and 10°C- 15°C intervals. The second stage of these experiments can be

visualized as the results we obtained between 15℃ to 30℃. During this period, we found that SIF metrics clearly disconnected from the temperature increase, while reflectance-based indices (CCI and PRI) continued to change. Recent work by Yang et al. (2022) using tower-based data, suggests that SIF becomes less dependent on temperature after the spring, when other environmental factors come into play. Apparently, SIF parameters, while closely correlated with CCI and PRI at colder temperatures (5-15 degrees C), later decoupled from CCI and PRI during this period when temperatures were in the 15℃ - 30℃ range. The exact cause of the divergence of SIF parameters from temperature and related photoprotective mechanisms in this second experiment remains unknown. However, it is possible that slight water stress occurred at these higher temperatures (20-30℃), and that this might have affected SIF and pigment responses in slightly different ways. Soil moisture (SM) deficit and vapour pression deficit (VPD) are key factors that can increase or decrease photosynthetic activity (Yu et al. 2022). These contrasting results show the necessity for more leaf-level experiments, through which we can explore the responses of SIF and carotenoid-based indices to additional environmental drivers, including SM and VPD, in addition to temperature. Within the context of global climate change, a rise in vapor pressure deficit (VPD) (Green et al. 2020; Yuan et al. 2019) and soil moisture deficit (Deng et al. 2020; Dorigo et al. 2012) may limit plant photosynthesis and carbon uptake. Further mechanistic leaf-level experiments are needed, and this topic should remain an active area of research.

Our results support a body of literature that demonstrates that remotely sensed vegetation tools, such as PRI and CCI, are sensitive to temperature and seasonal changes in foliar carotenoid and xanthophyll cycle pigment content and activity (Wong and Gamon, 2015; Gamon et al. 2016; Seyednasrollah et al. 2020; Yang et al. 2022). As such, they may be generally useful for tracking and quantifying the “invisible” seasonal changes in pigment content across evergreen conifer tree

species. Besides this, our findings provide important information that can be used in future interpretations of SIF and carotenoid reflectance-based vegetation indices in various spatial and temporal domains. Such leaf-level mechanistic understanding is fundamental to support the interpretation of SIF data obtained using global remote sensing technology, designed to measure entire ecosystems, such as the upcoming FLuorescence EXplorer (FLEX) mission of the European Space Agency (ESA) (Kraft et al. 2017). The Boreal ecosystem is a major contributor to the global climate system. Thus, reducing uncertainties in the timing and drivers of the spring transition could generate a better understanding of how this biome is responding to a changing climate, and how it may in turn affect climate.

Literature cited

Adams III, W. W., & Demmig-Adams, B. (1994). Carotenoid composition and down regulation of photosystem II in three conifer species during the winter. *Physiologia Plantarum*, *92*(3), 451–458. https://doi.org/https://doi.org/10.1111/j.1399-3054.1994.tb08835.x

Bandopadhyay, S., Rastogi, A., & Juszczak, R. (2020). Review of Top-of-Canopy Sun-Induced Fluorescence (SIF) Studies from Ground, UAV, Airborne to Spaceborne Observations. *Sensors* , Vol. 20. https://doi.org/10.3390/s20041144

Berra, E. F., & Gaulton, R. (2021). Remote sensing of temperate and boreal forest phenology: A review of progress, challenges and opportunities in the intercomparison of in-situ and satellite phenological metrics. *Forest Ecology and Management*, *480*, 118663. https://doi.org/https://doi.org/10.1016/j.foreco.2020.118663

Demmig-Adams, B, & Adams, W. W. (1992). Photoprotection and Other Responses of Plants to High Light Stress. *Annual Review of Plant Physiology and Plant Molecular Biology*, *43*(1), 599–626. https://doi.org/10.1146/annurev.pp.43.060192.003123

Demmig-Adams, Barbara, & Adams, W. W. (1996). The role of xanthophyll cycle carotenoids in the protection of photosynthesis. *Trends in Plant Science*, *1*(1), 21–26. https://doi.org/https://doi.org/10.1016/S1360-1385(96)80019-7

Gamon, J A, Peñuelas, J., & Field, C. B. (1992). A narrow-waveband spectral index that tracks diurnal changes in photosynthetic efficiency. *Remote Sensing of Environment*, *41*(1), 35–44. https://doi.org/https://doi.org/10.1016/0034-4257(92)90059-S

Gamon, John A, Field, C. B., Goulden, M. L., Griffin, K. L., Hartley, A. E., Joel, G., … Valentini, R. (1995). Relationships Between NDVI, Canopy Structure, and Photosynthesis in Three Californian Vegetation Types. *Ecological Applications*, *5*(1), 28–41. https://doi.org/10.2307/1942049

Gillies, S. L., & Vidaver, W. (1990). Resistance to photodamage in evergreen conifers. *Physiologia Plantarum*, *80*(1), 148–153. https://doi.org/10.1111/j.1399-3054.1990.tb04389.x

Jeong, S.-J., Schimel, D., Frankenberg, C., Drewry, D. T., Fisher, J. B., Verma, M., … Joiner, J. (2017).

Application of satellite solar-induced chlorophyll fluorescence to understanding large-scale variations in vegetation phenology and function over northern high latitude forests. *Remote Sensing of Environment*, *190*, 178–187. https://doi.org/https://doi.org/10.1016/j.rse.2016.11.021

Kraft, S., Bello, U. Del, Harnisch, B., Bouvet, M., Drusch, M., & Bézy, J.-L. (2017). Fluorescence imaging spectrometer concepts for the Earth explorer mission candidate flex. *Proc.SPIE*, *10564*. https://doi.org/10.1117/12.2309086

Louis, J., Ounis, A., Ducruet, J.-M., Evain, S., Laurila, T., Thum, T., … Moya, I. (2005). Remote sensing of sunlight-induced chlorophyll fluorescence and reflectance of Scots pine in the boreal forest during spring recovery. *Remote Sensing of Environment*, *96*(1), 37–48. https://doi.org/https://doi.org/10.1016/j.rse.2005.01.013

Luus, K. A., Commane, R., Parazoo, N. C., Benmergui, J., Euskirchen, E. S., Frankenberg, C., … Lin, J. C. (2017). Tundra photosynthesis captured by satellite-observed solar-induced chlorophyll fluorescence. *Geophysical Research Letters*, *44*(3), 1564–1573. https://doi.org/10.1002/2016GL070842

Magney, T., R. Bowling, D., A. Logan, B., Großmann, K., Stutz, J., D. Blanken, P., … Frankenberg, C. (2019). Mechanistic evidence for tracking the seasonality of photosynthesis with solar-induced fluorescence. *Proceedings of the National Academy of Sciences of the United States of America*. https://doi.org/10.1073/pnas.1900278116

Montgomery, R. A., Rice, K. E., Stefanski, A., Rich, R. L., & Reich, P. B. (2020). Phenological responses of temperate and boreal trees to warming depend on ambient spring temperatures, leaf habit, and geographic range. *Proceedings of the National Academy of Sciences*, *117*(19), 10397 LP – 10405. https://doi.org/10.1073/pnas.1917508117

Nichol, J. C., Drolet, G., Porcar-Castell, A., Wade, T., Sabater, N., Middleton, M. E., … Atherton, J. (2019). Diurnal and Seasonal Solar Induced Chlorophyll Fluorescence and Photosynthesis in a Boreal Scots Pine Canopy. *Remote Sensing* , Vol. 11. https://doi.org/10.3390/rs11030273

Öquist, G., & Huner, N. P. A. (2003). Photosynthesis of Overwintering Evergreen Plants. *Annual Review of Plant Biology*, *54*(1), 329–355. https://doi.org/10.1146/annurev.arplant.54.072402.115741

Pierrat, Z., Magney, T., Parazoo, N., Grossmann, K., Bowling, D., Seibt, U., … Stutz, J. (2022). Diurnal and seasonal dynamics of solar-induced chlorophyll fluorescence, vegetation indices, and gross primary productivity in the boreal forest. *Journal of Geophysical Research: Biogeosciences*. https://doi.org/10.1029/2021JG006588

Pierrat, Z., Nehemy, M., Roy, A., Magney, T., Parazoo, N., Laroque, C., … Stutz, J. (2021). Tower-Based Remote Sensing Reveals Mechanisms Behind a Two-phased Spring Transition in a Mixed-Species Boreal Forest. *Journal of Geophysical Research: Biogeosciences*, *126*. https://doi.org/10.1029/2020JG006191

R. Springer, K., Wang, R., & Gamon, J. (2017). Parallel Seasonal Patterns of Photosynthesis, Fluorescence, and Reflectance Indices in Boreal Trees. In *Remote Sensing* (Vol. 9). https://doi.org/10.3390/rs9070691

Raczka, B., Porcar-Castell, A., Magney, T., Lee, J. E., Köhler, P., Frankenberg, C., … Bowling, D. R. (2019). Sustained Nonphotochemical Quenching Shapes the Seasonal Pattern of Solar-Induced Fluorescence at a High-Elevation Evergreen Forest. *Journal of Geophysical Research: Biogeosciences*, *124*(7), 2005–2020. https://doi.org/https://doi.org/10.1029/2018JG004883

Rajewicz, A. P., Atherton, J., Alonso, L., & Porcar-Castell, A. (2019). Leaf-Level Spectral Fluorescence

Measurements: Comparing Methodologies for Broadleaves and Needles. *Remote Sensing* , Vol. 11. https://doi.org/10.3390/rs11050532

Rascher, U., Alonso, L., Burkart, A., Cilia, C., Cogliati, S., Colombo, R., … Zemek, F. (2015). Sun-induced fluorescence – a new probe of photosynthesis: First maps from the imaging spectrometer HyPlant. *Global Change Biology*, *21*(12), 4673–4684. https://doi.org/https://doi.org/10.1111/gcb.13017

Siegmann, B., Cendrero-Mateo, M. P., Cogliati, S., Damm, A., Gamon, J., Herrera, D., … Rascher, U. (2021). Downscaling of far-red solar-induced chlorophyll fluorescence of different crops from canopy to leaf level using a diurnal data set acquired by the airborne imaging spectrometer HyPlant. *Remote Sensing of Environment*, *264*, 112609. https://doi.org/https://doi.org/10.1016/j.rse.2021.112609

van der Tol, C., Rossini, M., Cogliati, S., Verhoef, W., Colombo, R., Rascher, U., & Mohammed, G. (2016). A model and measurement comparison of diurnal cycles of sun-induced chlorophyll fluorescence of crops. *Remote Sensing of Environment*, *186*, 663–677. https://doi.org/https://doi.org/10.1016/j.rse.2016.09.021

Verhoeven, A. (2014). Sustained energy dissipation in winter evergreens. *New Phytologist*, *201*(1), 57–65. https://doi.org/10.1111/nph.12466

Walter-McNeill, A., Garcia, M. A., Logan, B. A., Bombard, D. M., Reblin, J. S., Lopez, S., … Bowling, D. R. (2021). Wide variation of winter-induced sustained thermal energy dissipation in conifers: a common-garden study. *Oecologia*. https://doi.org/10.1007/s00442-021-05038-y

Walther, S., Voigt, M., Thum, T., Gonsamo, A., Zhang, Y., Köhler, P., … Guanter, L. (2016). Satellite chlorophyll fluorescence measurements reveal large-scale decoupling of photosynthesis and greenness dynamics in boreal evergreen forests. *Global Change Biology*, *22*(9), 2979–2996. https://doi.org/10.1111/gcb.13200

Wieneke, S., Ahrends, H., Damm, A., Pinto, F., Stadler, A., Rossini, M., & Rascher, U. (2016). Airborne based spectroscopy of red and far-red sun-induced chlorophyll fluorescence: Implications for improved estimates of gross primary productivity. *Remote Sensing of Environment*, *184*, 654–667. https://doi.org/https://doi.org/10.1016/j.rse.2016.07.025

Wong, C. Y. S., D'Odorico, P., Bhathena, Y., Arain, M. A., & Ensminger, I. (2019). Carotenoid based vegetation indices for accurate monitoring of the phenology of photosynthesis at the leaf-scale in deciduous and evergreen trees. *Remote Sensing of Environment*, *233*, 111407. https://doi.org/https://doi.org/10.1016/j.rse.2019.111407

Yang, J. C., Magney, T. S., Albert, L. P., Richardson, A. D., Frankenberg, C., Stutz, J., … Bowling, D. R. (2022). Gross primary production (GPP) and red solar induced fluorescence (SIF) respond differently to light and seasonal environmental conditions in a subalpine conifer forest. *Agricultural and Forest Meteorology*, *317*, 108904. https://doi.org/https://doi.org/10.1016/j.agrformet.2022.108904

Yu, T., Jiapaer, G., Bao, A., Zheng, G., Zhang, J., Li, X., … Umuhoza, J. (2022). Disentangling the relative effects of soil moisture and vapor pressure deficit on photosynthesis in dryland Central Asia. *Ecological Indicators*, *137*, 108698. https://doi.org/https://doi.org/10.1016/j.ecolind.2022.108698

Chapter 4 – General conclusions and future work

The present study provides strong evidence that during the spring recovery, SIF parameters, and carotenoid reflectance-based vegetation indices are closely tied to temperature changes and positively correlated with each other. Most important, we confirmed that two dominant conifer species from the boreal forest, present slightly different timing in their spring recovery of photosynthetic activity and in the related optical metrics (PRI, CCI and SIF metrics). While photosynthesis was not directly measured due to logistical constraints, we were able to track the relative-timing of the photosynthetic reactivation of both species during the spring recovery and we gained knowledge about how these two conifer species' metrics differ slightly in kinetics, in particular the activation of SIF emission, which was earlier in lodgepole pine (*P. contorta)* (starting under lower temperatures) than in black spruce (*P. mariana*).

We learned from our results that Sun induced chlorophyll fluorescence (SIF), is a reliable optical method for detecting spring transition. However, after the spring transition, the SIF signal became more variable and apparently decoupled from Chl:Car reflectance indices (CCI and PRI) and temperature. These confounding effects require further research to clarify the physiological and biological mechanisms driving the SIF fluorescence signal in different conditions, species, and ecosystems. In addition, as expected, NDVI failed to represent the spring recovery transition, showing that SIF and carotenoid reflectance-based indices are critical assets to improve the detection and monitoring of carbon cycle dynamics in evergreen forests.

Finally, we recommend the use of this combined methodology of proximal remote sensing tools to track and monitor evergreen conifers, we also encourage future studies to incorporate the carotenoid pigment content quantification to validate PRI and CCI. Together these remote sensing tools may offer a powerful means to monitor photosynthesis and phenology not only from a needle-

scale perspective but also from a canopy and satellite scale perspective. The metrics studied here can also be observed from different platforms and can be used not only to explore the phenology and physiological responses of evergreen conifers trees but also a diversity of natural ecosystems and crops. We suggest that future research on SIF could explore how the signal responds to other variables such as APAR, VPD and SWC after the spring transition.

Comprehensive bibliography

Adams III, W. W., & Demmig-Adams, B. (1994). Carotenoid composition and down regulation of photosystem II in three conifer species during the winter. *Physiologia Plantarum*, *92*(3), 451–458. https://doi.org/https://doi.org/10.1111/j.1399-3054.1994.tb08835.x

Allen, M., Barros, V., Broome, J., Cramer, W., Christ, R., Church, J., … Yohe, G. (2014). *{IPCC fifth assessment synthesis report - Climate Change 2014 synthesis report}* (P. Aldunce, T. Downing, S. Joussaume, Z. Kundzewicz, J. Palutikof, J. Skea, … Z. Xiao-Ye, eds.). Retrieved from citeulike-article-id:13416115

Angert, A., Biraud, S., Bonfils, C., Henning, C., Buermann, W., Pinzon, J., … Fung, I. (2005). Drier summers cancel out the CO_2 uptake enhancement induced by warmer springs. *Proceedings of the National Academy of Sciences of the United States of America*, *102*, 10823–10827. https://doi.org/10.1073/pnas.0501647102

Astrup, R., Bernier, P. Y., Genet, H., Lutz, D. A., & Bright, R. M. (2018). A sensible climate solution for the boreal forest. *Nature Climate Change*, *8*(1), 11–12. https://doi.org/10.1038/s41558-017-0043-3

Bandopadhyay, S., Rastogi, A., & Juszczak, R. (2020). Review of Top-of-Canopy Sun-Induced Fluorescence (SIF) Studies from Ground, UAV, Airborne to Spaceborne Observations. *Sensors* , Vol. 20. https://doi.org/10.3390/s20041144

Barichivich, J., Briffa, K. R., Myneni, R. B., Osborn, T. J., Melvin, T. M., Ciais, P., … Tucker, C. (2013). Large-scale variations in the vegetation growing season and annual cycle of atmospheric CO2 at high northern latitudes from 1950 to 2011. *Global Change Biology*, *19*(10), 3167–3183. https://doi.org/10.1111/gcb.12283

Berra, E. F., & Gaulton, R. (2021). Remote sensing of temperate and boreal forest phenology: A review of progress, challenges and opportunities in the intercomparison of in-situ and satellite phenological metrics. *Forest Ecology and Management*, *480*, 118663. https://doi.org/https://doi.org/10.1016/j.foreco.2020.118663

Bowling, D., Frankenberg, C., Logan, B., & G. J. G. 2019. (n.d.). *Collaborative Proposal: MRA: Seasonality of photosynthesis of temperate and boreal conifer forests across North America.*

Bowling, D., Logan, B., Hufkens, K., Aubrecht, D., Richardson, A., Burns, S., … Eiriksson, D. (2018). Limitations to winter and spring photosynthesis of a Rocky Mountain subalpine forest. *Agricultural and Forest Meteorology*, *252*, 241–255. https://doi.org/10.1016/j.agrformet.2018.01.025

Buermann, W., Forkel, M., O'Sullivan, M., Sitch, S., Friedlingstein, P., Haverd, V., … Richardson, A. D. (2018). Widespread seasonal compensation effects of spring warming on northern plant productivity. *Nature*, *562*(7725), 110–114. https://doi.org/10.1038/s41586-018-0555-7

Busch, F., Huner, N., & Ensminger, I. (2009). Biochemical constrains limit the potential of the photochemical reflectance index as a predictor of effective quantum efficiency of photosynthesis during the winter spring transition in Jack pine seedlings. *Functional Plant Biology*, *36*. https://doi.org/10.1071/FP08043

Butler, W., & Strasser, R. (1977). Tripartite model for the photochemical apparatus of green plant photosynthesis. *Proceedings of the National Academy of Sciences of the United States of America*, *74*, 3382–3385. https://doi.org/10.1073/pnas.74.8.3382

Chapin, F. S., Sturm, M., Serreze, M. C., McFadden, J. P., Key, J. R., Lloyd, A. H., … Welker, J. M.

(2005). Role of Land-Surface Changes in Arctic Summer Warming. *Science*, *310*(5748), 657 LP – 660. https://doi.org/10.1126/science.1117368

Demmig-Adams, B, & Adams, W. W. (1992). Photoprotection and Other Responses of Plants to High Light Stress. *Annual Review of Plant Physiology and Plant Molecular Biology*, *43*(1), 599–626. https://doi.org/10.1146/annurev.pp.43.060192.003123

Demmig-Adams, Barbara, & Adams, W. W. (1996a). The role of xanthophyll cycle carotenoids in the protection of photosynthesis. *Trends in Plant Science*, *1*(1), 21–26. https://doi.org/10.1016/S1360-1385(96)80019-7

Demmig-Adams, Barbara, & Adams, W. W. (1996b). The role of xanthophyll cycle carotenoids in the protection of photosynthesis. *Trends in Plant Science*, *1*(1), 21–26. https://doi.org/https://doi.org/10.1016/S1360-1385(96)80019-7

Drusch, M., Moreno, J., Del Bello, U., Franco, R., Goulas, Y., Huth, A., … Verhoef, W. (2016). The FLuorescence EXplorer Mission Concept-ESA's Earth Explorer 8. *IEEE Transactions on Geoscience and Remote Sensing*, *PP*, 1–12. https://doi.org/10.1109/TGRS.2016.2621820

Du, S., Liu, L., Liu, X., & Hu, J. (2017). Response of Canopy Solar-Induced Chlorophyll Fluorescence to the Absorbed Photosynthetically Active Radiation Absorbed by Chlorophyll. *Remote Sensing* , Vol. 9. https://doi.org/10.3390/rs9090911

Estiarte, M., & Peñuelas, J. (2015). Alteration of the phenology of leaf senescence and fall in winter deciduous species by climate change: effects on nutrient proficiency. *Global Change Biology*, *21*(3), 1005–1017. https://doi.org/10.1111/gcb.12804

Francis, J., & Skific, N. (2015). Evidence linking rapid Arctic warming to mid-latitude weather patterns. *Philosophical Transactions. Series A, Mathematical, Physical, and Engineering Sciences*, *373*. https://doi.org/10.1098/rsta.2014.0170

Frankenberg, C., B. Fisher, J., Worden, J., Badgley, G., Saatchi, S., Lee, J.-E., … Yokota, T. (2011). New global observations of the terrestrial carbon cycle from GOSAT: Patterns of plant fluorescence with gross primary productivity. In *GEOPHYSICAL RESEARCH LETTERS* (Vol. 38). https://doi.org/10.1029/2011GL048738

Fréchette, E., Wong, C., Junker-Frohn, L., Chang, C., & Ensminger, I. (2015). Zeaxanthin-independent energy quenching and alternative electron sinks cause a decoupling of the relationship between the photochemical reflectance index (PRI) and photosynthesis in an evergreen conifer during spring. *Journal of Experimental Botany*, *66*. https://doi.org/10.1093/jxb/erv427

Friedl, M. A., Gray, J. M., Melaas, E. K., Richardson, A. D., Hufkens, K., Keenan, T. F., … O'Keefe, J. (2014). A tale of two springs: using recent climate anomalies to characterize the sensitivity of temperate forest phenology to climate change. *Environmental Research Letters*, *9*(5), 54006. https://doi.org/10.1088/1748-9326/9/5/054006

Friedman, A. R., Hwang, Y.-T., Chiang, J. C. H., & Frierson, D. M. W. (2013). Interhemispheric Temperature Asymmetry over the Twentieth Century and in Future Projections. *Journal of Climate*, *26*(15), 5419–5433. https://doi.org/10.1175/JCLI-D-12-00525.1

Gamon, J., Fred Huemmrich, K., Wong, C., Ensminger, I., Garrity, S., Y. Hollinger, D., … Penuelas, J. (2016). A remotely sensed pigment index reveals photosynthetic phenology in evergreen conifers. In *Proceedings of the National Academy of Sciences* (Vol. 113). https://doi.org/10.1073/pnas.1606162113

Gamon, J A, Peñuelas, J., & Field, C. B. (1992). A narrow-waveband spectral index that tracks diurnal

changes in photosynthetic efficiency. *Remote Sensing of Environment*, *41*(1), 35–44. https://doi.org/https://doi.org/10.1016/0034-4257(92)90059-S

Gamon, J A, Serrano, L., & Surfus, J. S. (1997). The Photochemical Reflectance Index: An Optical Indicator of Photosynthetic Radiation Use Efficiency across Species, Functional Types, and Nutrient Levels. *Oecologia*, *112*(4), 492–501. Retrieved from http://www.jstor.org/stable/4221805

Gamon, John A, & Berry, J. A. (2012). Facultative and constitutive pigment effects on the Photochemical Reflectance Index (PRI) in sun and shade conifer needles. *Israel Journal of Plant Sciences*, *60*(1–2), 85–95. https://doi.org/10.1560/IJPS.60.1-2.85

Gamon, John A, & Bond, B. (2013). Effects of irradiance and photosynthetic downregulation on the photochemical reflectance index in Douglas-fir and ponderosa pine. *Remote Sensing of Environment*, *135*, 141–149. https://doi.org/https://doi.org/10.1016/j.rse.2013.03.032

Gamon, John A, Field, C. B., Goulden, M. L., Griffin, K. L., Hartley, A. E., Joel, G., … Valentini, R. (1995). Relationships Between NDVI, Canopy Structure, and Photosynthesis in Three Californian Vegetation Types. *Ecological Applications*, *5*(1), 28–41. https://doi.org/10.2307/1942049

Gauthier, S., Bernier, P., Kuuluvainen, T., Shvidenko, A. Z., & Schepaschenko, D. G. (2015). Boreal forest health and global change. *Science*, *349*(6250), 819 LP – 822. https://doi.org/10.1126/science.aaa9092

Gillies, S. L., & Vidaver, W. (1990). Resistance to photodamage in evergreen conifers. *Physiologia Plantarum*, *80*(1), 148–153. https://doi.org/10.1111/j.1399-3054.1990.tb04389.x

Gilmore, A. M., & Yamamoto, H. Y. (1993). Linear models relating xanthophylls and lumen acidity to non-photochemical fluorescence quenching. Evidence that antheraxanthin explains zeaxanthin-independent quenching. *Photosynthesis Research*, *35*(1), 67–78. https://doi.org/10.1007/BF02185412

Gitelson, A. A., & Gamon, J. A. (2015). The need for a common basis for defining light-use efficiency: Implications for productivity estimation. *Remote Sensing of Environment*, *156*, 196–201. https://doi.org/https://doi.org/10.1016/j.rse.2014.09.017

Goetz, S., Bunn, A., Fiske, G., & Houghton, R. (2005). Satellite-observed photosynthetic trends across boreal North America associated with climate and fire disturbance. In *Proceedings of the National Academy of Sciences of the United States of America* (Vol. 102). https://doi.org/10.1073/pnas.0506179102

Gonsamo, A., Chen, J. M., & Ooi, Y. W. (2018). Peak season plant activity shift towards spring is reflected by increasing carbon uptake by extratropical ecosystems. *Global Change Biology*, *24*(5), 2117–2128. https://doi.org/10.1111/gcb.14001

Hänninen, H. (2016). *Boreal and Temperate Trees in a Changing Climate*. https://doi.org/10.1007/978-94-017-7549-6

Hari, P., & Kulmala, L. (2009). Boreal Forest and Climate Change. In *Advances in Global Change Research*. https://doi.org/10.1007/978-1-4020-8718-9_9

Hogg, E. H. (Ted), Brandt, J. P., & Michaelian, M. (2008). Impacts of a regional drought on the productivity, dieback, and biomass of western Canadian aspen forests. *Canadian Journal of Forest Research*, *38*(6), 1373–1384. https://doi.org/10.1139/X08-001

Huner, N., Öquist, G., & Melis, A. (2003). Photostasis in Plants, Green Algae and Cyanobacteria: The Role of Light Harvesting Antenna Complexes. In *Light-Harvesting Antennas in Photosynthesis*

(Vol. 13, pp. 401–421). https://doi.org/10.1007/978-94-017-2087-8_14

Huner, N. P. A., Öquist, G., & Sarhan, F. (1998). Energy balance and acclimation to light and cold. *Trends in Plant Science*, *3*(6), 224–230. https://doi.org/https://doi.org/10.1016/S1360-1385(98)01248-5

Jeong, S.-J., Schimel, D., Frankenberg, C., Drewry, D. T., Fisher, J. B., Verma, M., … Joiner, J. (2017). Application of satellite solar-induced chlorophyll fluorescence to understanding large-scale variations in vegetation phenology and function over northern high latitude forests. *Remote Sensing of Environment*, *190*, 178–187. https://doi.org/https://doi.org/10.1016/j.rse.2016.11.021

Joiner, J., Yoshida, Y., Vasilkov, A. P., Yoshida, Y., Corp, L. A., & Middleton, E. M. (2011). First observations of global and seasonal terrestrial chlorophyll fluorescence from space. *Biogeosciences*, *8*(3), 637–651. https://doi.org/10.5194/bg-8-637-2011

Keenan, R. J., Reams, G. A., Achard, F., de Freitas, J. V, Grainger, A., & Lindquist, E. (2015). Dynamics of global forest area: Results from the FAO Global Forest Resources Assessment 2015. *Forest Ecology and Management*, *352*, 9–20. https://doi.org/https://doi.org/10.1016/j.foreco.2015.06.014

Kraft, S., Bello, U. Del, Harnisch, B., Bouvet, M., Drusch, M., & Bézy, J.-L. (2017). Fluorescence imaging spectrometer concepts for the Earth explorer mission candidate flex. *Proc.SPIE*, *10564*. https://doi.org/10.1117/12.2309086

La Roi, G. H. (1967). Ecological Studies in the Boreal Spruce-Fir Forests of the North American Taiga. I. Analysis of the Vascular Flora. *Ecological Monographs*, *37*(3), 229–253. https://doi.org/10.2307/1948439

Lian, X., Piao, S., Li, L. Z. X., Li, Y., Huntingford, C., Ciais, P., … McVicar, T. R. (2020). Summer soil drying exacerbated by earlier spring greening of northern vegetation. *Science Advances*, *6*(1), eaax0255. https://doi.org/10.1126/sciadv.aax0255

Linkosalo, T., Heikkinen, J., Pulkkinen, P., & Mäkipää, R. (2014). Fluorescence measurements show stronger cold inhibition of photosynthetic light reactions in Scots pine compared to Norway spruce as well as during spring compared to autumn . *Frontiers in Plant Science* , Vol. 5. Retrieved from https://www.frontiersin.org/article/10.3389/fpls.2014.00264

Louis, J., Ounis, A., Ducruet, J.-M., Evain, S., Laurila, T., Thum, T., … Moya, I. (2005). Remote sensing of sunlight-induced chlorophyll fluorescence and reflectance of Scots pine in the boreal forest during spring recovery. *Remote Sensing of Environment*, *96*(1), 37–48. https://doi.org/https://doi.org/10.1016/j.rse.2005.01.013

Luus, K. A., Commane, R., Parazoo, N. C., Benmergui, J., Euskirchen, E. S., Frankenberg, C., … Lin, J. C. (2017). Tundra photosynthesis captured by satellite-observed solar-induced chlorophyll fluorescence. *Geophysical Research Letters*, *44*(3), 1564–1573. https://doi.org/10.1002/2016GL070842

Magney, T., R. Bowling, D., A. Logan, B., Großmann, K., Stutz, J., D. Blanken, P., … Frankenberg, C. (2019). Mechanistic evidence for tracking the seasonality of photosynthesis with solar-induced fluorescence. *Proceedings of the National Academy of Sciences of the United States of America*. https://doi.org/10.1073/pnas.1900278116

Manabe, S., Stouffer, R. J., Spelman, M. J., & Bryan, K. (1991). Transient Responses of a Coupled Ocean–Atmosphere Model to Gradual Changes of Atmospheric CO2. Part I. Annual Mean Response. *Journal of Climate*, *4*(8), 785–818. https://doi.org/10.1175/1520-0442(1991)004<0785:TROACO>2.0.CO;2

Meroni, M., Rossini, M., Guanter, L., Alonso, L., Rascher, U., Colombo, R., & Moreno, J. (2009). Remote sensing of solar-induced chlorophyll fluorescence: Review of methods and applications. *Remote Sensing of Environment*, *113*(10), 2037–2051. https://doi.org/https://doi.org/10.1016/j.rse.2009.05.003

MICHAELIAN, M., HOGG, E. H., HALL, R. J., & ARSENAULT, E. (2011). Massive mortality of aspen following severe drought along the southern edge of the Canadian boreal forest. *Global Change Biology*, *17*(6), 2084–2094. https://doi.org/10.1111/j.1365-2486.2010.02357.x

Mohammed, G. H., Colombo, R., Middleton, E. M., Rascher, U., van der Tol, C., Nedbal, L., … Zarco-Tejada, P. J. (2019). Remote sensing of solar-induced chlorophyll fluorescence (SIF) in vegetation: 50 years of progress. *Remote Sensing of Environment*, *231*, 111177. https://doi.org/https://doi.org/10.1016/j.rse.2019.04.030

Monteith JL. (1977). Climate and the efficiency of crop production in Britain. *Philosophical Transactions of the Royal Society of London. B, Biological Sciences*, *281*(980), 277–294. https://doi.org/10.1098/rstb.1977.0140

Montgomery, R. A., Rice, K. E., Stefanski, A., Rich, R. L., & Reich, P. B. (2020). Phenological responses of temperate and boreal trees to warming depend on ambient spring temperatures, leaf habit, and geographic range. *Proceedings of the National Academy of Sciences*, *117*(19), 10397 LP – 10405. https://doi.org/10.1073/pnas.1917508117

NASA's Earth Observatory. (2013). Arctic amplification. Retrieved May 10, 2019, from https://climate.nasa.gov/news/927/arctic-amplification/

Nichol, J. C., Drolet, G., Porcar-Castell, A., Wade, T., Sabater, N., Middleton, M. E., … Atherton, J. (2019). Diurnal and Seasonal Solar Induced Chlorophyll Fluorescence and Photosynthesis in a Boreal Scots Pine Canopy. *Remote Sensing* , Vol. 11. https://doi.org/10.3390/rs11030273

Öquist, G., & Huner, N. P. A. (2003). Photosynthesis of Overwintering Evergreen Plants. *Annual Review of Plant Biology*, *54*(1), 329–355. https://doi.org/10.1146/annurev.arplant.54.072402.115741

ÖQUIST, G., & MARTIN, B. (1980). Inhibition of photosynthetic electron transport and formation of inactive chlorophyll in winter stressed Pinus silvestris. *Physiologia Plantarum*, *48*(1), 33–38. https://doi.org/https://doi.org/10.1111/j.1399-3054.1980.tb03215.x

Pan, Y., Birdsey, R. A., Fang, J., Houghton, R., Kauppi, P. E., Kurz, W. A., … Hayes, D. (2011). A Large and Persistent Carbon Sink in the World's Forests. *Science*, *333*(6045), 988 LP – 993. https://doi.org/10.1126/science.1201609

PEÑUELAS, J., FILELLA, I., & GAMON, J. A. (1995). Assessment of photosynthetic radiation-use efficiency with spectral reflectance. *New Phytologist*, *131*(3), 291–296. https://doi.org/https://doi.org/10.1111/j.1469-8137.1995.tb03064.x

Peñuelas, J., Filella, I., Gamon, J. A., & Field, C. (1997). Assessing photosynthetic radiation-use efficiency of emergent aquatic vegetation from spectral reflectance. *Aquatic Botany*, *58*(3), 307–315. https://doi.org/https://doi.org/10.1016/S0304-3770(97)00042-9

Pierrat, Z., Magney, T., Parazoo, N., Grossmann, K., Bowling, D., Seibt, U., … Stutz, J. (2022). Diurnal and seasonal dynamics of solar-induced chlorophyll fluorescence, vegetation indices, and gross primary productivity in the boreal forest. *Journal of Geophysical Research: Biogeosciences*. https://doi.org/10.1029/2021JG006588

Pierrat, Z., Nehemy, M., Roy, A., Magney, T., Parazoo, N., Laroque, C., … Stutz, J. (2021). Tower-Based Remote Sensing Reveals Mechanisms Behind a Two-phased Spring Transition in a Mixed-Species

Boreal Forest. *Journal of Geophysical Research: Biogeosciences*, *126*. https://doi.org/10.1029/2020JG006191

Pinto, F., Celesti, M., Acebron, K., Alberti, G., Cogliati, S., Colombo, R., … Rascher, U. (2020). Dynamics of sun-induced chlorophyll fluorescence and reflectance to detect stress-induced variations in canopy photosynthesis. *Plant, Cell & Environment*, *43*(7), 1637–1654. https://doi.org/https://doi.org/10.1111/pce.13754

Porcar-Castell, A., Garcia Plazaola, J. I., J Nichol, C., Kolari, P., Olascoaga, B., Kuusinen, N., … Nikinmaa, E. (2012). Physiology of the seasonal relationship between Photochemical Reflectance Index and photosynthetic Light Use Efficiency. In *Oecologia* (Vol. 170). https://doi.org/10.1007/s00442-012-2317-9

Porcar-Castell, A., Tyystjärvi, E., Atherton, J., Tol, C., Flexas, J., E Pfündel, E., … Berry, J. (2014). Linking chlorophyll a fluorescence to photosynthesis for remote sensing applications: Mechanisms and challenges. In *Journal of experimental botany* (Vol. 65). https://doi.org/10.1093/jxb/eru191

Powles, S. (2003). Photoinhibition of Photosynthesis Induced by Visible Light. *Annu Rev Plant Physiol*, *35*, 15–44. https://doi.org/10.1146/annurev.pp.35.060184.000311

R. Springer, K., Wang, R., & Gamon, J. (2017). Parallel Seasonal Patterns of Photosynthesis, Fluorescence, and Reflectance Indices in Boreal Trees. In *Remote Sensing* (Vol. 9). https://doi.org/10.3390/rs9070691

Raczka, B., Porcar-Castell, A., Magney, T., Lee, J. E., Köhler, P., Frankenberg, C., … Bowling, D. R. (2019). Sustained Nonphotochemical Quenching Shapes the Seasonal Pattern of Solar-Induced Fluorescence at a High-Elevation Evergreen Forest. *Journal of Geophysical Research: Biogeosciences*, *124*(7), 2005–2020. https://doi.org/https://doi.org/10.1029/2018JG004883

Rajewicz, A. P., Atherton, J., Alonso, L., & Porcar-Castell, A. (2019). Leaf-Level Spectral Fluorescence Measurements: Comparing Methodologies for Broadleaves and Needles. *Remote Sensing* , Vol. 11. https://doi.org/10.3390/rs11050532

Rangwala, I., Sinsky, E., & Miller, J. (2013). Amplified warming projections for high altitude regions of the Northern Hemisphere mid-latitudes from CMIP5 models. *Environmental Research Letters*, *8*, 24040. https://doi.org/10.1088/1748-9326/8/2/024040

Rascher, U., Alonso, L., Burkart, A., Cilia, C., Cogliati, S., Colombo, R., … Zemek, F. (2015). Sun-induced fluorescence – a new probe of photosynthesis: First maps from the imaging spectrometer HyPlant. *Global Change Biology*, *21*(12), 4673–4684. https://doi.org/https://doi.org/10.1111/gcb.13017

Richardson, A., Black, T., Ciais, P., Delbart, N., Friedl, M., Gobron, N., … Varlagin, A. (2010). Influence of spring and autumn phenological transitions on forest ecosystem productivity. *Philosophical Transactions of the Royal Society B-Biological Sciences, v.365, 3227-3246 (2010)*, *365*. https://doi.org/10.1098/rstb.2010.0102

Richardson, A. D., Keenan, T. F., Migliavacca, M., Ryu, Y., Sonnentag, O., & Toomey, M. (2013). Climate change, phenology, and phenological control of vegetation feedbacks to the climate system. *Agricultural and Forest Meteorology*, *169*, 156–173. https://doi.org/https://doi.org/10.1016/j.agrformet.2012.09.012

Ronald, S., Manabe, S., & Bryan, K. (1989). Interhemispheric asymmetry in climate response to a gradual increase of atmospheric CO2. *Nature*, *342*. https://doi.org/10.1038/342660a0

Rossini, M., Nedbal, L., Guanter, L., Ač, A., Alonso, L., Burkart, A., … Rascher, U. (2015). Red and far

red Sun-induced chlorophyll fluorescence as a measure of plant photosynthesis. *Geophysical Research Letters*, *42*(6), 1632–1639. https://doi.org/https://doi.org/10.1002/2014GL062943

Savitch, L. V, Leonardos, E. D., Krol, M., Jansson, S., Grodzinski, B., Huner, N. P. A., & Öquist, G. (2002). Two different strategies for light utilization in photosynthesis in relation to growth and cold acclimation. *Plant, Cell & Environment*, *25*(6), 761–771. https://doi.org/https://doi.org/10.1046/j.1365-3040.2002.00861.x

Shvidenko, A., & Schepaschenko, D. (2013). Climate Change and Wildfires in Russia. *Contemporary Problems of Ecology*, *6*, 683–692. https://doi.org/10.1134/S199542551307010X

Siegmann, B., Cendrero-Mateo, M. P., Cogliati, S., Damm, A., Gamon, J., Herrera, D., … Rascher, U. (2021). Downscaling of far-red solar-induced chlorophyll fluorescence of different crops from canopy to leaf level using a diurnal data set acquired by the airborne imaging spectrometer HyPlant. *Remote Sensing of Environment*, *264*, 112609. https://doi.org/https://doi.org/10.1016/j.rse.2021.112609

Springer, K. (2018). *Monitoring Phenology of Boreal Trees Using Remote Sensing*. University of Alberta.

Sun, Y., Frankenberg, C., Jung, M., Joiner, J., Guanter, L., Köhler, P., & Magney, T. (2018). Overview of Solar-Induced chlorophyll Fluorescence (SIF) from the Orbiting Carbon Observatory-2: Retrieval, cross-mission comparison, and global monitoring for GPP. *Remote Sensing of Environment*, *209*, 808–823. https://doi.org/https://doi.org/10.1016/j.rse.2018.02.016

Sutinen, M.-L., Arora, R., Wisniewski, M., Ashworth, E., Strimbeck, R., & Palta, J. (2001). *Mechanisms of Frost Survival and Freeze-Damage in Nature*. https://doi.org/10.1007/978-94-015-9650-3_4

Ulsig, L., Nichol, J. C., Huemmrich, F. K., Landis, R. D., Middleton, M. E., Lyapustin, I. A., … Porcar-Castell, A. (2017). Detecting Inter-Annual Variations in the Phenology of Evergreen Conifers Using Long-Term MODIS Vegetation Index Time Series. *Remote Sensing* , Vol. 9. https://doi.org/10.3390/rs9010049

van der Tol, C., Rossini, M., Cogliati, S., Verhoef, W., Colombo, R., Rascher, U., & Mohammed, G. (2016). A model and measurement comparison of diurnal cycles of sun-induced chlorophyll fluorescence of crops. *Remote Sensing of Environment*, *186*, 663–677. https://doi.org/https://doi.org/10.1016/j.rse.2016.09.021

Van Wittenberghe, S; Verrelst, J; Alonso L; Hermans, I; Delegido, J; Valcke, R; Moreno, J; Samson, R. (2013). Methodology, Fluowat leaf clip develped by Luis Alonso. In *Enviromental Pollution* (pp. 29–37). Valencia.

Van Wittenberghe, S., Alonso, L., Verrelst, J., Hermans, I., Delegido, J., Veroustraete, F., … Samson, R. (2013). Upward and downward solar-induced chlorophyll fluorescence yield indices of four tree species as indicators of traffic pollution in Valencia. *Environmental Pollution*, *173*, 29–37. https://doi.org/https://doi.org/10.1016/j.envpol.2012.10.003

Verhoeven, A. (2014). Sustained energy dissipation in winter evergreens. *New Phytologist*, *201*(1), 57–65. https://doi.org/10.1111/nph.12466

Walter-McNeill, A., Garcia, M. A., Logan, B. A., Bombard, D. M., Reblin, J. S., Lopez, S., … Bowling, D. R. (2021). Wide variation of winter-induced sustained thermal energy dissipation in conifers: a common-garden study. *Oecologia*. https://doi.org/10.1007/s00442-021-05038-y

Walther, S., Voigt, M., Thum, T., Gonsamo, A., Zhang, Y., Köhler, P., … Guanter, L. (2016). Satellite chlorophyll fluorescence measurements reveal large-scale decoupling of photosynthesis and greenness dynamics in boreal evergreen forests. *Global Change Biology*, *22*(9), 2979–2996.

https://doi.org/10.1111/gcb.13200

Wang, X., Piao, S., Xu, X., Ciais, P., MacBean, N., Myneni, R. B., & Li, L. (2015). Has the advancing onset of spring vegetation green-up slowed down or changed abruptly over the last three decades? *Global Ecology and Biogeography*, *24*(6), 621–631. https://doi.org/10.1111/geb.12289

Wieneke, S., Ahrends, H., Damm, A., Pinto, F., Stadler, A., Rossini, M., & Rascher, U. (2016). Airborne based spectroscopy of red and far-red sun-induced chlorophyll fluorescence: Implications for improved estimates of gross primary productivity. *Remote Sensing of Environment*, *184*, 654–667. https://doi.org/https://doi.org/10.1016/j.rse.2016.07.025

Williams, C. M., Henry, H. A. L., & Sinclair, B. J. (2015). Cold truths: how winter drives responses of terrestrial organisms to climate change. *Biological Reviews*, *90*(1), 214–235. https://doi.org/https://doi.org/10.1111/brv.12105

Wong, C. (2014). *Seasonal photosynthetic activity in evergreen conifer leaves monitored with spectral reflectance*. Univesity of Alberta.

Wong, C. Y. S., D'Odorico, P., Arain, M. A., & Ensminger, I. (2020). Tracking the phenology of photosynthesis using carotenoid-sensitive and near-infrared reflectance vegetation indices in a temperate evergreen and mixed deciduous forest. *New Phytologist*, *226*(6), 1682–1695. https://doi.org/10.1111/nph.16479

Wong, C. Y. S., D'Odorico, P., Bhathena, Y., Arain, M. A., & Ensminger, I. (2019). Carotenoid based vegetation indices for accurate monitoring of the phenology of photosynthesis at the leaf-scale in deciduous and evergreen trees. *Remote Sensing of Environment*, *233*, 111407. https://doi.org/https://doi.org/10.1016/j.rse.2019.111407

Wong, C. Y. S., & Gamon, J. A. (2015). The photochemical reflectance index provides an optical indicator of spring photosynthetic activation in evergreen conifers. *New Phytologist*, *206*(1), 196–208. https://doi.org/10.1111/nph.13251

Yang, J. C., Magney, T. S., Albert, L. P., Richardson, A. D., Frankenberg, C., Stutz, J., … Bowling, D. R. (2022). Gross primary production (GPP) and red solar induced fluorescence (SIF) respond differently to light and seasonal environmental conditions in a subalpine conifer forest. *Agricultural and Forest Meteorology*, *317*, 108904. https://doi.org/https://doi.org/10.1016/j.agrformet.2022.108904

Yang, Q., Blanco, N., Hermida Carrera, C., Lehotai, N., Hurry, V., & Strand, Å. (2020). Two dominant boreal conifers use contrasting mechanisms to reactivate photosynthesis in the spring. *Nature Communications*, *11*, 128. https://doi.org/10.1038/s41467-019-13954-0

Yu, T., Jiapaer, G., Bao, A., Zheng, G., Zhang, J., Li, X., … Umuhoza, J. (2022). Disentangling the relative effects of soil moisture and vapor pressure deficit on photosynthesis in dryland Central Asia. *Ecological Indicators*, *137*, 108698. https://doi.org/https://doi.org/10.1016/j.ecolind.2022.108698

Appendix A – Leaf-Clip Methodology – Collecting and analyzing sun induced chlorophyll fluorescence SIF and needle-reflectance data with a FluoWat leaf-clip.

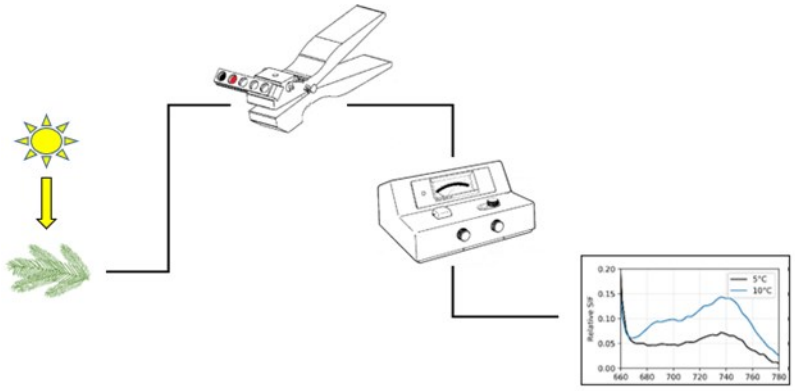

Materials and Methods

- Section 1. Background

In order to measure the reflectance and the fluorescence signal for this experiment, we used the FluoWat leaf-clip designed by (Van Wittenberghe, S; Verrelst, J; Alonso L; Hermans, I;

Delegido, J; Valcke, R; Moreno, J; Samson, 2013) (Figure 1). The FluoWat leaf-clip is a newly developed tool designed to conduct proximal optical sampling of individual leaves (Mohammed et al., 2019; Van Wittenberghe et al. 2013, 2014). The leaf-clip was specifically designed to hold leaves and to measure the energy emitted by the SIF signal in the red and far-red under sunlight or artificial light (see figure 2). The design of the leaf-clip allows us to collect the SIF signal of groups of needles or individual leaves, using a high spectral resolution spectrometer (UniSpec-SC, PP Systems, Amesbury, MA, USA), that was also attached to an optical fibre (UNI684, PP Systems, Amesbury, MA, USA). For the purposes of this experiment, we set the needles in bunches of 6 to 8 in a black electric tape, the needles were carefully arranged one next to the other (see figure 2B), trying to avoid gaps (to eliminate transmittance), however, the instrument can also clip leaves too.

Details on needle collection, groups of 6-8 needles were carefully removed from the sunny side of the tree and mounted on a black electric tape like in Figure 2-b. All the processes were performed outside in the rooftop, where the needles were constantly exposed to natural air temperature. The needles were positioned with the tops towards one side of the tape and the bottom's situated in the opposite direction. (Important: during winter because of very low temperatures setting the needles in the masking tape was more challenging than during spring or summer). Immediately after this, the black masking tape holding the needles was located in the FluoWat leaf-clip (Figure 1). We assumed there was no change in air temperature at the time of collecting the SIF signal and reflectance.

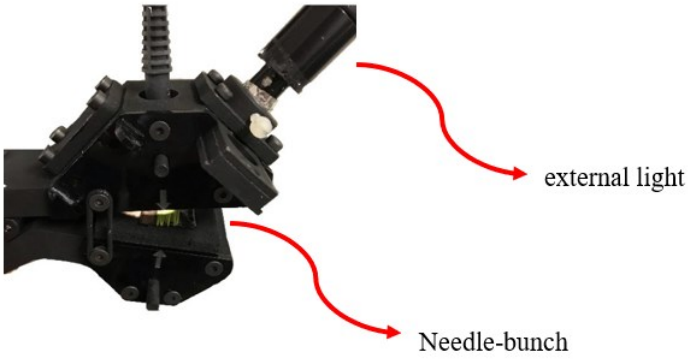

Figure 1. FluoWat leaf-clip design (Alonso et al. 2007).

- Section 2. Setting up the instrument and collecting data with a FluoWat leaf-clip.

Each leaf measurement was performed according to a fixed protocol (Figure 3). First, we mounted the leaf clip on a tripod with an adjustable arm and set the leaf clip to point towards the sun (Figure 2a), allowing maximal radiation to enter the port illuminating the interior of the clip. Before the insertion of the needles into the leaf-clip, a dark current (DS) was measured. After this, we collected the incoming sunlight or irradiance (*I*). This was measured as the reflected radiance of a white reference (WR) – (10 mm thick ODM98 panel, designed by (Gigahertz-Optic, 2021) placed inside the clip. Next, the bundle of needles was inserted into the clip, and leaf reflectance was measured, one time without the filter (REF) and three times with the 650 filter (SIF) using time intervals of 60s (during three times). Finally, incoming solar irradiance (*I*) was measured as the reflected radiance of a white reference with the filter (WR650). The protocol used to collect data for this experiment is presented as a series of sample spectra in Figure 4, and an example of unprocessed SIF spectral data is presented in Figure 6.

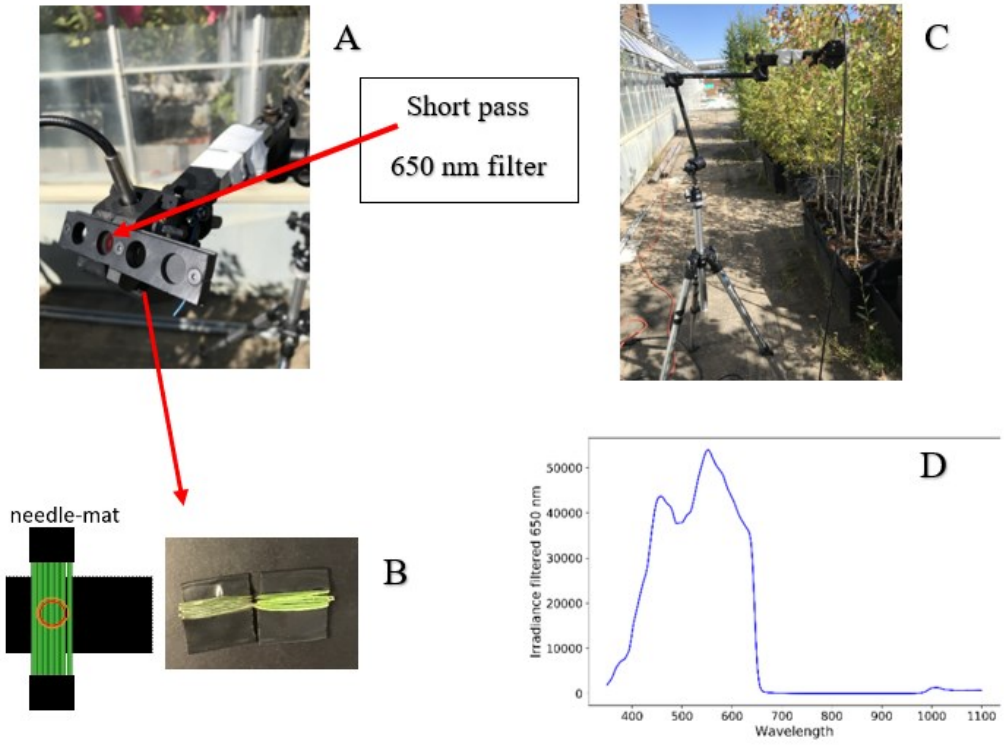

Figure 2. (A) FluoWat leaf-clip (Van Wittenberghe et al. 2013) coupled with a spectrometer (UniSpec, PP Systems, Amesbury MA), which enables measurement of the sun induced fluorescence spectrum by selectively filtering the incoming light. (B) Needle bunches arranged on black electric tape. (C) Leaf-clip set on the tripod. (D) Spectral measurement of white reference with a 650 nm short pass filter.

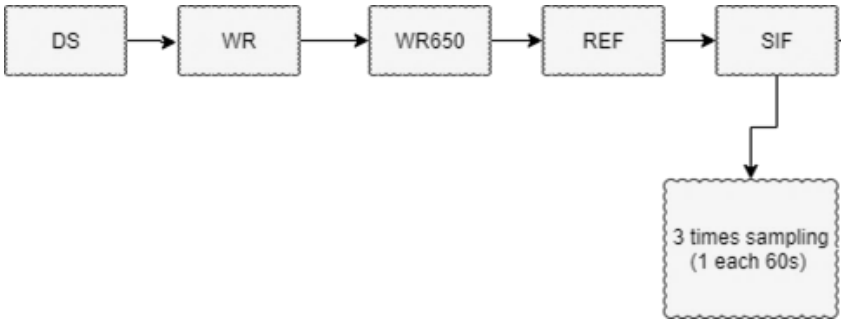

Figure 3. Work-flow used to collect spectral data from needles during the experiment.

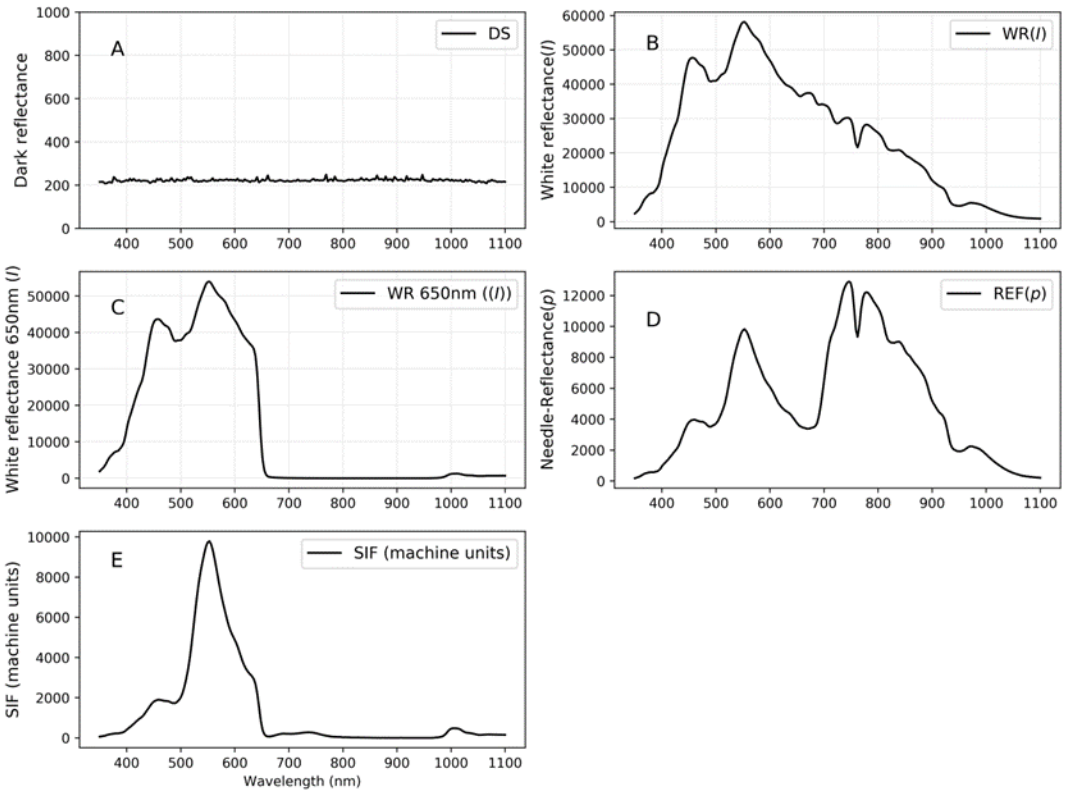

Figure 4. Spectral examples of the protocol used to collect data under natural sunlight, this protocol was applied to each bundle of needles a) a dark reflectance was collected using a black filter positioned to block the incoming light, b) white reference was using a ODM85 white filter, c) a second reflectance was collected with a 650nm filter, d) needle spectral reflectance was collected with the filter not positioned and not corrected, and e) Sun induced chlorophyll fluorescence was collected with the 650 nm filter, in machine units, without corrections.

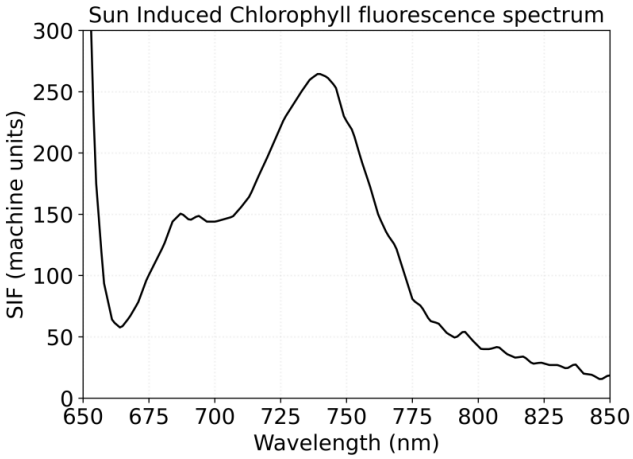

Figure 5. SIF spectrum collected using a FluoWat leaf-clip (raw data and before corrections). Data displayed is from a Black Spruce's bundle-needle, taken on August 19th, 2020, under sunny and clear sky conditions.

- Section 3. Correcting and calibrating spectral data

In order to calculate reflectance vegetation indices, we first calibrated the raw reflectance that was obtained in machine units, using the next procedure (see equation 1 and Figure 6). The corrected reflectance (ρ) was calculated as the obtained raw-reflected radiance of the needle (L_λ) divided by incoming solar irradiance (I_λ). The latter is given by the radiance reflected by the WR.

Equation (1)

$$\rho\lambda = L_\lambda / I_\lambda$$

ρ_λ, reflectance
L_λ, radiance
I_λ, irradiance

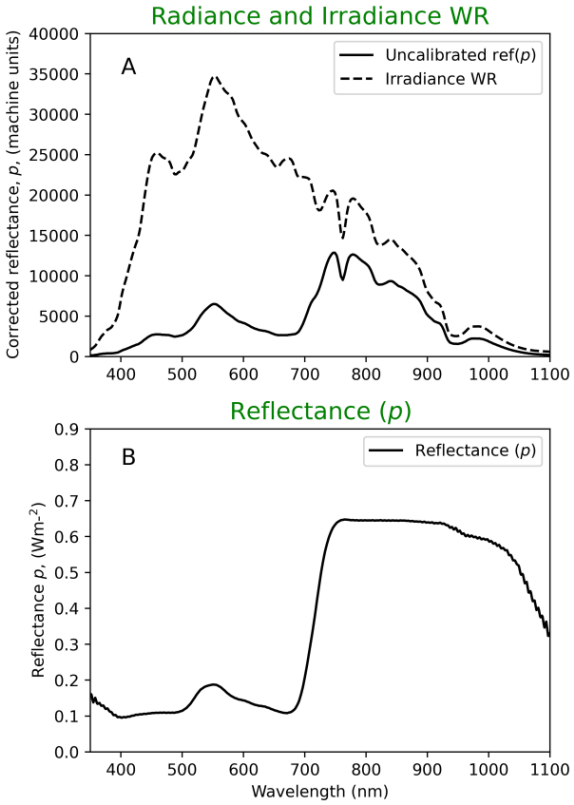

Figure 6. Chart shows: a) Obtained raw-reflected radiance of the needle (uncalibrated reflectance) divided by incoming solar irradiance (I_λ) (White reference). b) Corrected reflectance ($\rho\lambda$).

After this procedure, optical reflectance indices were calculated using the leaf reflectance (ρλ) from each measurement and the following equations:

Normalized difference vegetation index NDVI	$\frac{\rho 800\text{nm} - \rho 630\text{nm}}{\rho 800\text{nm} + \rho 630\text{nm}}$
Photochemical reflectance index PRI	$\frac{\rho 531\text{nm} - \rho 570\text{nm}}{\rho 531\text{nm} + \rho 570\text{nm}}$
Chlorophyll/carotenoid index CCI	$\frac{\rho 531\text{nm} - \rho 630\text{nm}}{\rho 531\text{nm} + \rho 630\text{nm}}$

- Section 3.1. Correcting for light-leaks in the SIF spectral data.

While using the 650nm filter needed to collect the SIF spectral signal, the incoming light is cut off beyond 650 nm. This cut-off is not perfect, and some radiation still passes the filter, leading to a slight "leak" of reflected radiation into the spectral region of the fluorescence spectrum. This residual light can reach as far as 800 nm (Mohammed et al. 2019; Van Wittenberghe et al., 2013, 2014). The majority of the light below 700 nm will become absorbed by the leaf, contributing to the SIF signal measured. However, a minor amount of the light-leakage reflected by the leaf will be added to the measured SIF emission (uncalibrated SIF), causing a slight error in SIF estimation(see Figure 7A). This light leakage can be accounted for and removed. In this project, the amount of residual light (or the light leakage) was calculated as the radiance sampled when using the filter (WR_{650}) times the reflectance (ρ) of the leaf (Reflectance (ρ) Wm^{-2}) (equation 2). The residual leaked light is then subtracted from the measured Chl fluorescence (uncalibrated SIF), to lead to Chl fluorescence without contamination by residual reflected light (corrected Chl fluorescence or corrected SIF) (Eq 3, Figure 7B). This correction must be done using the corrected leaf reflectance before transforming the uncalibrated SIF units into radiance units.

Equation (2)

$$\text{Residual light (light} - \text{ leakage)} = \rho_\lambda * I_{650\,\lambda\,\text{nm}}$$

ρ_λ, corrected reflectance

$I_{650\,\lambda\,\text{nm}}$, irradiance from the white reference using the short pass filter 650nm.

Equation (3)

$$\text{Corrected SIF} = \text{Uncalibrated SIF} - \text{Residual light(light leakage)}$$

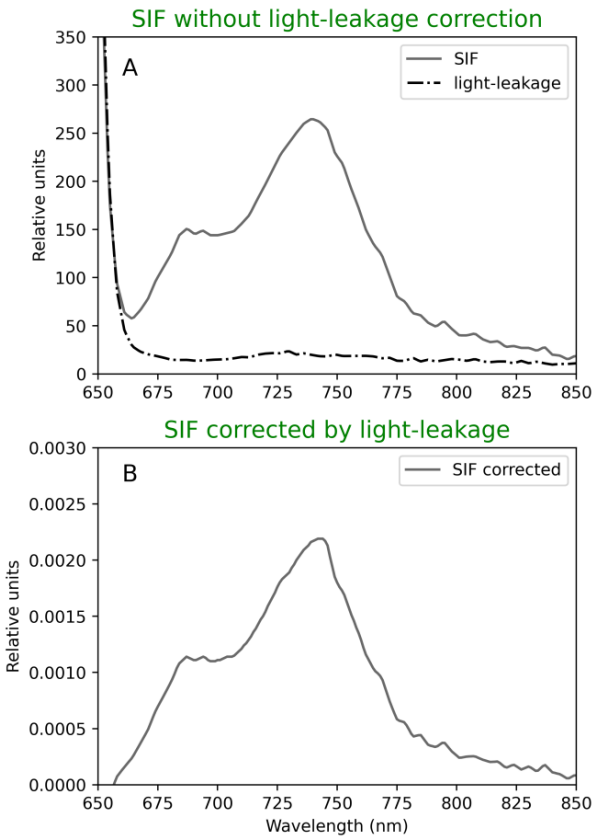

Figure 7. Spectral representation of a) the SIF signal (dark grey line) without correction and the calculated light-leakage (black dashed line) b) Light-leakage removed from SIF signal.

- Section 3.2. Radiometric calibration methodology

To obtain radiometric units for SIF calculation, the UniSpec field spectrometer must be calibrated against a radiometrically calibrated instrument or light source. For this calibration, a field spectrometer (PSR-3500, Spectral Evolution, Haverhill MA, USA) was used as the calibrated (reference) instrument, and a standard reference panel (Spectralon, LabSphere, North Sutton, NH, USA) was used to transfer the radiometric units ($Wm^{-2}sr^{-1}nm^{-1}$), units needed to correct Sun Induced Fluorescence (SIF) data collected in apparent reflectance (machine units). To complete this task, the following equipment and setting-up were required.

- UniSpec field spectrometer (not radiometrically calibrated)

- 2mm Optic Fiber (Uni684, PP Systems)
- Bubble Level & Tripod
- White Panel, size 26 cm (Spectralon, LabSphere, North Sutton, NH, USA)
- Spectral Evolution field spectrometer (radiometrically calibrated)
- 2 mm and 2.5 mm optical fiber (provided with Spectral evolution radiometer)
- Laptop computer

- Calibration Setup and measurements

Measurements were made under sunny conditions with no clouds blocking the sun. The first step was to turn on the spectrometers to let them warm up and adjust for the ambient outside temperature (15 minutes according to manuals). Next, we set up the tripod and installed and leveled the white panel (See Figure 8). After this, we inserted and secured the fiber optics into their respective spectrometer (Unispec, 2m, UNI684, PP Systems, Amesbury, MA, USA) and radiometer (PSR-3500, Spectral Evolution, with2mm optic fibre and 2.5 mm). We connected the spectrometers to the laptop computer and made initial test measurements (collecting samples every 10 seconds with both devices, with the integration time set to 20 ms). After this we collected the data from both devices (12 scans each time).

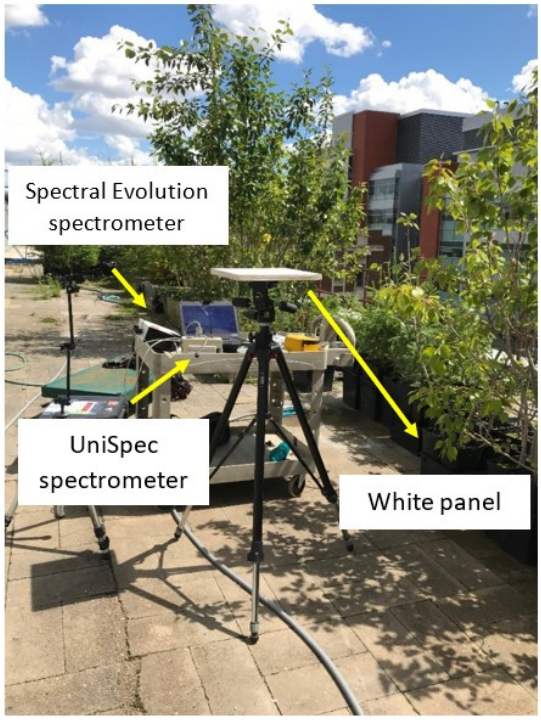

Figure 8. Instruments set-up during cross-calibration data collection. During calibration, each instrument foreoptic was pointed towards the white panel under identical sunny conditions.

After this, we downloaded the data from both devices and converted them into comma separated value files. For the data collected with UniSpec we used Multispec-v4.0 (http://specnet.info) and, for data collected with Spectral evolution spectrometer we used the Darwin SP software (Spectral Evolution, Haverhill MA, USA). We convolved the Spectral Evolution data using "SED-channel-spacing-to-1nm-Converter" software (Spectral Evolution, Haverhill MA, USA) to obtain 1nm band spectral resolution. This process was necessary to match the Unispec data, which was corrected to 1nm when processing through Multispec-v4.0.

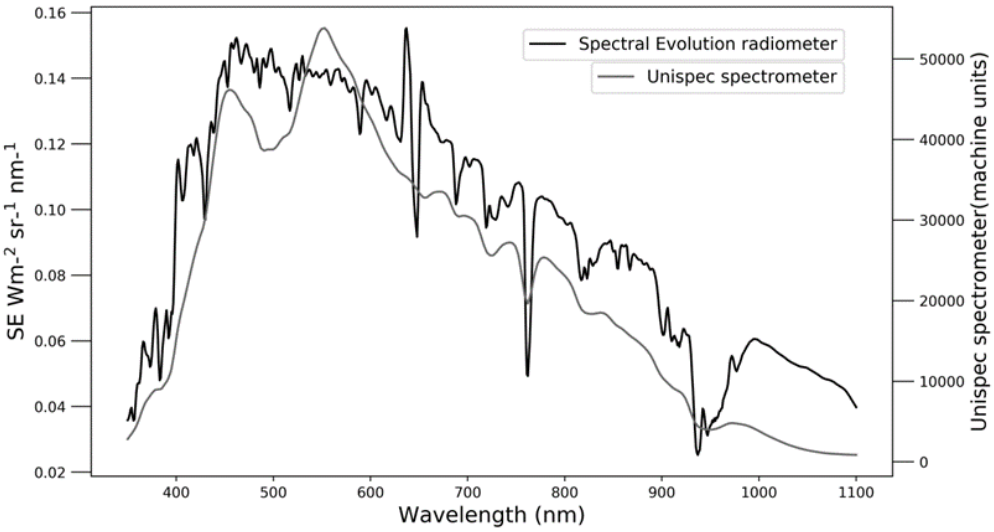

Figure 9. Radiance collected under a sunny and clear sky day during May 2020. Black lines show data collected using the Spectral Evolution radiometer, (expressed in Wm-2sr-1nm-1) and grey lines show the data collected with the Unispec spectrometer (expressed in machine units). Note: the higher spectral resolution of the Spectral Evolution yields more atmospheric absorption features.

Later, we used the measurements from both instruments to calculate a ratio of the radiometrically-calibrated spectrum (Figure 9) to the uncalibrated spectrum. This ratio was later used to convert sun induced fluorescence from uncalibrated machine units into radiometric units. The ratio was calculated using an average of 12 measurements from each spectrometer, measurements collected over the same timeframe (several minutes) and under similar sunny conditions. Because the resulting calibration included slight artifacts associated with the different spectral resolutions of the instruments, we applied a 20% smoothing kernel-filter, and the resulting ratio spectrum is shown in Figure 10.

Equation (4)

$$Ratio = \frac{calibrated\ L_{Spectral\ Evolution}}{uncalibrated\ L_{\text{Unispec}}}$$

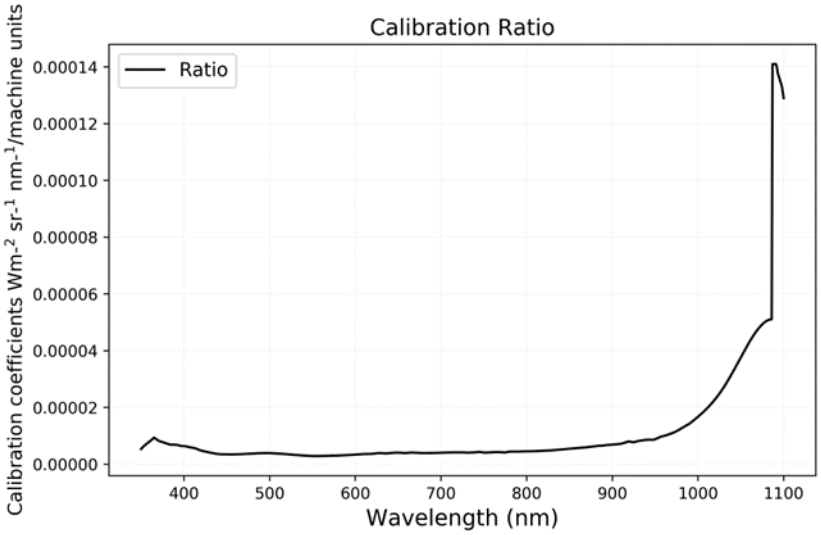

Figure 10. Ratio calculated using equation 1. Later the cross-calibration ratio was multiplied for each wavelength to convert SIF collected from the Unispec (in apparent reflectance units) to radiometric units ($Wm^{-2}sr^{-1}nm^{-1}$).

This radiometric calibration of the sun induced fluorescence (SIF) data must be done after correcting by the light leakage, examples are shown in figure 11. The SIF data was calculated by multiplying each measurement by the calibration ratio previously obtained (Figure 10). Results are presented as radiometric units $Wm^{-2}sr^{-1}nm^{-1}$.

Equation (5)

$$\text{Calibrated SIF} = Ratio\ x\ Corrected\ SIF_{\lambda} = Wm^{-2}sr^{-1}nm^{-1}.$$

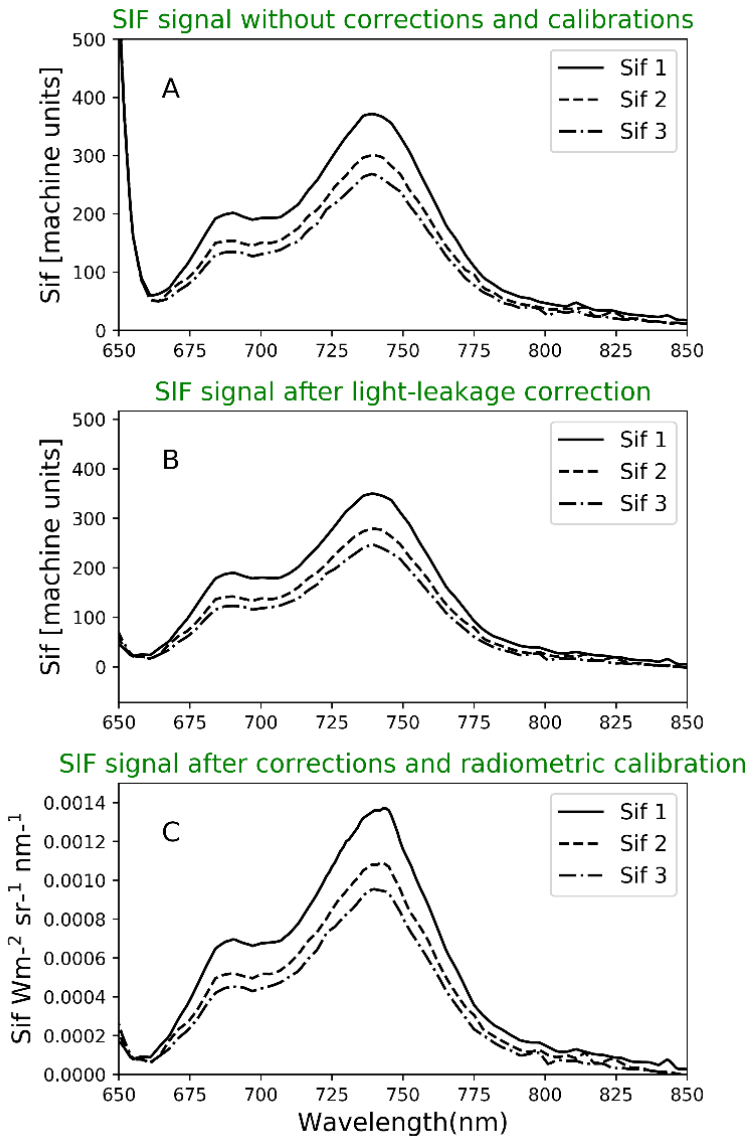

Figure 11. a) Sun induced fluorescence (Sif) spectral signal in machine units before cross-calibration and light leakage correction, b) Sun induced fluorescence spectral signal after light leakage correction and c) SIF after cross-calibration in radiometric units and light-leakage.

Section 2.3. Derivation of sun induced chlorophyll fluorescence yield parameters.

- *Calculating Fluorescence yield (FY)*

In order to obtain FY, we need to obtain absorbed PAR (APAR) which is obtained using equation 9. In this project, transmittance (T) was assumed to be zero because the leaves (evergreen needles) are optically thick. In equation 10, we set the limit between 650 to 850 because in this interval is

where we find the fluorescence signal and both chlorophyll fluorescence peaks (wavelengths of these peaks at 685 and 740 nm (Rossini et al., 2015).

Equation (6) $$APAR = PAR\ (W\text{m}^2)x\ FPAR$$

Equation (7) $$\text{FY} = \int_{690}^{740} f(\lambda)\, d\lambda / APAR(\text{W m}^2)$$

- *Calculating Fluorescence yield (FY) at peaks.*

Equation (8)

$$\text{FY}_{685} = \frac{SIF\ 685\ \lambda}{APAR}$$

Equation (9)

$$\text{FY}_{745} = \frac{SIF\ 745\ \lambda}{APAR}$$

- *Calculating Fluorescence yield (FY) ratio.*

$$\text{FY}_{\text{ratio}} = \frac{FY\ 685\ \lambda}{FY\ 745\ \lambda}$$

Literature Cited

Gigahertz-Optic. (2021). ODM98 Properties and Specifications. Retrieved June 4, 2021, from https://light-measurement.com/ODM98-specifications/

Mohammed, G. H., Colombo, R., Middleton, E. M., Rascher, U., van der Tol, C., Nedbal, L., … Zarco-Tejada, P. J. (2019). Remote sensing of solar-induced chlorophyll fluorescence (SIF) in vegetation: 50 years of progress. *Remote Sensing of Environment*, *231*, 111177. https://doi.org/https://doi.org/10.1016/j.rse.2019.04.030

Rossini, M., Nedbal, L., Guanter, L., Ač, A., Alonso, L., Burkart, A., … Rascher, U. (2015). Red and far red Sun-induced chlorophyll fluorescence as a measure of plant photosynthesis. *Geophysical Research Letters*, *42*(6), 1632–1639. https://doi.org/https://doi.org/10.1002/2014GL062943

Van Wittenberghe, S; Verrelst, J; Alonso L; Hermans, I; Delegido, J; Valcke, R; Moreno, J; Samson, R. (2013). Methodology, Fluowat leaf clip developed by Luis Alonso. In *Enviromental Pollution* (pp. 29–37). Valencia.

Van Wittenberghe, S., Alonso, L., Verrelst, J., Hermans, I., Delegido, J., Veroustraete, F., … Samson, R. (2013). Upward and downward solar-induced chlorophyll fluorescence yield indices of four tree species as indicators of traffic pollution in Valencia. *Environmental Pollution*, *173*, 29–37. https://doi.org/https://doi.org/10.1016/j.envpol.2012.10.003